



UNIVERSITAT POLITÈCNICA DE CATALUNYA
BARCELONATECH
Escola d'Enginyeria de Telecomunicació
i Aeroespacial de Castelldefels

TREBALL DE FI DE GRAU

TFG TITLE: DESIGN OF A HYPERSONIC AIRBREATHING CRUISE MISSILE

DEGREE: Grau en Enginyeria d'Aeronavegació

AUTHOR: Eduard Graells Pina

ADVISOR: Fernando Pablo Mellibovsky Elstein

DATE: August 27, 2019

Title : DESIGN OF A HYPERSONIC AIRBREATHING CRUISE MISSILE

Author: Eduard Graells Pina

Advisor: Fernando Pablo Mellibovsky Elstein

Date: August 27, 2019

Overview

In this project, a hypersonic airbreathing cruise missile is designed through an optimization process. The main use of this futuristic weapon technology is to be employed against enemy ships while being launched from an Mk-41 VLS launcher, the most widespread VLS in the world.

In this optimization process and for this type of missile, Genetic Algorithms and Monte Carlo simulations are used to find an optimal solution for the rocket booster engine, the scramjet engine, aerodynamics and warhead sizing. With this data, trajectory, stability and manoeuvrability is studied to determine the performance of the missile. Other aspects concerning the missile materials of the airframe and dome are discussed on a qualitative way and no structural analysis is studied within this project.

It should be noted that hypersonic weapons are mature technologies, and the only information about them are research papers regarding their aerodynamics and propulsion systems. Then, the only built hypersonic vehicles are experimental, meaning that the baseline data to start design process scarce. This brings a great challenge to this project, where creativity and the use of analytical expressions for rapid missile synthesis and conceptual design is a must.

On the other side, due to the complex behaviour of hypersonic flows, this adds difficulties to our research since most of the methods employed are numerical, which can be calculated easily on a CFD in the final stages of the design, but they are not fast enough to be implemented on the initial stages of design. The final results prove that the methods employed for initial sizing are accurate enough to model a CAD design which can be used as a baseline for future research in this technology.

To conclude with, the final results obtained with the algorithms helps us to understand the effects on design, especially when flying at high Mach numbers where the classical configuration of airframe, wings and tail must be radically redesigned to more aerodynamic efficient bodies such as Waveriders.

Regarding to the optimization process, objective functions were changed manually to find better results at each iteration of the optimization process but better techniques such as local search methods used in artificial intelligence could be employed.

CONTENTS

Introduction	1
CHAPTER 1. Aerodynamics	9
1.1. Fundamentals of hypersonic aerodynamics	9
1.1.1. Newtonian flow theory	11
1.1.2. Shock expansion theory	12
1.1.3. Van Driest method (II)	12
1.2. Nose cone aerodynamics	12
1.3. Missile body aerodynamics	13
1.4. Tail aerodynamics	14
1.5. Aerothermodynamics and materials selection	15
1.5.1. Airframe materials	15
1.5.2. Insulation materials	15
1.5.3. Seeker dome	16
1.5.4. Surface heating	16
1.6. Computational fluid dynamics	16
CHAPTER 2. Propulsion system	19
2.1. Solid rocket booster	19
2.1.1. Star grain configuration	20
2.1.2. Solid rocket propellant chemistry and composition	22
2.1.3. Booster's casing materials selection	23
2.2. Scramjet and ramjet engines	23
2.2.1. Scramjet thermodynamic cycle	23
2.2.2. Intake considerations	25
2.2.3. Mixed compression analysis	26
2.2.4. Burner and combustion analysis	27
2.2.5. Expansion and nozzle analysis	28
CHAPTER 3. Stability & Control	31
3.1. Stability and manoeuvrability	31

3.2. Missile body with booster	31
3.3. Missile body	32
CHAPTER 4. Flight trajectory	33
4.1. Hypersonic missile trajectory overview	33
4.2. Trajectory optimization methods	34
4.3. Proposed trajectory	35
4.4. Navigation and guidance	36
CHAPTER 5. Warhead	39
5.1. Introduction to warheads	39
5.2. Warhead design	39
5.3. Penetrator design	41
CHAPTER 6. Genetic algorithms and Monte Carlo simulation	43
6.1. Missile design as an iterative process	43
6.2. Genetic algorithms	43
6.2.1. Crossover and Mutation	44
6.3. Monte Carlo simulation	44
6.4. Structure of the problem	44
CHAPTER 7. Results	51
7.1. Warhead	51
7.2. Aerodynamics	52
7.3. Booster	56
7.4. Scramjet	57
7.5. Trajectory	59
7.6. General aspects	61
Conclusions	63

Bibliography	65
APPENDIX A. Atmosphere model	71
APPENDIX B. Aerodynamic design equations	73
APPENDIX C. Stability, Maneuverability and control	85
APPENDIX D. Solid booster design equations	89
APPENDIX E. Scramjet design equations	95
APPENDIX F. Trajectory design equations	101
APPENDIX G. Warhead and Penetrator design equations	105

LIST OF FIGURES

1	Typical missile subsystems distribution. Figure extracted from [49]	2
2	Hypersonic missiles from the USA and Russia	3
3	Surface to Air missiles from the Aegis Combat System	5
4	First set of missile correlations	7
5	Second set of missile correlations	8
1.1	Dissociation of N_2 and O_2 molecules as a function of velocity and altitude for different aircrafts. Figure extracted from [32]	10
1.2	L/D ratio as a function of volume parameter for different body shapes. Figure extracted from [7]	13
1.3	Body differentials of elliptical cross-section	14
1.4	2D nose cone with splitted fluid domain to apply an overset meshing	17
1.5	Mesh sizing on the nose cone and intake	17
2.1	Types of missile-booster integration. Figure extracted from [4]	19
2.2	Grain port geometries and the corresponding thrust as a function of time. Figure extracted from [39]	20
2.3	Cross-section shape and parameters. Figures extracted from [39]	21
2.4	Analysis of the burnback scenario. Figures extracted from [39]	21
2.5	Scramjet stages and thermodynamic cycle. Figures extracted from [40]	24
2.6	Compression efficiency as a function of number of shocks n and temeprature ratio Ψ . Figure extracted from [40]	24
2.7	Types of scramjet and ramjet intakes. Figure extracted from [4]	25
2.8	advantages and drawbacks of each type of intake. Figure extracted from [4]	26
2.9	Mixed compression inlet. Figure extracted from [40]	27
2.10	Characteristic lines and the corresponding notation	29
3.1	Force diagram of our designed missile with the booster	31
3.2	Force diagram of our designed missile	32
4.1	Trajectories for different hypersonic vehicles. Figure extracted from [51]	34
4.2	Proposed trajectory for the hypersonic airbreathing cruise missile	36
5.1	Blast pressure at miss distance as a function of time. Figure extracted from [54]	40
6.1	Crossover method for rocket booster and scramjet analysis	44
6.2	Flow chart diagram of the design process	46
7.1	Nose and Scramjet inlet at $M = 7.35$ and $\alpha = 0^\circ$	54
7.2	Nose and Scramjet inlet at $M = 7.35$ and $\alpha = 6^\circ$	54
7.3	Nose and Scramjet inlet at $M = 7.35$ and $\alpha = 12^\circ$	55
7.4	Nose and Scramjet inlet at $M = 7.35$ and $\alpha = 20.5^\circ$	55
7.5	Propellant grain cartridge in different views	56
7.6	Missile booster technical data plots	57

7.7 Characteristics method for Scramjet Nozzle	59
7.8 Take-off phase trajectory plots	60
7.9 Gliding phase trajectory plots	61
7.10 Final missile model with the booster in different views	62

LIST OF TABLES

2.1	List of Solid Rocket Propellants and their properties. See reference [44] for more information about the propellant names	22
2.2	List of Scramjet Hydrocarbon fuels and their properties	28
5.1	List of High Explosives Charges and their properties	41
6.1	List of constraints applied in the random individual creation of the warhead	47
6.2	List of constraints applied in the random individual creation of the body aerodynamics	48
6.3	List of constraints applied in the random individual creation of the propellant grain	48
6.4	List of constraints applied in the random individual creation of the scramjet engine	49
6.5	List of constraints applied in the random individual creation of the constant climb angle phase	49
7.1	Final Warhead dimensions and performance	51
7.2	Final Missile aerodynamics and missile flight performance	53
7.3	Final propellant grain dimensions and rocket performance	56
7.4	Final Scramjet dimensions and performance on cruise conditions	58
7.5	Parameters of the missile flying at a constant pitch angle	60
7.6	Technical data of the hypersonic missile	62

INTRODUCTION

Cruise missile fundamentals

The primary mission of any cruise missile consists in the delivery of a lethal payload (usually known as warhead) accurately to a distant target, trying to avoid the enemy defences. Basically cruise missiles were designed to improve the old and well-known ballistic missiles as SAM sites were improving their capacity to defeat ballistic threats. With the new emerging cruise missile technology, some nations could strike targets thousands kilometres away by flying at lower altitudes, remaining inside the Earth's atmosphere along their trajectory. Obviously, it had its drawbacks since those cruise missiles flew in a subsonic regime, compared to the high hypersonic regimes of ballistic missiles when entering again into the Earth's atmosphere.

Despite their lower speed they were smaller than ballistic missiles, making them easier to deploy in a variety of launch platforms from air, ground, sea and submarine. On the ground, cruise missiles are launched from road-mobile systems or fixed platforms. On the sea, they can be launched from ships and submarines, and the last are capable of launching them while submerged from Vertical launch systems or torpedo tubes. Cruise missiles can be classified according to their type of target: Land attack missiles (LACM) and Anti-ship missiles (AShM).

LACM permit striking land-based heavily defended targets thousands of kilometres away. USA and Russia are leaders on this category, followed by some European countries and developed countries in Asia. The most famous LACM is the Tomahawk missile. AShM are designed to sink war ships, differing from LACM in their guidance systems and warheads. The Soviets were the first on developing those type of missiles, most of them supersonic. The initial and the most widespread method of propulsion are the jet engines (turbofan and turbojet). The less common methods are ramjet propulsion and the scramjet for hypersonic missiles, but the main disadvantages of those methods of propulsion are the initial boost phase to produce thrust, although they have greater specific impulses than conventional rocket engines.

The flight trajectory of a subsonic or supersonic cruise missile remains few meters above the ground, using sea-skimming or TERCOM guidance techniques. The main advantage of this trajectory it's the capacity to avoid any ground radar detection. Other missiles (especially supersonic and hypersonic), fly a higher altitudes to be more fuel efficient and thus, increasing their range to finally dive to their target at their terminal phase. Radar sensor can detect them easily, so they must trust on their high speed and manoeuvrability to increase survivability when penetrating enemy defences. Obviously, cruise missiles can mix the different available trajectories to benefit from their positive properties.

Cruise missiles can use a huge variety of guidance systems, like inertial guidance, TERCOM (Terrain contour matching), GNSS for the initial and cruise phase of the flight. At the terminal phase (or end-game) they rely on more accurate systems like lasers, TV guidance, active and passive RF seekers, and IR seekers. Another important system is the DSMAC (Digital Scene Matching Area Correlation), which is a more "automated" version of the TV guidance.

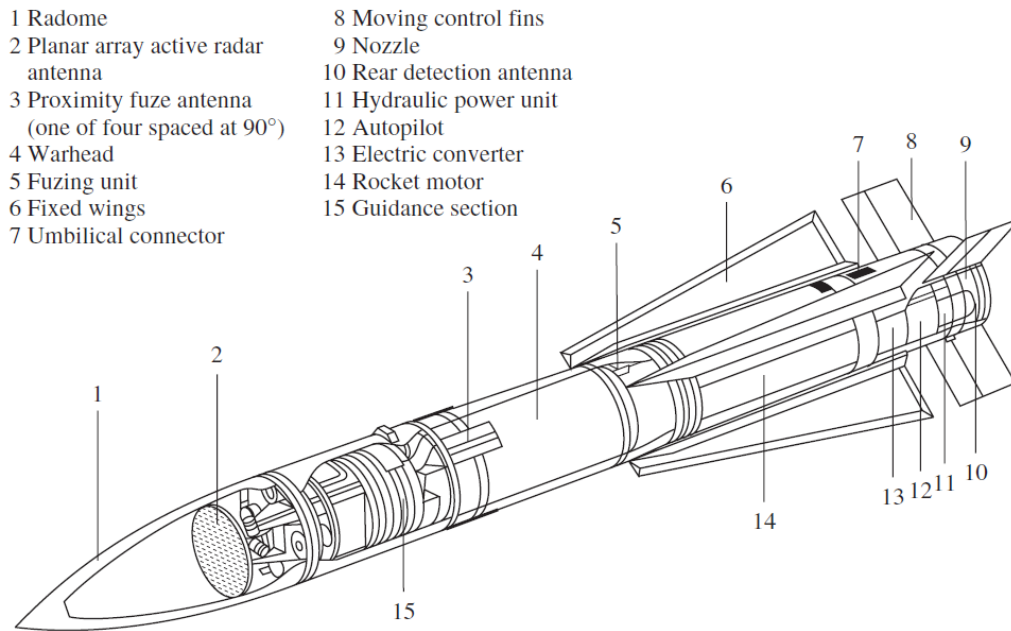


Figure 1: Typical missile subsystems distribution. Figure extracted from [49]

The race for hypersonics

Hypersonic vehicles are those which fly between Mach 5 and Mach 25. When talking about missiles, they fall in two categories: Hypersonic cruise missiles and Hypersonic boost glide vehicles. The reason why some nations are starting a new hypersonic arms race is because this new weapon system is capable of rapid delivery of warheads, providing the enemy a minimum reaction time. The main thread involving this new weapons systems are their capability to deploy nuclear warheads, which could risk the escalation of conflict between countries.

Hypersonic vehicles have been in development since 1950's, but only after 1998 when a US Tomahawk subsonic cruise missile failed to reach a time critical target in Afghanistan, the government concerned about the usefulness of this weapon system. Previously, we talked about how the cruise missiles improved some vulnerabilities of classical ballistic missiles, although in the vast majority of cases they fly at subsonic speeds (or supersonic in some cases). Hypersonic cruise missiles want to solve the problem of speed of actual cruise missile, increasing it above Mach 5, while having high manoeuvrability during the entire flight making the trajectory unpredictable and thus, more difficult to track. This new type of technology offers an opportunity to respond to many type of threats, including time-critical, hardened, buried and heavily defended targets. They will have the capacity to strike targets from any direction, a fact that improves lethality in front of ballistic missiles.

This new type of weapons represents a new challenge for the aerospace industry, since new materials to enhance aerothermal survivability and new methods of propulsion must be tested. The engine that has been proven to withstand those requirements is the Scramjet, a type of air-breathing engine where the combustion occurs at supersonic speeds. This propulsion system promises to be lighter, and thus easier to carry heavy warheads at greater ranges. As far as we know, some boosters are required to accelerate the scramjet

to supersonic/hypersonic speeds which can be tandem or side-mounted boosters, always depending on the launching platform.

Some fuels are under study, but hydrogen and hydrocarbons are the perfect candidates. Although hydrogen is easily flammable and then less energy is required to ignite and mix it, it has the lowest density compared to hydrocarbons, making the storage more complicated. Hydrocarbons are more dense and easy storable fuels, enabling missiles flying longer ranges with the same amount of fuel in the tank with increased safety.

To make this weapon affordable to many nations, engineers must study affordable methods of production. The nations that are leading the development of this type of weapon are USA, Russia and China (see reference [1]). USA is working on the Advanced Hypersonic Weapon (AHW), which is a boost-glide weapon with long range capability. Moreover, Lockheed Martin is developing the Falcon Hypersonic Technology, another boost-glide vehicle that reaches speeds of Mach 20 with high manoeuvrability to avoid enemy defences.

China has been developing since early 2014, the two brands of hypersonic weapons including the hypersonic glide vehicles (HGV) and the hypersonic cruise missiles. The DF-ZF is a HGV that reaches a maximum speed of Mach 10 during the glide phase and which can carry nuclear or conventional warheads. The DF-ZF is mounted on the top of a ballistic missile, evading defences when gliding.

Russia is the country that has advantage on this field. Since 2012, when they were concerned about the threat that US X-51 Waverider could suppose to the country, Russia has encouraged itself to invest in hypersonic weapons. Their HGV names as Avangard has been tested multiple times, reaching speeds up to Mach 20 with the ability to perform evasive manoeuvres. Apart from this, Russia is developing with India an evolution of the supersonic cruise BrahMos, the BrahMos-II, an air-breathing cruise missile which can reach speeds of Mach 7. Another missile that has been tested successfully in 2017 is the 3M22 Zircon, an anti-ship cruise missile capable of reaching speeds up to Mach 8 and with a theoretical range between 500 km and 750 km, although some experts extends the range to 1000 km. Finally, the KH-47M2 Kinzhal is a modification of the Surface-to-Surface Iskander missile but it is launch from an aircraft and reaching speeds of Mach 10.



(a) AHW developed by DARPA



(b) MiG 31 carrying a Kinzhal missile

Figure 2: Hypersonic missiles from the USA and Russia

Defense against hypersonic missiles

To defeat hypersonic weapons, there must be a perfect integration of aerospace defence systems comprising air and missile defence systems, missile early warning attack and space controls. Some weapons like the directed energy weapons are one of the best options, but they are still on their infancy. Those type of weapons would be used especially for HGV in their initial boost phase. Other options include jamming or the use of rail guns when the warheads enter to the lower layers of the atmosphere. The systems mentioned above are only ideas proposed by the US Missile Defence Agency, but nowadays there are any system capable of defending against hypersonic weapons.

Actually, the best option to defeat a hypersonic weapon seems to be destroying it while still attached to the aircrafts, submarines, boats or Transporter Erector Launchers (TELs). Hence, to defeat hypersonic weapons, adopting an offensive strategy can ensure good defence. But as always, the best defence against this new type of weapons consists to apply non-proliferation measures in order to prevent the spread of this technology.

Defense systems

The reason why hypersonic missiles can suppose a serious threat to modern ships are because of high speed can penetrate de multi-layered defences where ships rely on. Those multi-layered systems consists on radars to detect and track, and Surface to Air missiles (SAM) which destroys the upcoming threats. In addition, those systems were designed in the past to defeat ballistic missiles, easy to track due to their non-changing suborbital trajectory.

One of those defenses is the Aegis Combat System designed by the US to defeat against aircraft and ballistic missiles. This system contains a AN/SPY-1 S-band passive electronically scanned array radar, a MK 99 Fire Control System, a WCS (Weapon Control System) to track and destroy targets, a Command and Decision Suite and finally the SM-2 Standard Missile family (RIM-66, RIM-67) for aircrafts and cruise missiles, and SM-3 (RIM-161, RIM-174) for ballistic threats. Both missile families communicates with the radar, receiving updates on target position and performing changes on its course (semi-active radar homing).



(a) RIM-67 Standard Missile



(b) RIM-161 Standard Missile 3 launched from a Mk-41 VLS

Figure 3: Surface to Air missiles from the Aegis Combat System

Background on missile design

Before starting our project, it is quite useful to have some feedback on other projects and research regarding to missile design. However, not only research about missiles will be considered but also hypersonic vehicles for transport or SSTO applications.

Ender, et al. [9] studied the conceptual hypersonic missile sizing by using different disciplinary analysis platforms (commercially available codes and MATLAB codes). In those codes they tested inlet and propulsion performance, geometry, aerodynamics, structural analysis, stability analysis, trajectory and sizing. Some of those commercial codes are fast prediction tools that can help engineers to develop new concepts in a much simpler way (like DATCOM software). DATCOM is a Fortran 90 semi-empirical software based on component build up method, used for the preliminary design and analysis of missile aerodynamics and performance. This type of method analyses each component of the missile separately, and finally computes the interferences between them (interference factors). This software is only supplied by the United States Air Force to American defence contractors, so we are not allowed to use it. Other software for preliminary design aerodynamic prediction includes MISL3, SUPL and AP09.

Demiral [11] studied the aerodynamics of a ramjet missile by employing fast prediction

tools (DATCOM) to calculate aerodynamic coefficients and validating them through a more accurate analysis using CFD (Fluent). Other objective of his thesis consists on designing a ramjet with meta-heuristic optimization algorithms under the restriction of some geometrical constraints and aerodynamic performance requirements, and determine which of those algorithms gives better results.

Regarding to CFD, most researchers that will be mentioned in this project are more likely to use ANSYS Fluent, however there exists other CFD more suitable to missile design (and other military and aerospace applications) like the CFD-FASTRAN, which is famous and well-known for its user-friendly usage and the speed of processing. This CFD software uses density based compressible Euler and Navier-Stokes solver with moving multi-body dynamics, generalized finite rate chemistry and thermal non-equilibrium modules.

Anderson [12] bases his research on a genetic algorithm consisting in a total of 29 variables from solid rocket design code, aerodynamic design code and a three-loop autopilot optimized for defeating ICBM and high manoeuvrable targets. In this case, the main goals of the genetic algorithm are minimizing intercept time and miss distance.

Redmon [13] performs the most complex design compared to the previous ones as it takes into account more parameters, and moreover, he only uses analytical equations in each phase of the design. However in his thesis he doesn't consider genetic algorithms to find the optimal solution which gives the best performance.

Not only the aerodynamics and engine performance but also the trajectory optimization should be considered to maximize range amongst others. In most cases trajectory design of a hypersonic vehicle has a maximum heat transfer constraint where descent velocity and flight profile plays an important role. Ul Islam Rizvi, S. T., et al. [48] studied in their paper the variation of the optimal burnout angle at the end of the ascent phase carried by the solid booster, and the optimal control deflection during the glide phase. This deflection would maximize the downrange performance of a hypersonic boost-glide waverider with a variation in heat rate.

With the previous thesis in mind we have a baseline to design our missile and which methods are the most practical and accurate. MATLAB with genetic algorithms and CFD to validate our results are the best candidates to start the conceptual designing process. Notice that all the equations will be listed on annexes, each of them containing the most important subsystems of the missile.

Establishing a baseline

Although no much data on hypersonic missiles is available, we must feed our algorithms with other Anti-Ship missiles data to get better configurations, and the best option is with supersonic missiles (see reference [14]).

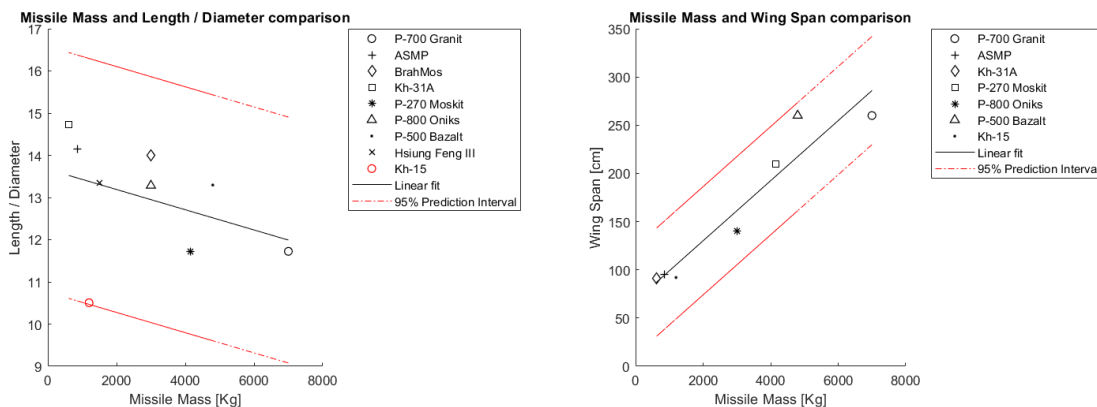
In this case, all the data of different parameters concerning a missile (weight, speed, range, wing span, warhead weight, length to diameter ratio, etc.) has been plotted and estimation is done by plotting a least squares regression line. However, the different data points of the missile are not close enough to the regression line, meaning that a standard error of the regression must be studied. This standard error measures the distance from the real values to the predicted ones, and the space between them is the margin where we

are going to set our constants to be evaluated both in genetic algorithm and Montecarlo simulation.

The missiles analysed in this project are the ASMP, BrahMos, BrahMos II, CVS401 Perseus, Hsiung Feng III, Kh-15, Kh-31A, P-270 Moskit, P-500 Bazalt, P-700 Granit, P-800 Oniks, P-900 Alfa, X-51 Waverider and the 3M22 Zircon.

The data of those missiles must be correlated in a logical way, for example, studying the relationship between missile weights and their length over diameter ratio. Other correlations between the warhead weight and the length over diameter ratio can be quite useful to study but for a conceptual design point of view doesn't make any sense. On the other way, we must define initial requirements of the missile, and for this case a cruise speed corresponding to a dynamic pressure of 48 KPa and a missile mass of 1800 Kg are the best options.

In figures 4(a) and 4(b) there are different correlations concerning the missile mass with the length/diameter ratio and the wingspan. The first one is important specially when a missile doesn't have restrictions of width. In our case, the VLS has a length/diameter about 10.6, which is in the frontier of the lower limit of the prediction interval. The Kh-15 is an aero-ballistic hypersonic missile having a similar length/diameter ratio. Regarding to the wingspan, in a Mk-41 VLS the restriction is stronger than for an air-launched missile since the width of the cannister is smaller compared with the P-500 cannisters. Despite the control surfaces are folded, a drastic reduction of the span is required.

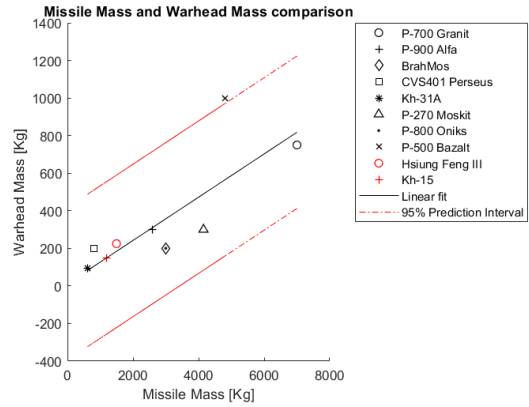
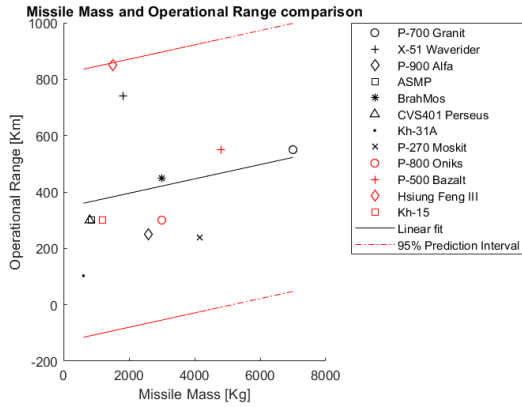


(a) Missile Mass and Length / Diameter comparison

(b) Missile Mass and Wing Span comparison

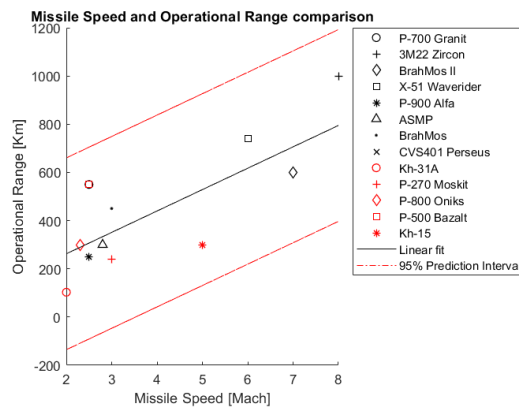
Figure 4: First set of missile correlations

Another considerations to be studied are the range, the speed and the warhead mass of the missile (see figures 5(a), 5(b) and 5(c)). Operational range helps us to understand how much fuel must carry the missile, while warhead mass gives us an estimate of the mass fraction required for the explosive. Speed and range correlation can be used to evaluate the efficiency of our propulsion system and drag.



(a) Missile Mass and Operational Range comparison

(b) Missile Mass and Warhead Mass comparison



(c) Missile Speed and Operational Range comparison

Figure 5: Second set of missile correlations

CHAPTER 1. AERODYNAMICS

1.1. Fundamentals of hypersonic aerodynamics

When starting the conceptual design phase, and thus aerodynamics, it is always important to have an idea of which calculation methods one should apply according to the missile flight speed. Accurate methods need to be applied to calculate precisely the range, manoeuvrability, miss distance and stability. Other aspects such as aeroheating allows to choose the correct materials to withstand the structural and heat loads, especially on the nose and the leading edge.

Those computations must be easy enough to set up in a computer, especially when multiple configurations and trade studies involving the engine type and performance, warheads, aerodynamics and trajectory requirements are going to be performed. Since in our study we are not provided with a hypersonic wind tunnel or specialized software for missile aerodynamic analysis or super computers to perform numerical simulations (Finite Element Methods) in detail, analytical equations are our best solution referring to their ease to use, robustness computationally affordable (some of those calculations could take weeks or even months, being so expensive). Concerning the detailed phase of the missile where the accuracy is the most important requirement, ANSYS Fluent will be the key of the analysis.

But going back to the analytical methods, aerodynamic researchers from Agard [17] have dealt with the solution, providing us a manual where analytical tools (amongst others) are applied according the flight regime of the missile (hypersonic in our case). According to this manual, we have to use the following methods (or similar) to calculate lift and drag in hypersonic regime for the body:

- Nose wave drag: SOSET (Second-Order-Shock-Expansion Theory) plus IMNT (Improved Modified Newtonian Theory) Modified for Real Gases.
- Boattail or Flare Wave Drag: SOSET for Real Gases.
- Skin Friction Drag: Van Driest Method (II).
- Base Drag: Improved Empirical Method.
- Aeroheating Information: SOSET plus IMNT for Real Gases.
- Inviscid Lift and Pitching Moment: SOSET for Real Gases.
- Viscous Lift and Pitch Moment: Improved Allen Perkins Crossflow. Then, for the wing alone and interference aerodynamics (body plus wing), they recommend us to apply the following methods:
- Wave drag: SE (Shock Expansion) plus MNT (Modified Newtonian Theory) for Real Gases along Strips.
- Skin Friction Drag: Van Driest II.
- Trailing Edge Separation Drag: Empirical.

- Body Base Pressure Caused by Tail Fins: Improved Empirical.
- Inviscid Lift and Pitching Moment (Linear/Nonlinear): 3DTWT or SE Empirical.
- Wing-Body, Body-Wing Interference (Linear/Nonlinear): Slender-Body Theory or Linear Theory Modified for Short Afterbodies, Empirical.
- Wing-Body Interference due to δ (Linear/Nonlinear): Slender-Body Theory, Empirical.
- Wing Tail Interference: Line Vortex Theory with Empirical Modifications for $k_w(B)$ Term and Nonlinearities.
- Aeroheating: SE plus MNT for Real Gases.

Some of the previous methods mentioned before, have good performance only when analysing the 3D model, like shock expansion theory. Since we want to take advantage of an axisymmetric design, those methods for 3D analysis will be ignored until our CAD design can be implemented in a CFD software.

Research from Moore, et al. [18] is useful for calculating the previous parameters, since they perform a deep study in the mathematics and physical relations of Newtonian theories and Shock expansion methods applied for real gases (see eqs. (B.1) to (B.7)). At this point, the reader may ask himself what real gas effects are and why we should be aware of them.

Assuming perfect gas flying at speeds above Mach 6, the temperature behind the shock wave will be higher for a perfect gas than for a real gas. The physical phenomenon behind this occurs when the air is heated above 2000K, the molecules of N_2 and O_2 begin to dissociate and chemically react and forming other species. This transfer of energy to vibration and the dissociation process that accounts for the fact that the temperature is much lower for a real gas than for a perfect gas at high Mach numbers. In other words, other types of energy apart from heat are involved in the process.

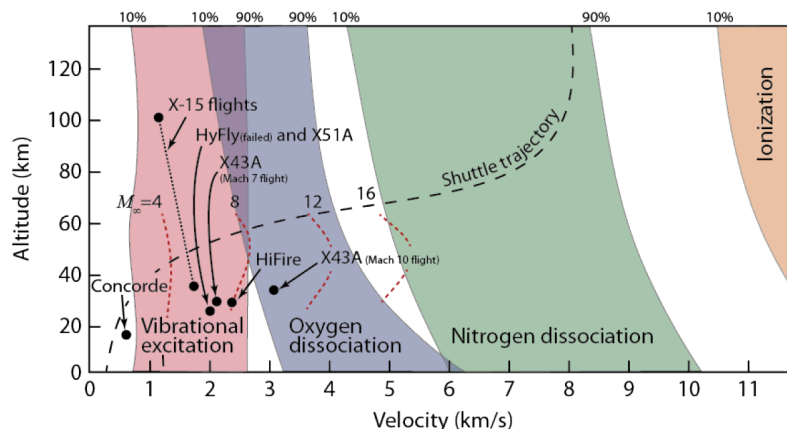


Figure 1.1: Dissociation of N_2 and O_2 molecules as a function of velocity and altitude for different aircraft. Figure extracted from [32]

Another important fact is pressure, which is also affected but at much less extent than temperature. That is the reason why aerodynamic forces and moments can still be computed assuming perfect gas with reasonable results.

1.1.1. Newtonian flow theory

When referring to hypersonic flow, it is strictly a non-linear flow. Complex phenomena such as high-temperature chemically reacting flows, viscous interaction, entropy layers, etc, makes impossible the possibility to be described by simple linear relationships. One of the most important equations to describe the pressure coefficient as a function of local deflection angle θ , can be found on [19]. However, this equation is not valid for hypersonic flow.

The simplicity of this equation, makes aerodynamicists think about if it is possible to apply a similar equation to rapidly estimate the pressure coefficient in terms of local surface inclination angle. Newtonian theory was initially really inaccurate with low speed flows (subsonic), but only with the advent of modern hypersonic aerodynamics it became a useful theory. There are two other primary methods to calculate the surface pressure in a hypersonic flow, called the tangent-wedge / tangent-cone method and the shock-expansion methods. Those methods are slightly more elaborated than Newtonian theory and provide better accuracy. However we are going to focus on Newtonian flow, since it is the basis of the others.

According to Isaac Newton, when a stream of particles following a rectilinear direction strike over a surface, they lose all their momentum normal to the surface, but moving tangentially to the surface without loss of tangential momentum. This phenomena is called the famous Newtonian sine-squared law for pressure coefficient. (see eq. (B.8))

Another important fact of the Newtonian flow is that the particles in the free stream impacting on the frontal area cannot curl around the body and impact on the back surface. In this area the total pressure coefficient will be 0.

Notice that the classical Newtonian flow theory is Mach number independent since it considers that Mach number is infinite over the surface. The Modified Newton Law proposed by Lester Lees solves this problem, by calculating the pressure coefficient as a function of the maximum pressure coefficient evaluated at the stagnation point behind the shock wave. The resulting equation equals the Newtonian law when Mach number is infinite and γ (heat ratio) equals 1. This theory is more accurate, especially when calculating the pressure distributions over blunt-nosed bodies. (see eqs. (B.9) to (B.11))

When considering the centrifugal force effects over curved surfaces in hypersonic flow, this theory is often called as Newtonian-Busemann theory. However, the results obtained with this theory are neither qualitatively nor quantitatively correct being in many cases worse than the Straight Newtonian approach (for example when calculating biconvex airfoils). (see eq. (B.12))

The final aspects to remark about the Newtonian theory are that the final result improves as the freestream Mach number increases. Secondly, Newtonian theory is usually more accurate for three-dimensional bodies than for two-dimensional bodies. The problem of less accuracy in low hypersonic regime can be a serious problem when studying the aerodynamics of the cruise missile.

1.1.2. Shock expansion theory

Shock expansion theory computes the flow parameters at the leading edge of a two-dimensional surface with the oblique shock wave relations and with the solution for a cone at the tip of a three-dimensional body. Later, Prandtl-Meyer expansion is applied through the surface behind the leading edge or tip and finally, all the pressure distribution along the body surface. The main idea is to divide the surface in many points as possible to get more accurate pressure distribution. The Second-order Shock-expansion Theory is a theory proposed by Syvertson applicable on pointed bodies with sharp airfoils. The theory has proven to give good results from low to moderate angles of attack and speeds above Mach 2.

1.1.3. Van Driest method (II)

Van Driest Method (II) is used to calculate skin friction drag, and it is obtained by differentiating the Kármán-Schoenherr equation respect to the length of the Reynolds number [20]. This method is applicable where the flow on the lifting surfaces is turbulent, two dimensional and the viscous region is located near the surface (boundary layer) (see eqs. (B.16) to (B.32)).

1.2. Nose cone aerodynamics

Nose cones or ogives must be designed to decrease the amount of drag and heating, while considering other important factors not accounted in the present work, such as structural integrity and signal transmission of the seeker. Pressure wave drag is higher than skin friction at supersonic speeds, meaning that it must be optimized to decrease the amount of drag to maximize range.

Nose cones are classified according to their shape, most common of which are conical, ogival and power-series. A trade-off analysis must be studied to determine which gives the better performance given specific flight conditions. Fortunately, those conical and ogival shapes were studied in the past and they have different performance according to the flight speed. In hypersonic regime, the best nose cones and ogives in terms of performance are Von Kármán (based on Haack series), 3/4 power series and 0.6 power series (see eqs. (B.13) to (B.15)).

To study the flow over a cone at hypersonic speeds, different analytical methods have been studied (see references [21], [22] and [23]) and some tested in wind tunnel, however the shape of our missile is more complex to study since it must house the different compression ramps for the scramjet, leave enough volume for the seeker and provide lift. The resulting cone shape has an elliptical cross section with a decreasing eccentricity as the distance from the nose start decreases. Different researchers like Ming Lee, et al. in [24] studied flow characteristics over elliptical cross section forebodies, but after a long literature review and for an efficient calculation, we have based the nose design on the research of H. Jorgensen (see references [25] and [26]).

1.3. Missile body aerodynamics

The main function of the missile body housing of the seeker, flight computer, warhead, fuel and engines. The final objective of the body is to provide the highest L/D ratio, while fitting properly in the VLS launcher.

One of the most important parameters when designing the body of the missile is the non-dimensional volume parameter $\frac{V^{2/3}}{S}$ [7]. High lifting bodies become progressively more wing-like and the L/D increases continuously as the volume parameter decreases. This is an important statement since less volume implies less fuel, less range and less warhead weight while a high L/D ratio can increase range according to the Breguet equation. This is one of the most important trade-off analysis we must face off in the design of the missile system.

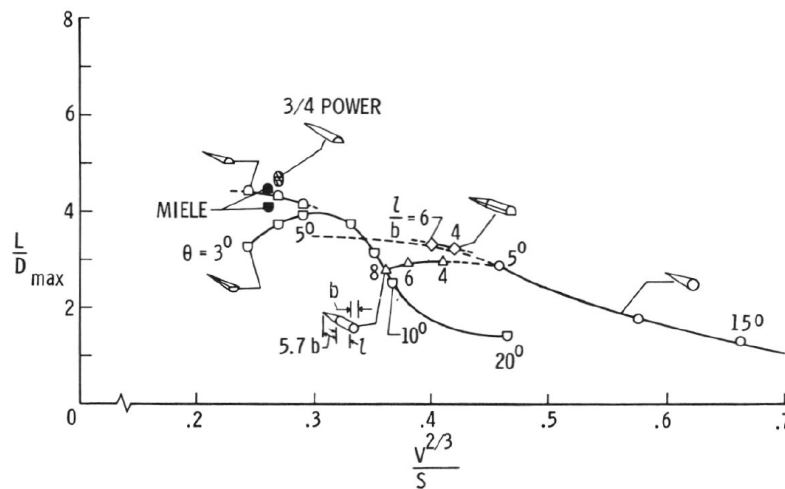


Figure 1.2: L/D ratio as a function of volume parameter for different body shapes. Figure extracted from [7]

To calculate the aerodynamic coefficients of a non-axisymmetric body (alone and with lifting surfaces), H. Jorgensen [26] has developed engineering-type methods based on Slender body theory and Newtonian theory for bodies with elliptical cross-section at high angles of attack (from 0° to 90°). Those coefficients are the normal-force coefficient, axial-force coefficient and pitching moment coefficient. Those methods are very powerful since they may be applicable for use at subsonic, supersonic and low hypersonic Mach numbers. In eqs. (B.33) to (B.43) the mathematical analysis of this method is explained in detail. The method is applied by splitting all the missile airframe in many differentials of elliptical cross-section (see figure 1.3).

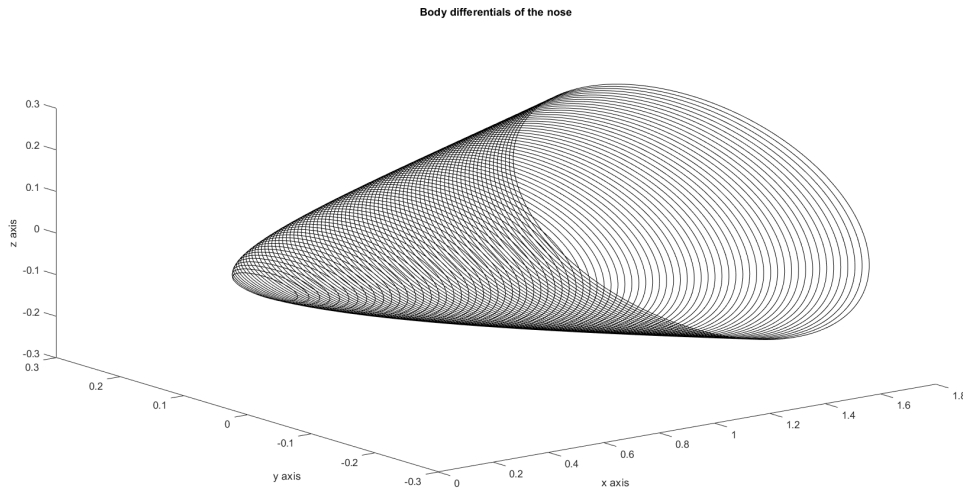


Figure 1.3: Body differentials of elliptical cross-section

1.4. Tail aerodynamics

The most common control type in airbreathing hypersonic / supersonic cruise missiles is tail control. This type of control has a large pitching moment and has a low level of hinge moment only when the tail has no adverse downwash due to the movement of forward surfaces. We must consider those facts since the tail control of the booster

Airfoil aerodynamics are strong dependent on the the airfoil geometric shape (chord and thickness) (see eqs. (B.44) to (B.49)), and the airspeed around them. When designing a tail fin flying at hypersonic speeds, heat is one of the most important constraints. Other important aspects related to airfoil selection is the structural efficiency and manufacturing costs, always taking into account the aerodynamic efficiency of the airfoil.

The typical supersonic airfoils are the double wedge, the modified double wedge, biconvex and blunt trailing edge. The benefits of using blunt trailing edge over the other airfoils are drag reduction, increase in lift curve slope and an increase in L/D ratios. In addition, this type of airfoil has a low tendency of flow separation on the afterward section (less difference in base pressure).

Schwarz [31] thesis studies the heat effects on a Wing/Fin root heating at Mach 8 speed, and also demonstrates the effectiveness and limitations of the Van Driest solution for laminar and turbulent flow on a flat plate. Since this experiment is performed by analysing flight conditions similar to ours, it will be an important reference to compare results and prove that we are dealing with reasonable solutions.

We based our airfoil conceptual design on W. Cleary et al. [27] research, where they study the aerodynamics of sharp and circularly blunt-wedge airfoils (see eqs. (B.50) to (B.60)). As we said before, heating on the leading edge play an important role while designing, since less radius means more heat. However, large leading edge radius may introduce three effects: A negative lift contribution of the leading edge, induced effects of bluntness on the flat surfaces of the airfoil, and the fact that modified Newtonian theory is a relative

poor estimate of the correct level of pressure coefficient on the flat windward surface. It is important to say that in order to simplify calculations, a constant leading edge radius and wedge angle that do not change with the chord has been studied.

1.5. Aerothermodynamics and materials selection

One of the most important challenges of this missile is the selection of materials to withstand the enormous heat when flying at high speeds on the atmosphere, transferring some of the kinetic energy to potential and internal energy of the gas due to vibration of molecules. To select properly those materials, is useful to simulate the amount of heat absorbed by the most heating-sensitive parts of the missile (nose and leading edges of the fins) (see eqs. (B.84) to (B.85)). More information about the structural design of a hypersonic vehicles and their cooling techniques are detailed on reference [28].

1.5.1. Airframe materials

In missiles flying above Mach 5.5 and without external insulation, the materials used are very expensive, such as titanium aluminide, single crystal nickel aluminides and ceramic matrix composites, being all of them a substitution of the classical nickel-based alloys for supersonic flight. To avoid the use of those materials and a hot structure, active cooling, thermal sink and external insulation should be considered, especially the external insulation which is the best approach for short-duration and one-way missions.

1.5.2. Insulation materials

The insulation can be internal, one-piece self-insulating composite structure and external insulation. For short duration flight at hypersonic speeds, the option of external insulation over a cold metal airframe with internal insulation has the lowest weight. The objective of external insulation is to protect the airframe from extreme heating while the internal insulation protects missile subsystems.

The design and selection of an insulation material include thermal conductivity, maximum Mach number, maximum temperature, tensile strength, maximum strain, density outgassing (loss of weight) and cost. For propulsion systems, the most used are medium density phenolic composites (nylon phenolic, silica phenolic, glass phenolic, carbon phenolic, graphite phenolic) and low density composites (micro-quartz paint, glass-cork-epoxy, carbon-silicone rubber).

Phenolics have good resistance to erosion, allow temperatures of almost 2500°C and maintain the aerodynamic shape since they only char at good temperatures, losing about 20% of their weight. On the other hand, low density composites are used for temperatures up to 1600°C and lose between the 30 and 60% of their weight in charring. For hypersonic missiles, the best option are medium density phenolic composites for their high temperature, while development on new high density insulation materials are still on development, and will help to improve the amount of fuel of the missile and the maximum range.

1.5.3. Seeker dome

A vast majority of missiles have a seeker on-board located at the nose, which can be Infrared (IR) and Radar frequency (RF). Anti-ship cruise missiles are more likely to use active RF seekers, and the seeker dome covering the RF seeker must have low dielectric constant, high transverse strength, low thermal expansion, high erosion resistance, and high temperature capability for short duration flight. The dome materials used for RF only seekers are quartz/fused silica, silicon nitride, diamond, pyroceram, polyimide and magnesium fluoride. For hypersonic missiles, the most popular and cost-effective domes are those made of silicon nitride. Diamond domes are slightly better, especially in max allowable temperature, but has higher cost.

The transmission efficiency of the radar signal is a function of the dome thickness, the wavelength of the radar, the dielectric constant and the incidence angle of the radar signal with the dome surface.

More information about the structural analysis and manufacturing of a silicon nitride radome can be found on reference [29]. Additional information on how silicon nitride radomes react in front of electromagnetic fields can be found reference [30].

1.5.4. Surface heating

The easier approximation to compute the heat on a stagnation point is given by Anderson, which tells to us that speed and leading edge radius play an important role on heating. However in reference [32] explains that the heat drops drastically after the leading edge eqs. (B.84) to (B.85). Moreover, in his thesis he also performs a deep study on the wall heat transfer and wall temperature effects which will be discussed here only in qualitative terms.

1.6. Computational fluid dynamics

Analytical calculations must be validated through a CFD simulation, and specially for the nose cone. Our reference in this case for studying hypersonic flow on a body is the thesis from Olliden [33], which is based on the study of a hypersonic flow field around a scramjet intake and over a cone-ogive with flare at speeds above Mach 7. Moreover, he explains in detail which turbulence models perform at their best depending on the analysis (in our case a 4 equation Transition SST model), and also he considers chemical reactions of the flow. The SST model gives accurate results at predicting the boundary layer transition from laminar to turbulent regime, one of the most crucial factors in hypersonic regime.

The size of the model is in scale 1:1 and thus, our contour volumes for the 2D nose cone have been divided in different parts in order to optimize the meshing process (see figure 1.4). First of all, the dimensions of this contour volume are a height of 4 m and a width of 5 m. The highest meshing density is located near the boundaries of the objects (wall of missile nose cone), and it decreases as the distance from the object increases. Specifically, the most detailed part has an element size of 0.004 m, while the frontal hemispherical area has an element size of 0.03 m and the upper areas an element size of 0.01 m (see figures 1.5(a) and 1.5(b)).

Appart from this, the simulation has been performed with different angles of attack (0, 6, 12 and 20.5) degrees, which will be explained later. (Notice that the ramps of the nose in the following figures are not designed until the Scramjet chapter.)

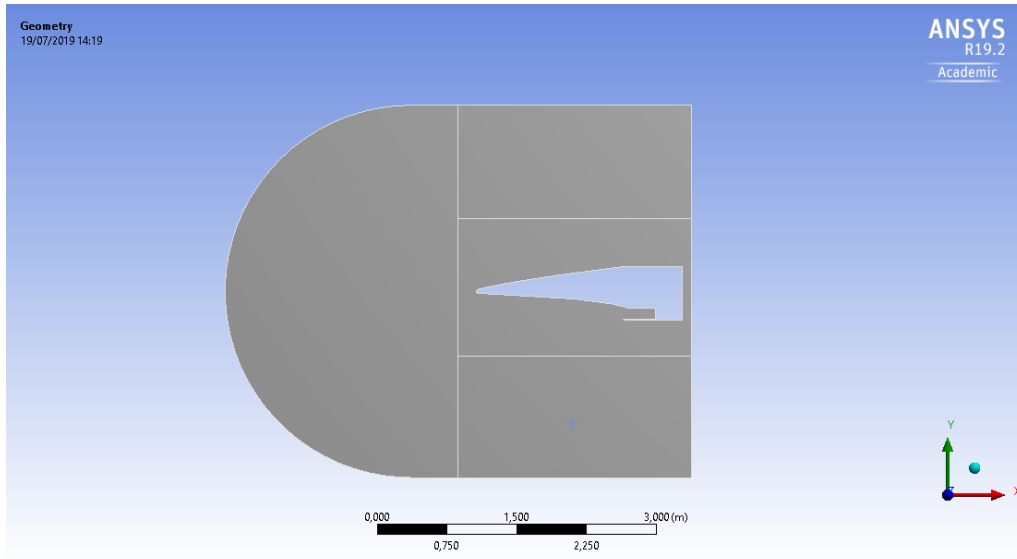
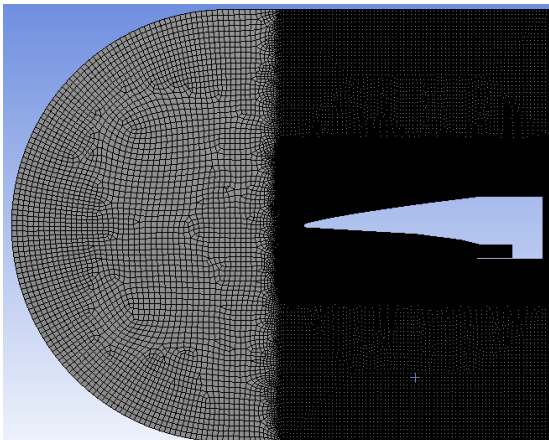
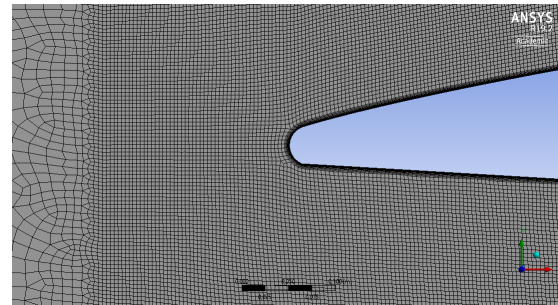


Figure 1.4: 2D nose cone with splitted fluid domain to apply an overset meshing

And then for the meshing:



(a) Meshing of the full nose cone and intake



(b) Zoom of the 10 inflation layers to study boundary layer effects

Figure 1.5: Mesh sizing on the nose cone and intake

CHAPTER 2. PROPULSION SYSTEM

In the initial chapters, when talking about cruise missiles and their features, some propulsion types were mentioned according to the missile flight speed. The most widespread engines were inside the category of reaction engines, including the turbofan and the turbojet, but also ramjet for supersonic cruise missiles was used and finally new methods of propulsion when reaching speeds beyond Mach 5.

2.1. Solid rocket booster

Ramjets cannot produce thrust until reaching high subsonic speed, while scramjets needs to fly at high supersonic speeds to work. One of the main problems about those engines requirements is the integration of the booster in the cruise missile, and always fulfilling the constraints of the launching system (weight, length, diameter, etc.). The governing physics of solid rocket motors are exactly the same than liquid rocket engines (see eqs. (D.1) to (D.14)), but the first provide high reliability, low weight and easy usage.

		Selection Factors								
		Length	Diameter	Weight	Ejectables	Cruise Drag	Carry Drag	Cost	Eng. - Booster Compatibility	Engine - Inlet Compatibility
Integral Rocket – Ramjet (IRR)		●	●	●	●	●	●	●	●	●
Aft Booster (Drop-off)		–	●	○	–	●	●	●	●	●
Forward Booster		–	●	○	●	●	○	○	○	○
Podded Booster (Drop-off)		●	–	○	–	●	○	●	●	●
Podded Ramjet		●	–	○	●	–	○	○	○	–
Podded IRR		●	–	●	●	–	○	○	○	–
Podded Ramjet Aft Booster (Drop-off)		○	–	–	–	–	●	○	○	–

● Superior ● Good ○ Average – Poor

Figure 2.1: Types of missile-booster integration. Figure extracted from [4]

The previous figure characterizes the different types of ramjet / scramjet engine integration with the booster. When low cruise drag is a priority as in a hypersonic cruise missile, the best options are the Integral Rocket – Ramjet (IRR) and the Aft Booster (Drop-off) configurations, however, the IRR is more suitable to ramjets than scramjets since the IRR uses the empty volume of the booster as the combustion chamber. When explaining the scramjets, we'll see how different is the combustion of a scramjet compared to a ramjet and the reason why the Drop-off configuration is better. The main disadvantages of this configuration is the long length, an important fact to consider when launching from Mk-41 VLS launcher with length constraints.

Some research has been made in the past on internal ballistics to provide guidelines for preliminary designs of rocket motors. Those guidelines are based on repetitive and estimated calculations that must be performed iteratively. Hartfield, et al. [43] derived different analytical methods for various grain ports using analytical methods, and according to their conclusions, such analytical methods are more efficient than grid-based techniques. Their research have become a basis for different researchers around the world to study in an

effective manner grain regression, pressure chamber and thrust.

In this project, our calculations are based on Tola's and Nikbay's [39] studies, which implement different analytical burnback solutions based on reference [43] in order to determine the total grain regression y and thus, the thrust and chamber pressure profiles. When calculating the total thrust which varies as a function of time, additional calculus is required, especially when the grain regression increases as rate of burn increases, due to the fact that port area is increasing.

There exists multiple grain configurations according to the desired thrust profile of a rocket or missile, or in other words, regressive, neutral and progressive thrust. Those thrust profiles allow a missile to climb at constant dynamic pressure, fast launch and sustain for cruising, etc. Since TWR tends to be very large, and hypersonic cruise missiles are designed to operate at high altitudes with low density, neutral thrust is the most suitable option for a constant dynamic pressure ascent of 96 kPa, the maximum recommended for scramjet engines structures, according to reference [40]. The most common configurations are the Star, Wagon wheel, Multiperforated, Dog bone and Dendrite, being the Star the easiest one to study for its regular shape.

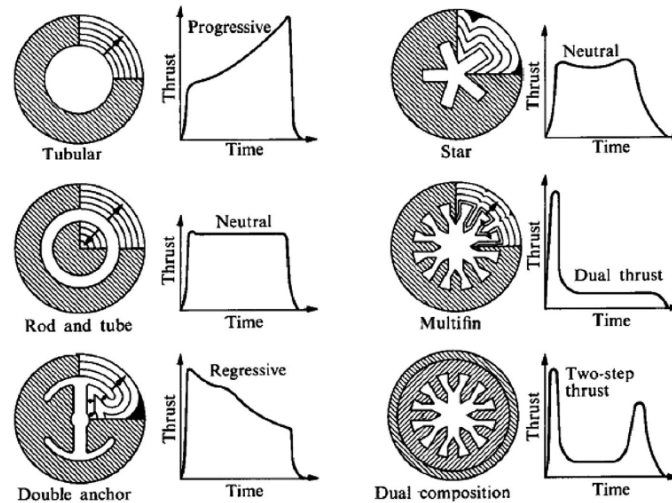


Figure 2.2: Grain port geometries and the corresponding thrust as a function of time. Figure extracted from [39]

In this project, complex phenomenon such as erosive burning due to high speed of the flow and grain stress and surface cracks have been ignored for simplicity, and due to the fact that length/diameter ratio of the propellant grain is below 5.

2.1.1. Star grain configuration

As we said before, solid rocket motor thrust change over time as a function of the port geometry, which must be studied carefully to design a missile using the applied science of internal ballistics. The first parameters that are going to be defined to run calculations are the outer radius of the propellant R_o , the inner radius of the propellant R_i , the slot length R_p , the slot tip radius f and the number of slots N .

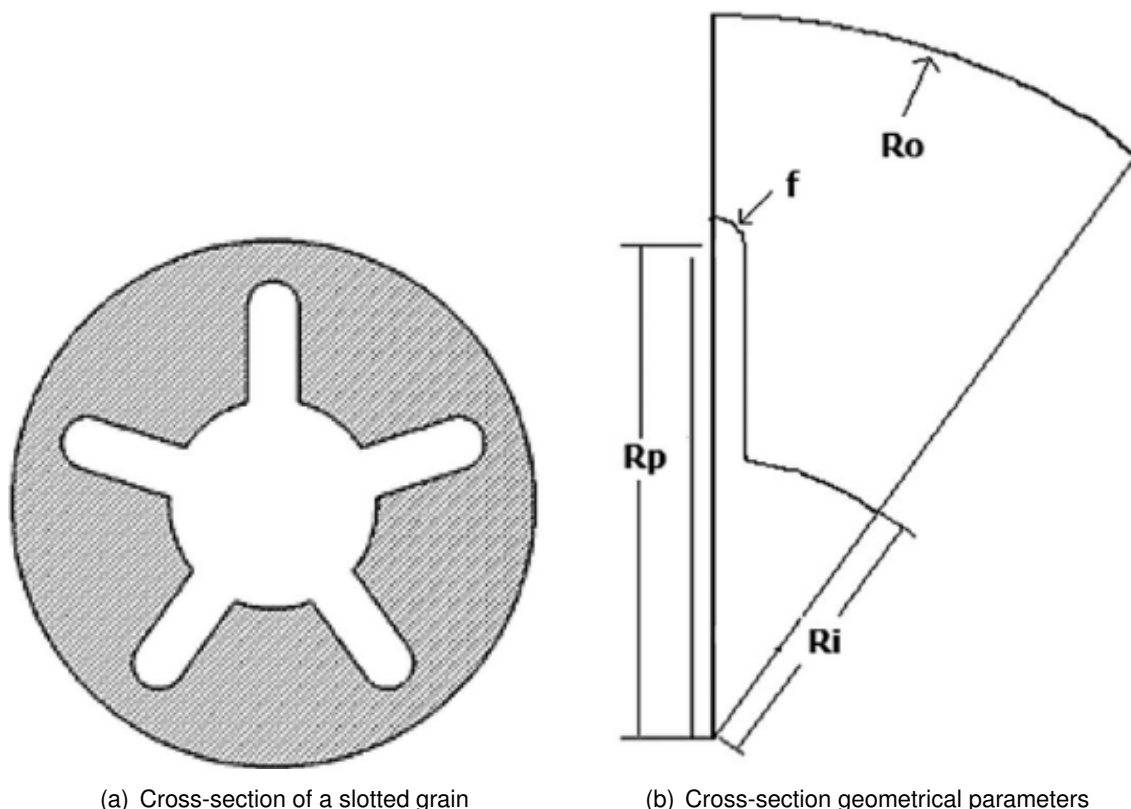


Figure 2.3: Cross-section shape and parameters. Figures extracted from [39]

The analytical equations describing the grain regression y , the port area A_p , the burn area A_b and the port volume V_p followed by the thrust and chamber pressure calculations, are described in (see eqs. (D.15) to (D.36)). To understand better the parameters and subscripts of those equations, the following figures may help the reader to visualize the concept. Other expressions can be found on their study, only consisting on different ways to solve the problem.

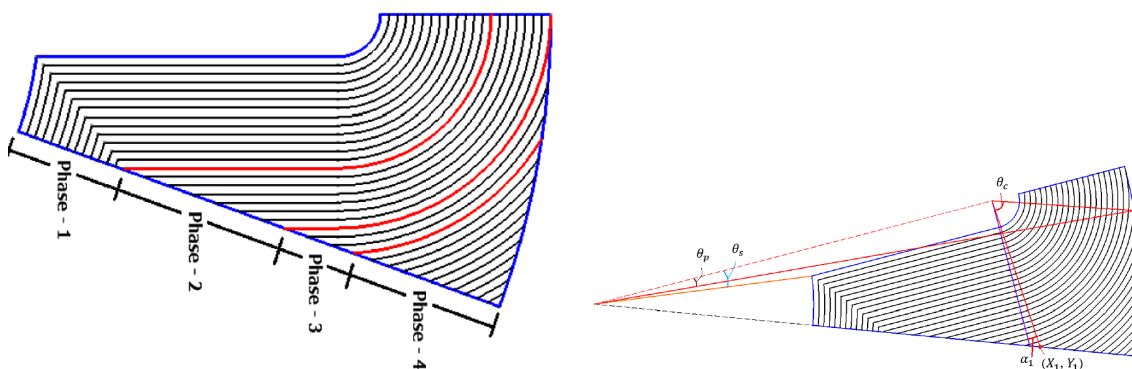


Figure 2.4: Analysis of the burnback scenario. Figures extracted from [39]

2.1.2. Solid rocket propellant chemistry and composition

Although in this part of the project only the grain burnback is analysed, chemistry plays an important role on the maximum thrust that a propellant can deliver regardless from nozzle geometry. Kubota [44] explains on his book the basics of propellants and explosives, from chemistry to performance. The main basis of any rocket propellant is the combustion of one or more fuels with oxidizing reactants, transforming those reactants into hot gas products. Those hot gases are thermodynamically expanded in a nozzle, and thus, producing thrust. To study the performance of each propellant is necessary to know exactly their chemical composition and the relative proportion, however this information is always simplified in some basic parameters like in table 2.1, which forces us to make some assumptions and the use of empirical equations mentioned before.

Propellants are classified in different groups according to their composition, and the main groups are DB (Double-Base), EDB (Extruded Double-Base), CDB (Cast Double-Base), EMCDB (Elastomer-Modified Cast Double-Base Propellants) and CMDB (Composite-Modified Double-Base propellant). DB propellants were the first used in rocketry until new polymers and binders were developed for the CMDB propellants. DB propellants were used in the past for small and tactical missiles but had low efficiency, while new type of composite propellants are made of Ammonium perchlorate crystals, Aluminium powder to increase density and specific impulse and a binder to hold the mixture, usually HTPB (Polybutadiene). In military applications however, it is important to consider how visible the smoke trail is, and Al_2O_3 solid particles released to the atmosphere are the most visible ones. More information about the chemistry and different applications of the previous propellants can be found on reference [45].

The table 2.1 presents the most important parameters about different solid propellants, being the most important ones specific impulse, burn rate at 1000 psi, density, pressure exponent and flame temperature, all measured in sea level conditions. Hazard classification is an additional parameter to classify the propellants if they are made from a detonable (class 1.1) or non-detonable material (class 1.3), like solid high explosives (HMX, RDX) which in fact, give the best performance.

Propellant type	Specific Impulse s	Flame Temperature K	Density kg/m ³	Metal content (wt %)	Burning rate mm/s	Pressure exponent	Hazard classification
DB	230	2530	1605.4	0	11.43	0.3	1.1
DB/AP/AI	265	3860	1799.2	21	19.81	0.4	1.3
DB/AP-HMX/AI	270	3970	1799.2	20	13.97	0.49	1.1
PVC/AP/AI	265	3370	1771.5	21	11.43	0.35	1.3
PU/AP/AI	265	3590	1771.5	20	6.86	0.15	1.3
PBAN/AP/AI	263	3480	1771.5	16	13.97	0.33	1.3
CTPB/AP/AI	265	3480	1771.5	17	11.43	0.4	1.3
HTPB/AP/AI	265	3480	1854.6	17	10.16	0.4	1.3
PBAA/AP/AI	265	3590	1771.5	14	8.13	0.35	1.3
AN/Polymer	180	1550	1467	0	1.52	0.6	1.3
XLDB/AP-HMX/AI	269	3620	1854.6	19	8.89	0.5	1.1
PVC/AP	240	2810	1688.5	0	11.43	0.38	1.3
PS/AP	240	2860	1716.2	0	8.89	0.43	1.3
PS/AP/AI	250	3030	1716.2	3	7.87	0.33	1.3
NEPE	269	3620	1854.6	19	15.24	0.5	1.3

Table 2.1: List of Solid Rocket Propellants and their properties. See reference [44] for more information about the propellant names

2.1.3. Booster's casing materials selection

The case containing the propellant grain must be able to withstand the pressure loads on the structure due to aerodynamic forces and also the pressure coming from the combustion chamber. The design of the casing is based on an iterative process based on the vehicle performance and manufacturing requirements. The most important loads and stresses that the case must withstand come from the internal pressure, the thrust force, nozzle and the aerodynamic surfaces coupled on the external part.

The most common materials used in casing are made of metal and composites, but the last ones can only withstand low temperatures. In our case, where we have constrained diameter imposed by the VLS and high volumetric efficiency is a priority, steel casing is the most common one. This casing allows less thickness to contain the same propellant and little insulation material.

In order to save more weight, a conical nozzle is selected in missiles instead of a countered nozzle.

2.2. Scramjet and ramjet engines

Ramjets and scramjets are classified inside the group of "athodyne" engines, which stands for Aero Thermodynamic Duct. The difference between those engines compared to the turbojet and turbofan is the absence of turbomachinery (fan/compressor and turbine), which decreases weight and complexity of the engine. The resulting engine is the composition of an entry duct, a combustion chamber and a nozzle. Main disadvantages of this type of engines are high fuel consumption and poor efficiency compared with the turbojet and turbofan.

Ramjets and scramjets make use of the ram compression effect, where the compression made outside the engine is enough to overcome the need of mechanical compression. The difference between the ramjet and the scramjet is that the last one makes the combustion supersonically (Supersonic Combustion ramjet), allowing it to operate at higher speeds. When using a ramjet, there is a limit of cruise speed where subsonic combustion becomes inefficient and supersonic combustion must be used. This upper limit on ramjet falls about Mach 5.5, but can differ slightly depending on the fuel used.

At the early days of supersonic cruise missiles, the solid rocket motor was preferred since was the most feasible technology. Then some ramjet configurations appeared, which allowed to increase range. The most famous supersonic ground launched anti-ship cruise missiles with ramjet were the P-270 Moskit, P-700 Granit, P-800 Oniks, P-1000 Vulcan, Brahmos.

2.2.1. Scramjet thermodynamic cycle

When studying the scramjet performance across its different parts (compression, combustion and expansion), the reader must be familiarized with the notation given to the scramjet (see figures 2.5(a) and 2.5(b)).

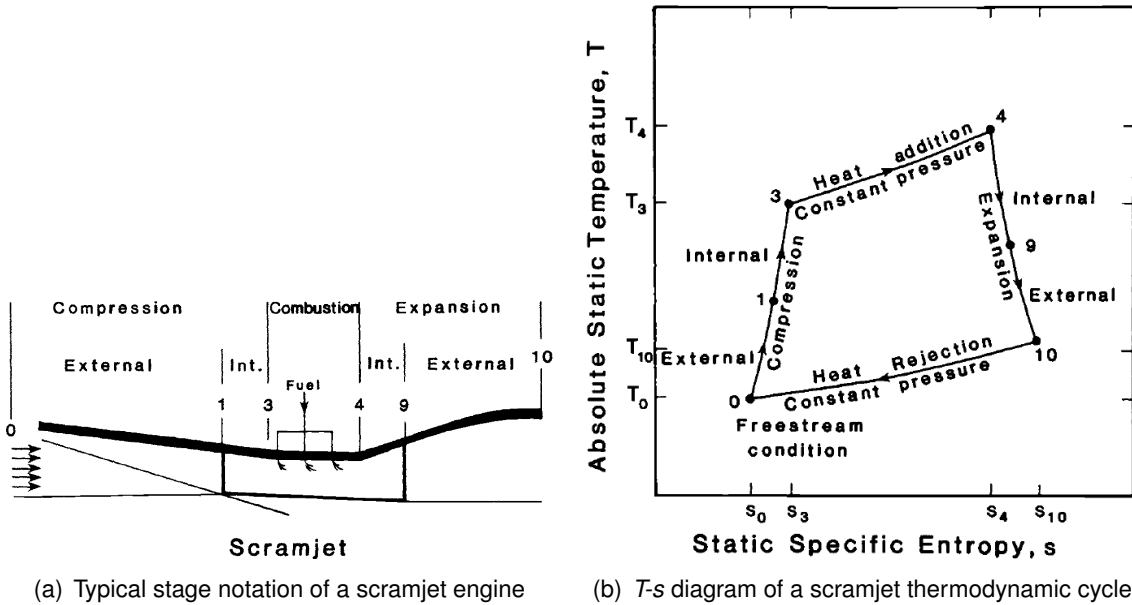


Figure 2.5: Scramjet stages and thermodynamic cycle. Figures extracted from [40]

- Between point 0 and point 3 there is an adiabatic compression from the freestream flow, increasing the static temperature from T_0 to T_3 . This compression process includes irreversibilities due to skin friction of the flow in the inlet ramps and the shockwaves across each ramp, causing entropy to increase between s_0 and s_3 . When irreversibilities are absent in the compression, we name this phenomena an isentropic compression. Isentropic inlets require infinite oblique shock waves to take advantage of this type of compression (see figure 2.6).

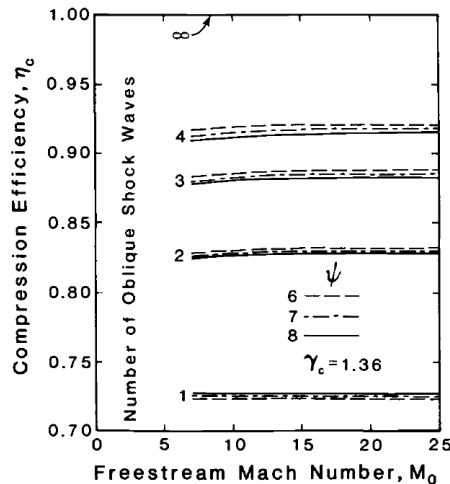


Figure 2.6: Compression efficiency as a function of number of shocks n and temperature ratio Ψ . Figure extracted from [40]

- Between point 3 and point 4 combustion of the fuel occurs. During the combustion process, constant static pressure, frictionless heat addition from the burner entry static temperature T_3 is assumed. There are 4 main reasons to assume constant

static pressure. The first is to prevent boundary-layer separation, secondly, because in the analysis of gas turbine and ramjets constant static pressure is assumed since velocity is brought close to 0 (not the case for scramjets). The third reason is that constant area combustors operate at constant pressure. The last reason is the simplicity of mathematical operations.

- Between point 4 and point 10 there is an adiabatic expansion from the burner static pressure $p_3 = p_4$ to the freestream static pressure $p_{10} = p_0$ (assuming adapted nozzle for maximum thrust). The entropy increases in the adiabatic expansion process due to skin friction between s_4 and s_{10} .
- Between point 10 and point 0 the thermodynamic cycle is closed with an imaginary constant static pressure and frictionless process. This assumes that heat is rejected from the exhaust air and returned to its original temperature-entropy state.

2.2.2. Intake considerations

One of the main design drivers for those types of missiles is the intake type and configuration. This is an important fact in our study too, since each intake configuration has its own advantages and drawbacks.







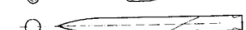

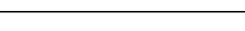




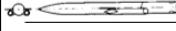
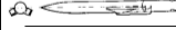
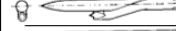
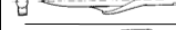

Type Inlet	Sketch	Placement
Nose		Annular nose inlet
Chin		Forward underside in nose compression field - partial annular
Forward Cruciform Annular		Forward in nose compression field - cruciform (four) annular inlets
Aft Cruciform Annular		Aft-cruciform (four) annular inlets
Under Wing Annular		In planar wing compression field - twin annular inlets
Twin Two-dimensional		Aft - twin cheek-mounted two dimensional inlets
Underslung Annular		Aft underside - full annular
Underslung Two-dimensional		Aft underside - belly mounted two dimensional inlet
Aft Cruciform Two-dimensional		Aft - cruciform (four) two dimensional inlets

Figure 2.7: Types of scramjet and ramjet intakes. Figure extracted from [4]

Type Inlet	Selection Factors										
	Pressure Recovery	Carriage Envelope	Alpha Capability	Weight	Drag	Warhead Shrouding	Inlet Cost	Preferred Steering	Preferred Control	Prime Mission Suitability	
	●	●	○	●	●	—	●	STT	W, C	ATS, STA	
	●	●	●	○	●	○	○	BTT	T	ATS, ATA, STA	
	○	○	●	—	○	—	—	STT	T	ATS, ATA, STA	
	○	●	○	●	○	●	○	STT	T	ATS	
	●	—	●	●	○	●	●	BTT	T	ATS, ATA, STA	
	●	○	●	●	●	●	○	BTT	T	ATS, ATA, STA	
	○	—	○	●	○	●	●	BTT	T	ATS	
	—	—	●	●	●	●	●	BTT	T	ATS, ATA, STA	
	○	●	○	●	●	●	○	STT	T	ATS	

Note:
 BTT = Bank to Turn
 STT = Skid to Turn
 W = Wing C = Canard
 T = Tail

● Superior ● Good ○ Average — Poor

Figure 2.8: advantages and drawbacks of each type of intake. Figure extracted from [4]

In figures 2.7 and 2.8 there are some of the most used inlet types for ramjet / scramjet missiles with their main features regarding to engine and aerodynamic performance. In the case of a hypersonic cruise missile the best option seems to be a “Chin” intake type due to its performance and compact size. Other variables such as the tail control for this configuration and the bank-to-turn will be useful when studying the stability and control of the missile.

When the type of intake has been selected, the type of compression inlet must be studied. The correct selection for the integration of the inlet to the airframe involves a host of considerations, including the swallow capacity, minimizing the drag and minimizing the pressure oscillation. There are three types of supersonic / hypersonic intakes, known as external compression, internal compression and mixed compression. For supersonic / hypersonic missiles the mixed compression type is selected due to the low forebody deflection drag, relatively low pressure oscillation and relatively low inlet start Mach number.

2.2.3. Mixed compression analysis

The primary mission of the compression system is to provide an increase of T_3 high enough at the combustor entry to maintain continuous combustion. When a scramjet engine must operate at different speeds, the shape of the inlet must be changed during flight to remain “on design” conditions, thus increasing complexity and weight. In the case of air-breathing missiles, fixed geometry intakes are preferred.

Two types of intakes have been studied in scramjet engines field. The first and the most common (and also studied in the present work) is the intake based on planar flow design or in other words planar shocks and Prandtl-Meyer flow. The other type of intake is based on axial flow which has a smaller surface area, meaning lower heating transfer rates and small boundary layer losses. The design of this intake is based on Busemann flow and wavecatching [34], which are beyond the scope of this project. The last type of intake is still under research and at this moment any hypersonic cruise missile developed or under

development incorporates it.

But now, let's focus on the mixed compression type inlet. Mixed compression inlet consists on different shockwaves outside and inside the inlet, providing the desired amount of compression and flow turning (see figure 2.9). The difference with external compression is that mixed compression can use multiple internal weaker shock reflections, leading to less entropy increase but with larger inlet length. The geometry of the inlet will be adapted for cruise flight conditions, flying at constant altitude and speed and the flow will be treated as one-dimensional and calorically perfect.

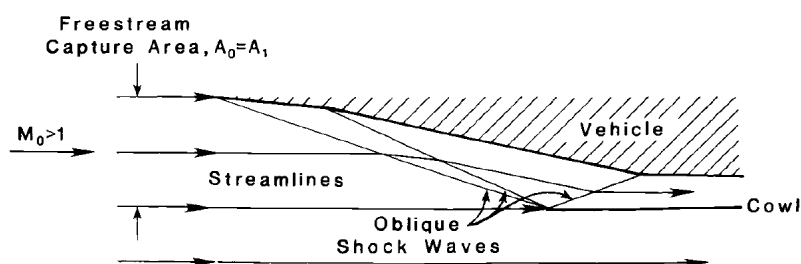


Figure 2.9: Mixed compression inlet. Figure extracted from [40]

Performance measures to analyse the intake include compression efficiency, kinetic energy efficiency, engine overall efficiency, propulsive efficiency and thermal efficiency. Moreover, detailed analysis on the inlet performance can be made by accounting the effects of skin friction and heat transfer and their detrimental effects on compression efficiency.

The physical and mathematical methods to design the inlet and its performance can be found on eqs. (E.1) to (E.19), which has also been designed using a genetic algorithm. Specialized software like HAP (Gas Tables) also allows performing calculations for scramjet design, however we have no access to this software and then solutions are obtained using MATLAB.

2.2.4. Burner and combustion analysis

The burner encounters the highest static pressure in the engine. Moreover, not only the highest pressure p_3 but also the combustor temperature T_4 is the highest, being the most challenging structure and requiring the most advanced materials and cooling techniques. Those cooling techniques may have some restrictions in missile design, since active cooling is not useful when designing missiles, so insulator materials must be chosen to isolate combustor from other subsystems.

During the combustion process, one should be familiarized with the stoichiometric fuel to air ratio and with the associated chemical equation eqs. (E.20) to (E.21). This equation tells us that the maximum combustion temperature occurs when hydrocarbon fuel molecules are mixed with just enough air so that all hydrogen atoms forms water vapour H_2O , and all of the carbon atoms form carbon dioxide CO_2 . Stoichiometric fuel to air ratios for the fuels used in the present work can be found on table 2.2.

Fuel type	Heat of reaction kJ/kg	x	y	Stoichiometric f/a
Methane	50010	1	4	0.0583
Ethane	47484	2	6	0.0624
Ethylene	47200	2	4	0.0680
Hexane	45100	6	14	0.0659
Octane	44786	8	18	0.0664

Table 2.2: List of Scramjet Hydrocarbon fuels and their properties

The combustion process in a hypersonic flow can be a complex phenomenon that will not be studied on this project, with the mixing of fuel in air the most challenging topic. Other important aspects is the properly calculation of the specific heat ratio in the combustion phase eq. (E.22), based on empirical models for stoichiometric and near stoichiometric fuel to air ratios which can be found in reference [46]. Other parameters of the combustor are calculated through eqs. (E.23) to (E.26).

2.2.5. Expansion and nozzle analysis

The primary function of the expansion components consists in providing acceleration of the flow from the burner exit static pressure to atmospheric static pressure (see eqs. (E.20) to (E.21)). The most common technique to design exhaust nozzles is the method of characteristics, which we have applied on this study and we are going to explain in detail.

Method of characteristics is useful especially for the case of a highly integrated scramjet engine on the airframe, where there is a variation on the classical nozzle shape. In this case, the exhaust nozzle is planar rather than circular like the classical circular bell-shaped de Laval nozzles. Those nozzles are usually heavier and present some disadvantages referring to geometry modification. This type of single expansion ramp nozzle was studied in reference [42] where they present their concept of an hypersonic aircraft, with the forebody (nose) acting as an inlet compression ramp, a center portion of the body containing the engine, and the remaining afterbody forming an exhaust-nozzle surface with aerodynamic drag penalty, a potential increase on lift and large thrust moment forces which must be counteracted for a stable flight condition.

Method of characteristics consists in a numerical technique to predict the nozzle shape of supersonic and hypersonic flow, which must deal with the complex nature of the fluid flow. The main advantages of this method are small computational time and acceptable accuracy. This method can be applied for one dimensional unsteady flow, two and three dimensional steady flows and axisymmetric steady flow despite the fact that the flow must be irrotational and isentropic.

Figure 2.10 is an additional extension to explain the related mathematical equations (see eqs. (E.30) to (E.35)). To better understand the nature of the problem, fewer shock reflections are calculated and can be numbered easily.

To start with, we must assume a set of different lines (7 in this case) departing from a and intersecting on a “flat plate”, and numbering this intersections 1, 9, 16, 22, 27, 31, 34. Those lines are named characteristics, and in this case where they are going downwards, are known as right running characteristics. The first right running characteristic is spaced

with an angle $\Delta\theta$, which has to be small enough. The exit Mach of the nozzle (which is a known variable), is used to study the maximum angle of the nozzle θ_{max} . Usually, the decimal part of this angle θ_{max} is taken as the reference value for the angle $\Delta\theta$, while the rest of characteristics have the same values of θ (same angles of separation).

Each of this right running characteristics will have a corresponding reflection (left running characteristic) which is going to interact with the right running characteristic, thus changing the new position of points 9 to 34. For example, point 2 is the intersection of $(s+)_{1}$ and $(s-)_{9}$, point 3 is the intersection of $(s+)_{2}$ and $(s-)_{16}$ until getting to point 7. Since point 9 is the only one affecting the right running characteristic (and of course the slope) of $(s-)_{9}$, the point 9 should be recalculated to study the position of the new points ranging from 10 to 14. Point 8, 15 and the rest of the nozzle wall have exactly the same Mach number and flow direction than those at point 7, 14, etc. Notice that the tangent line joining the points of the wall has to be small to be more accurate, or in other words, the characteristics method increases its accuracy as the number of characteristic points increases.

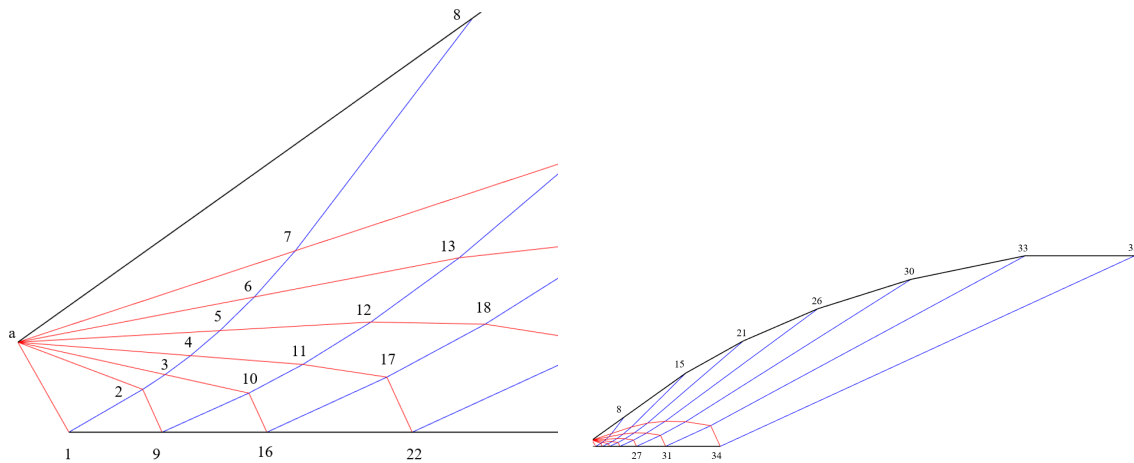


Figure 2.10: Characteristic lines and the corresponding notation

CHAPTER 3. STABILITY & CONTROL

3.1. Stability and manoeuvrability

Accuracy of any guided missile is strictly related to the response characteristics of the complete guidance, control and airframe loop. One of the most important requirements of any missile is to ensure enough natural static and dynamic airframe stability, and with this data the servo actuators for the control surfaces can be designed.

The airframe of a missile must be designed with enough load factor capability (or manoeuvrability) to perform turns with the minimum possible radius.

In this project we only consider the two-degree-of-freedom analysis (one rotational and one translational) since is the most useful to study the longitudinal stability and manoeuvrability of the missile in the conceptual phase, and damping terms will be neglected. In a steady flight condition, the summation of moments about the center of gravity of the missile is 0, and the condition for static stability is that C_{m_α} is negative, meaning a pitch down manoeuvre with an increase of the angle of attack. To determine the manoeuvrability, the load factor capability must be determined with the C_{N_δ} and the C_{m_δ} derivatives.

Those derivatives calculated in this project will be referred to the most critical conditions of flight, on the terminal phase of the flight.

3.2. Missile body with booster

In this case the tail of the body missile act as wings and the tails of the booster are moveable tails. The center of mass in this configuration is assumed to be at 50% of the total length. (see eqs. (C.1) to (C.4) for more information about the subscripts). Notice that in figures 3.1 and 3.2 it appears the normal force N instead of the normal force coefficient C_N of the equations. This is due to the fact that in the mentioned equations appear two additional terms, dynamic pressure q and reference surface S_{ref} .

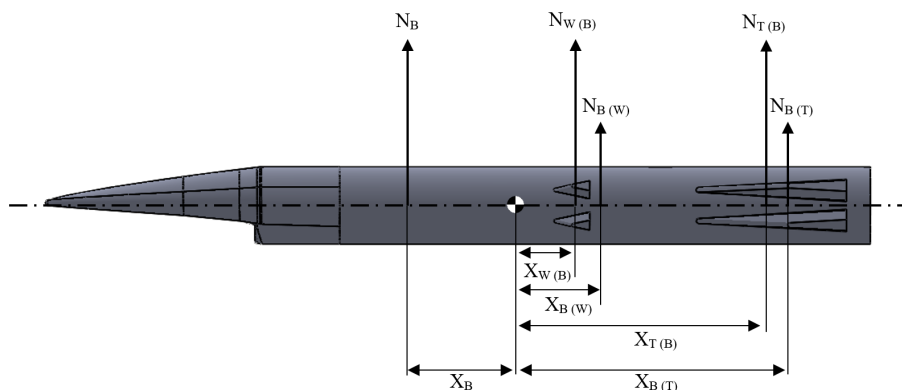


Figure 3.1: Force diagram of our designed missile with the booster

3.3. Missile body

Now the wings of the previous configuration act as tails. The center of mass of the current configuration is assumed to be at 40% of the length (more weight on the front due to radar seeker and other subsystems). eqs. (C.5) to (C.8)

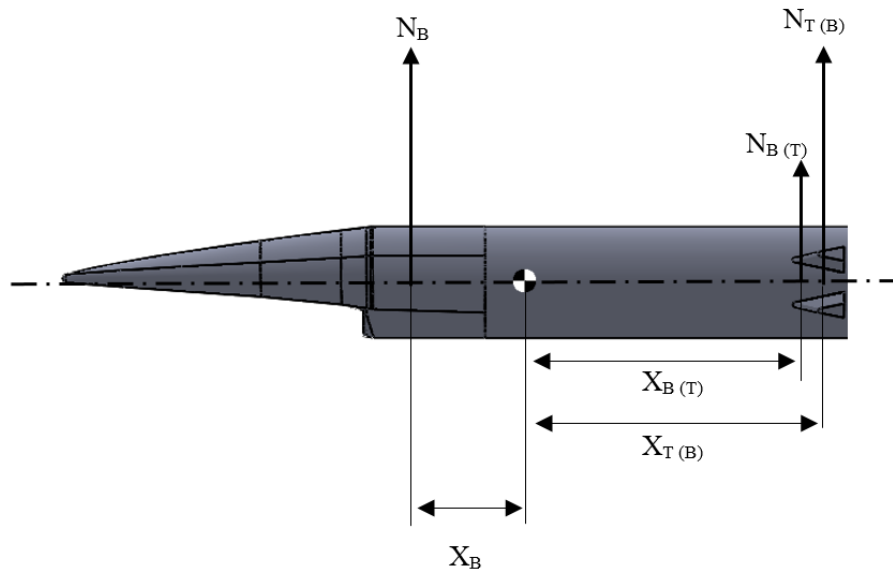


Figure 3.2: Force diagram of our designed missile

CHAPTER 4. FLIGHT TRAJECTORY

4.1. Hypersonic missile trajectory overview

Most anti-ship missiles have defined trajectories which are based on sea-skimming or in high altitude flight and dive. The flight phases of a typical high altitude cruising anti-ship missile are the following [5]:

- Boost phase, where alignment and target/platform data acquisition takes place.
- Climb phase, where missile performs updating of navigation and target data while flying using steerpoint navigation.
- Cruise phase, where seeker is activated when cruise starts and locked on target before start diving. Seeker activation include initialisation, target data and clutter rejection. When seeker locks on target, there is a navigation handover and ECCM (Electronic Counter-Counter Measures) are activated.
- Terminal phase, where proportional navigation is established, ECCM are engaged and missiles strikes on the target performing a variety of attack profiles like waving, straight and level high-speed attack, pop-up and dive and finally supersonic acceleration.

Although those flight trajectory has been tested successfully by many supersonic and subsonic anti-ship cruise missiles, hypersonic cruise missile may face-off different problems such as extreme heating in cruise phase and high drag while diving. This immense heating can play against the missile since high infrared radiation is emitted and tracked by GEO and HEO warning satellites like SBIRS (Space-Based Infrared System), DSP (Defense Support Program) satellites, Next-Gen OPIR (Next-Generation Overhead Persistent Infrared Program) and LEO tracking satellites such as STSS (Space Tracking and Surveillance System). Then, optimization of trajectory for maximum range and small heating rates must be optimized according to our mission requirements.

Figure 4.1 provides a reference on different altitudes and speeds according to the hypersonic vehicle involved. Hypersonic airbreathing cruise missile speed falls within the range of Mach 6 and Mach 10 while the altitude is between 20 and 30 kilometres of altitude. This data will feed our genetic algorithm, being one of the most meaningful parameters.

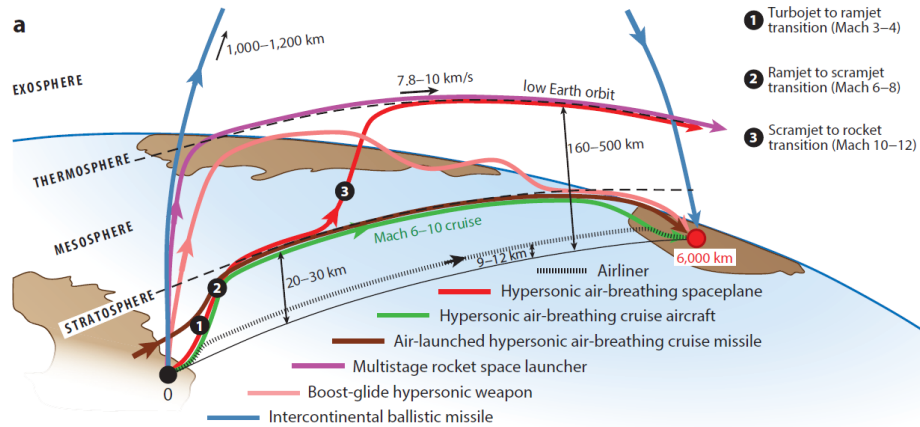


Figure 4.1: Trajectories for different hypersonic vehicles. Figure extracted from [51]

4.2. Trajectory optimization methods

The vast majority of research studies about optimal trajectory for hypersonic vehicles are focused on HGV and ballistic missiles, where constant thrust is assumed and other trajectory optimization techniques are studied.

Some research on missile trajectory optimization has been made by Ul Islam Rizvi, S. T., et al. [48] where they solve the nonlinear, multiphase, constrained optimal control problem by using an hp-adaptive Gauss pseudospectral method for an HGV. In their case the parameters to be optimized were the burnout angle and the control deflections of the aircraft.

Chai, Dong, et al. [53] optimize a boost-skipping trajectory by means of hp-adaptive Gauss pseudospectral method, transforming the optimal control problem into a nonlinear programming problem. Finally they adopt a sequential quadratic programming algorithm to obtain the trajectory and satisfying the constraints. Boost-skipping trajectory was proposed because its ability to improve missile penetration while increasing the overall range.

In addition, in their research explained that not only optimal control theory but also shooting techniques and heuristic algorithms are commonly used to solve trajectory optimization problems. The advantage of heuristic algorithms are easy implementation and are still widely used for problems where the variables are discrete, not in this case where there is a large number of points along the trajectory. However heuristic algorithms performed well to find an optimal solution for the solid rocket booster grain port and the scramjet inlet analysis, where they are simulated across a proposed trajectory to determine the relative performance.

Zhou, Hao, et al. [52] tried to find a history of control of the angle of attack to maximize the terminal velocity using genetic algorithms and including a heat rate constraint.

4.3. Proposed trajectory

Knowing the benefits and the drawbacks of genetic algorithms (and heuristic algorithms in general) applied to trajectory optimization, a vertical profile trajectory must be analysed not only for maximizing range and speed but also for booster, scramjet, aerodynamic surfaces and warhead sizing. Different genetic algorithms have been programmed and coupled together, but this will be explained in the next chapter, while explaining in detail the methodology.

- **Boost phase:** Solid rocket motor port has to be designed accordingly to provide the highest amount of TWR to reach the maximum speed to ignite the scramjet. Although high speed is also desirable to travel higher horizontal distances, high acceleration at low atmospheric layers mean higher dynamic pressure, causing the missile to break down. The most important parameters in gravity turn is the pitch rate $\dot{\theta}$, or the rate at which missile nose pitch down and the cut off θ , the final pitch where booster runs out of fuel (see eqs. (F.1) to (F.16)).
- **Climb phase:** When the booster drops-off, the scramjet is powered on but it has not the highest efficiency since intake and nozzle have no adapted geometry. This reduction in efficiency implies more fuel consumption \dot{m}_f to produce the required amount of thrust. For most missiles, the typical value of TWR in climb falls between 2 and 10 [4], and obviously, this TWR must overcome drag during the ascent. The parameters to optimize here are then the TWR and the angle of climb, while heating, initial and final velocities and cruise altitude will act as constraints (see eqs. (F.17) to (F.21)).
- **Cruise phase:** In the cruise phase scramjet engine must be optimized to maximize the range for different hydrocarbon fuels presented in the propulsion section. Here the inlet design takes place and also the nozzle design using the method of characteristics. Inlet and nozzle must always fulfil the dimension requirements of the Mk-41 VLS, so an optimal solution to those dimensions must be found. Then, aerothermal heating will be another aspect to consider especially because of the insulator materials point of view. Cruise phase is the longest of the flight, so heat transfer across the different materials (especially in nose) should be studied to determine the required thickness of the insulator. Regarding to aerodynamics, CG displacement and static stability margin must be determined for the correct sizing of the tail. Flying at some angle of attack α may influence the scramjet total performance (see eqs. (F.22) to (F.24)).
- **Gliding phase:** Within this phase, missile aerodynamics play an important role to maximize range. High L/D ratios obtained from an elliptical cross-section body and little effects of compression lift (despite the fact this is not a waverider configuration) should help to accomplish this objective, taking into consideration that scramjet remains unpowered. Tail must provide the required manoeuvrability in the last stage of gliding to defeat target defences and increase survivability. (see eqs. (F.25) to (F.28))
Then, the missile must coast to target at the highest possible speed, and maintain it until hitting the target, where hypersonic missile regard on their high speed for deep penetrations in the steel of the ship hull. The penetrator material of the warhead

and the warhead itself is dimensioned from the data obtained in the gliding phase. Notice that on figure 4.2 a solid line and a dashed line are represented on the gliding phase since two trajectories are possible. This assumption is based on references [48] and [53], where boost-skipping trajectories (dashed line) maximizes the range but decreases the terminal speed.

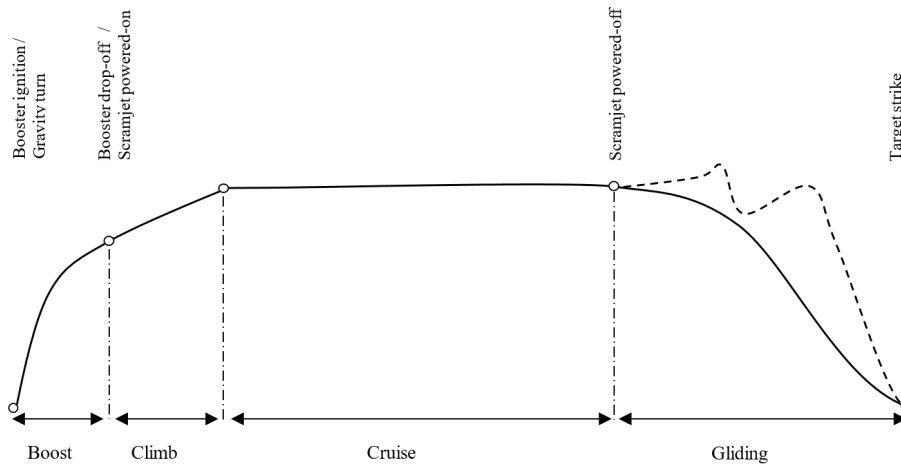


Figure 4.2: Proposed trajectory for the hypersonic airbreathing cruise missile

From the previous definitions it is obvious to say that aerodynamic surfaces will be dimensioned for the most critical stages of flight, first the boost phase and finally the gliding phase (see figure 4.2). In chapter 6, we explain in detail the methods to optimize the trajectory profile.

4.4. Navigation and guidance

Anti-Ship cruise missiles can use either two methods of homing guidance system on their terminal phase. The first is based on an active radar homing and the second on an active/passive radar homing. In active radar homing, the missile seeker consists on a radar transceiver emitting electromagnetic pulses to detect the target position while in active/passive radar homing where they track the target that is attempting to jam the missile electronics with noise. This capacity for the missile to track autonomously the target is also known as fire-and-forget, but the missile requires always sensing of target and it adds additional cost and weight to the missile. Moreover, the main requirement for any homing system is that the seeker must be perfectly aligned with the longitudinal body axis of the missile.

Apart from their main homing guidance system, Anti-ship missiles can track their position in cruise and ascent phase with an INS (Inertial Navigation System) alone or a GPS (Global Positioning System) coupled with an INS due to the fact that they have longer operational ranges compared to other Air to Air missiles. This additional guidance systems are required since missile on-board radar has small diameter antenna to fit inside the missile and thus, low effective radiated power (ERP) to track the target on the entire flight.

The GPS/INS receivers are based on a centralized Kalman filter that processes the data from all the sensors within the missile (GPS, seeker, INS, etc.). Tightly coupled GPS/INS can perform pseudorange measurements from three to only one satellite using a Kalman filter of 23 states, allowing high precision measurements of velocity and position and counteract the effects of jamming. Those 23 states are correcting the missile position error (3 states), velocity error (3 states), attitude error (3 states), accelerometer bias (3 states), gyro bias (3 states), GPS receiver clock bias (1 state), GPS receiver clock drift (1 state), data link radar misalignment (3 states) and launch position error (3 states).

Other emerging technologies that could replace seeker in near future are the data links. Data links can transmit target image data generated from sensors such as Synthetic Aperture Radar (SAR), reducing the possible collateral damage. However those technologies are more likely to be applied on missiles with loitering capability, and hypersonic missiles are discarded. Another important fact is that all modern homing systems employ proportional navigation as their guidance law (see reference [49] for more details and mathematical analysis of proportional navigation and GPS/INS navigation).

CHAPTER 5. WARHEAD

5.1. Introduction to warheads

Warhead design may differ according to the missile's target. The most famous and used warheads are blast warheads, fragmentation warheads, continuous rod warheads and shaped charge warheads, explained well in reference [56].

- Blast warhead: Consists of a high explosive filled inside a casing. When is detonated it creates a large wave front of positive pressure, and followed by a negative pressure burst. On the other hand, blast warheads are classified into internal and external blast. The internal blast warhead detonates once it is inside the target, requiring an armour piercing device on its head to penetrate armour (such as warships hull) without damaging the casing. If the target skin is softer, the blast of the explosion provides enough pressure to penetrate it (like in aircrafts), but the fuze must always be in contact with the target. External blast warhead are detonated while near the target using proximity type fuze.
- Fragmentation warhead: Consists of an explosive charge surrounded by metal fragments or a solid metal casing. When the charge detonates, the fragments are propelled at high speeds, and inflicts damage by delivering kinetic energy. They are used against air and surface targets, and the fragment size and mass is strong related with the target type. Proximity fuze is the most common detonator since this warhead is detonated by proximity.
- Continuous rod warhead: Consists of an explosive surrounded by a series of metal rods. Rods are some kind of metal fragments welded together on their sides, forming a circular hoop that expands radially when the explosive detonates. This hoop expands until the circumference exceeds the total sum of rod lengths, when it breaks up in several pieces. They are employed against air targets, cutting them and accomplishing a quick kill.
- Shaped charge warhead: Consists of an axially symmetric high order explosive disposed in a specific geometry, with a detonation point at the axis of one end of the charge and a symmetrically placed linear cavity on the other side. This cavity in most of the cases has a cone shape, although other shapes have been used. When the explosive detonates, the shock wave compresses some of the liner material forming a high velocity stream named as jet. This jet has the capability to penetrate against armoured targets of different thickness.

5.2. Warhead design

In reference [5], we are given technical data of warheads used in anti-ship missiles. Warhead weight is dependent on missile range, but the weight is usually between 120 and 450 kilogram, and must be able to defeat 100 m^3 compartments with wall thickness about 30 mm. Another important aspect are the fragments required to transmit kinetic energy and

damage the structure. For this purpose, fragment size around 120 and 250 g and speed of 1600 m s^{-1} are desirable. Then, a blast fragmentation warhead must be considered for this purpose. Another important data is that to ensure 100% lethality, the minimum blast pressure has to be about 1.5 MPa and for a building destruction about 80 kPa.

Blast fragmentation warheads provide high blast energies at low miss distances and high kinetic energy of fragments at high miss distances. When warhead detonates, a peak overpressure is generated from the explosive charge, and integrating all the overpressures in time, the total impulse is obtained (see figure 5.1). The pressure and the total impulse are strongly related to explosive charge weight, explosive composition, charge geometry, casing material and atmospheric conditions (essentially atmospheric pressure). When detonating, the pressure wave travels until reaching the target, at an arrival time t_a . Moreover, the shockwave is in contact with the target a time t_d and the damage to the target is high if duration time t_d remains as high as possible. Finally, a trade-off between the explosive charge mass and the fragment sized is required to find the best solution (see eqs. (G.1) to (G.15)).

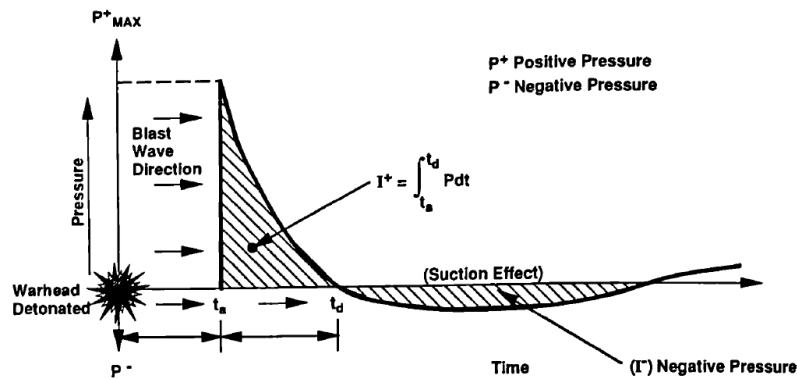


Figure 5.1: Blast pressure at miss distance as a function of time. Figure extracted from [54]

In table 5.1, different explosives and their technical data are presented.

Explosive	Density g cm^{-3}	Detonation velocity kms^{-1}
CH-6	1.72	8.55
COMP A-3 (91/9 RDX WAX)	1.65	8.47
COMP A-4	1.65	8.956
COMP A-5-I	1.65	8.931
COMP B (63/36/1 RDX/TNT/WAX)	1.71	7.92
HBX-1 (40/38/17/5 RDX/TNT/AL/WAX)	1.76	7.22
HBX-3	1.85	7.53
HMX	1.89	9.11
HNS	1.7	7
HTA-3 (49/29/22 HMX/TNT/AL)	1.9	7.866
LX-14 (95.5/4.5 HMX/Estane 5702)	1.835	8.83
NTO	1.871	8.12
OCTOL (75/25 HMX/TNT)	1.81	8.48
PBXN-5 (95/5 HMX/Vitrol)	1.89	8.82
PETN	1.78	8.59
RDX	1.77	8.7
TATB	1.88	7.76
TETRYL	1.71	7.85
TNETB	1.78	8.46

Table 5.1: List of High Explosives Charges and their properties

5.3. Penetrator design

Supersonic and hypersonic missiles have an advantage over other missiles when referring to penetration capabilities. To increase the kinetic energy of the penetrator, heavy metals such as tungsten or depleted uranium are used. But we must take into account that these heavy materials are not hard enough, meaning that some casing metal must protect them from a structural failure. Steel alloys are usually employed for this casing shells. This type of penetrators are known as armour-piercing penetrators.

In the research from Holkko [57], he found out interesting data from US Army Material Command where the hardness value of a typical nose shell ranges from 653 to 722 BHN (Brinell Hardness Number) and on the remaining casing the hardness values oscillates between 370 and 420 BHN. Eglin steel (ES-1) is a low cost steel developed by the US Air Force and the Ellwood National Forge Company and it is used for the new generation of penetrators such as the GBU-28 bomb. This metal is made up of different elements, but the most important ones are Iron, Chromium, Nickel and Tungsten.

According to the nose shape and the thickness of the structure to penetrate through, different fracture mechanisms appear like Dishing, Punching and Ductile hole enlargement. Another important fact from reference [57] is that he performs a better analytical study on penetration mechanisms eqs. (G.15) to (G.16).

But after all, when referring to penetration capabilities, the armour of the target must be studied since the yield strength and the density of the armour are fundamental data. Navy ships hull are usually made of structural steel or other heavy metal, but today's armour is

not thicker as in the World War II era. In World War II, battleships had armours ranging to 320 to 400 mm to withstand artillery shells, so it will be the reference data to do run the calculations.

Today's ship armour design is based on a belt armour, designed to absorb the impact of torpedoes and missiles. The belt armour covers the ship from the main deck to some distance below the water, and is tilted (armour sloping) so that when something strikes it encounters more distance to penetrate.

CHAPTER 6. GENETIC ALGORITHMS AND MONTE CARLO SIMULATION

6.1. Missile design as an iterative process

Missile design is a complex engineering system being formed by other subsystems related between them. The conceptual design is a creative and an iterative process requiring rapid evaluation of alternatives. The usage of a baseline missile to initiate the design process includes some benefits such as a faster design process and more accurate. The lack of hypersonic cruise missiles and the privacy of information in military technologies, force us to search and study the main characteristics of each missile subsystem individually.

One of the main objectives of our study was to find reliable information sources performing studies about rocket and scramjet propulsion, hypersonic aerodynamics (lifting bodies and fins), trajectory optimization and guidance. The mathematical equations of those investigations performed by researchers must be easy to implement in an optimization problem for a fast converging solution.

Arslan [15], explains in his thesis how to apply optimization techniques on the aerodynamics of missiles, while B. Anderson [12] uses a genetic algorithm to optimize the missile fulfilling the guidance requirements. Those studies can be used as guidelines to perform our study by applying specific constraints to our problem and get accurate results. Other authors such as Broglia [16], uses genetic algorithm to optimize the shape of a waverider configuration for a hypersonic flight.

6.2. Genetic algorithms

In our study, the variables to optimize varies accordingly to the subsystem of the missile. In the following chapters, we are going to explain in detail those variables but here we only detail the process followed by the genetic algorithm to optimize our design. Genetic algorithm is a method to solve constrained and unconstrained optimization problems based on natural selection. The genetic algorithm modifies in each generation a set of individual solutions, selecting random individuals to be parents and producing children for the next generation. Over successive generations, the population tends to find an optimal solution, known as the best fitness function value.

To find an optimal solution (and a fast converging one), some emphasis should be applied in the following genetic algorithm rules: Selection rules, Crossover rules and Mutation rules. Those rules say to the algorithm how the individuals will be selected, how the chromosomes of two parents will be combined and how some random changes will be applied to the children.

MATLAB offers the user a package named “Genetic Algorithm Toolbox” to apply the algorithm via a set of commands. However, due to the complexity of our problem and variables we are more likely to code our genetic algorithm, being more easy to understand but less efficient.

6.2.1. Crossover and Mutation

Crossover and mutation techniques are the same without taking into account which part is been analysed (scramjet or solid rocket booster). Restrictions in crossover are applied only if the fuel used from two parents are the same and only geometrical data is different, meaning that if one has less performance (higher values of the fitness function), less chromosomes of the worst individual will be selected for crossover (80% and 20%) (see figure 6.1(a)). In the opposite case where parents have different fuels, those restrictions moderate and only the difference between fitness functions are considered (60% and 40%) (see figure 6.1(b)). The reason for that is that bad performance of a fuel does not mean bad geometry design of the grain port.

Until now we have explained how much chromosomes of each individual will be considered for the crossover, but not which ones will be selected. For this study, the chromosomes to start the crossover are selected randomly, always ensuring that selected chromosomes are not the same.

In the case of mutation, it is based on probability to change all of the chromosomes of one or more individual (depends always on probability). Mutation is given as a percentage and tells us how much individuals will change their entire chromosomes out of 100 individuals (3% means that 3 individuals are mutated from 100).

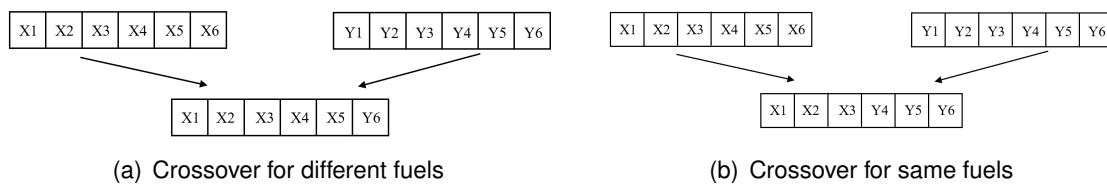


Figure 6.1: Crossover method for rocket booster and scramjet analysis

6.3. Monte Carlo simulation

The main difference between GA and Monte Carlo simulation is that the last one consists on a pure random search. However, pure randomness implies a large set of individuals to be created and running the calculations which can be sometimes cost prohibitive. It has been used for a while in missile conceptual design. The Monte Carlo method works by defining a domain of multiple inputs and generating pseudo-random numbers over that domain. The last phase consist on evaluating those inputs in the defined equations to solve the problem.

One of the most important facts of Monte Carlo simulation that hasn't been taken into account on this project is the search of influential variables through probabilistic analysis.

6.4. Structure of the problem

Due to the lack of computational power to find an optimal solution for the missile system in just one simulation program, we have divided our problem in many parts. The first part

consists on a Monte Carlo simulation for modelling the warhead. Secondly, one genetic algorithm is applied to find an optimal solution of the solid rocket booster grain and the initial ascent trajectory. The second genetic algorithm optimizes the scramjet performance for a given cruise flight conditions. The third algorithm based on a Monte Carlo simulation, optimizes the body and the aerodynamic control surfaces to provide adequate manoeuvrability and stability to the missile. Finally, the performance of the previous calculations are checked by evaluating the gliding trajectory towards the target.

Initially, we are given a constrained optimization problem of the form

$$\min_{x \in \mathbb{R}} f(x) \quad (6.1)$$

$$s.t. x \in \Omega \quad (6.2)$$

And the algorithm must find a solution that accomplishes

$$f(x^*) \leq f(x), \forall x \in \Omega \quad (6.3)$$

Where f is a scalar-valued function called fitness function, x are the decision variables and Ω is the constraint set. Finally, x^* will be the optimal solution of the fitness function inside the constraint set.

The constraints of this optimization problems will be strongly related with the missile platform integration, in this case the vertical launching system Mk-41. The dimensions and limitations of the VLS (length, width and weight) will put some limits in our missile dimensions and capabilities, not finding the best solution with the maximum range capability but enough considering our mission objective.

The Mk-41 launcher that we are going to use is the Strike version, which is used for the Tomahawk cruise missile. The dimensions are the following:

- Maximum weight, kg / (lb): 1814.37 / (4000)
- Maximum length, m / (in): 6.2738 / (247)
- Maximum diameter, m / (in): 0.5842 / (23)

Those dimensions are used in each step of the calculations, since rocket booster length is a limiting factor on how much thrust can deliver the engine, nose length must be large enough to provide the required compression but at the same time having enough volume for housing other subsystem, and the maximum diameter limits the span of the tail fins despite they are folded.

Since we must deal with huge amount of data at each design phase, a flow chart diagram must be designed, explaining in detail the order of execution.

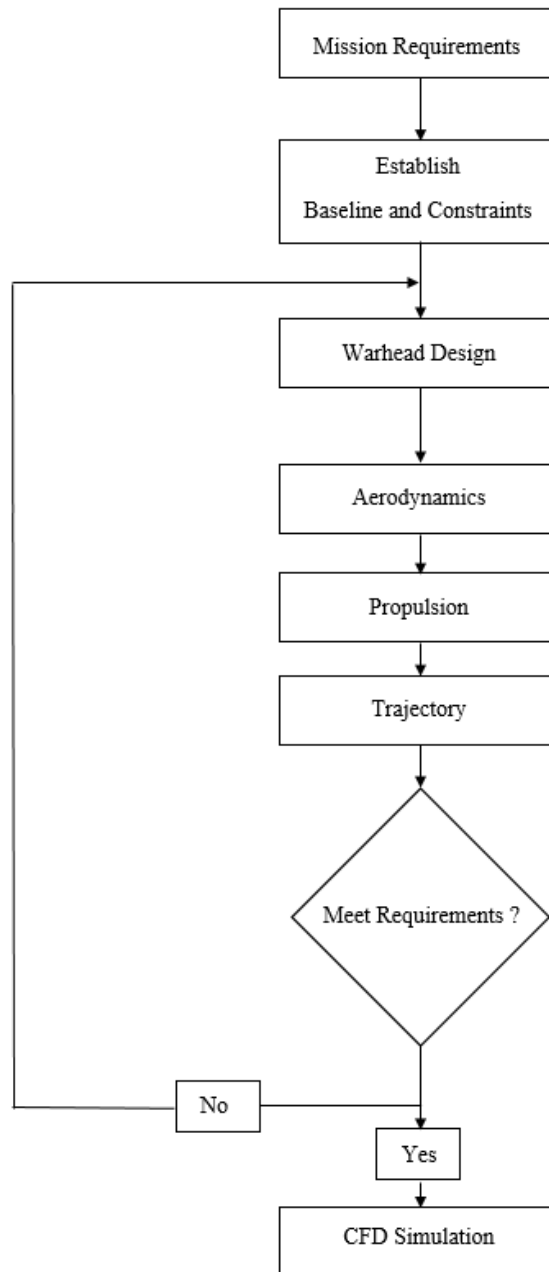


Figure 6.2: Flow chart diagram of the design process

- Warhead design: Maybe one of the most important design driver of the missile, where penetrator capabilities, blast pressure and velocity of fragments must be close enough to the requirements. The parameter that relates warhead performance and aerodynamic design is speed. When missile is closing to the target it must have enough manoeuvrability (between 40 and 60 g according to the baseline), and enough speed to penetrate inside the hull. Warhead mass must be high enough for high blast pressure and high fragment velocity but low enough to storage more fuel. It seems obvious that for a low volume warhead high density explosives will be preferred.

Another important parameter that appear not only on this objective function but also

on the others is the sigmoid function $S(x)$. The sigmoid function is an S-shaped curve that allows us to deal with possible negative values, returning the function a low value to better optimize the function. Apart from this, it can also be used when the values are non-negative.

$$S(x) = \frac{1}{1 + e^{-x}}$$

And the objective function:

$$f = \frac{M_T^2 S(M_P) S(L_c)}{S(p) S(p - p_k) S(E_T) S(v_f) S(t_k) S(t_d) S(v_{bl})}$$

Parameter	Minimum Value	Maximum Value	Step Size	Units
Casing inner radius	0.09	0.2150	10^{-4}	m
Casing outer radius	0.1	0.22	10^{-4}	m
Charge to Mass ratio	1	20	0.1	-
Terminal speed	700	1500	1	ms^{-1}
Length / Diameter penetrator	5	30	1	-
Nose length percentage	5	70	1	%
Total Warhead mass	200	600	1	kg

Table 6.1: List of constraints applied in the random individual creation of the warhead

- **Aerodynamics:** At this point, the missile aerodynamics must be evaluated at the most important critical points. The first is the moment before booster drop off where missile reaches the highest speed, altitude and is still performing a pitching manoeuvre at a constant pitch rate. To provide the desired manoeuvrability and static stability, the fins of the missile (both on booster and the missile itself) must be sized properly, but accounting the effects of drag and aeroheating on the nose and the fins. Moreover, the span of the fins have a restriction of length imposed by the canister width, where they must be folded. The fitness function for aerodynamics is splitted in two parts, the first considering the missile body and the booster and the second only the missile body.

– Missile body and booster:

$$f = \frac{S(\alpha_{(L/D)_{max,B}}) S(|\alpha_{(L/D)_{max,W}} - \alpha_{(L/D)_{max,T}}|) \dot{q} (C_{D_0})^8 S(b_W) S(b_T) S(\frac{n}{\delta})}{S((L/D)_{max,B}) S((L/D)_{max,W}) S((L/D)_{max,T}) S(R_{LE,T}) S(R_{LE,W}) S(\bar{X})}$$

– Missile body:

$$f = \frac{S(\alpha_{(L/D)_{max,B}}) S(\alpha_{(L/D)_{max,W}}) \dot{q} (C_{D_0})^8 S(b_W) S(\frac{n}{\delta})}{S((L/D)_{max,B}) S((L/D)_{max,W}) S(R_{LE,W}) S(\bar{X})}$$

Parameter	Minimum Value	Maximum Value	Step Size	Units
Nose length	1.5	1.8	0.01	m
Missile length (no booster)	4	4.1	0.01	m
Semi-major axis a	0.05	Missile radius	10^{-3}	m
Nose radius	10^{-4}	0.07	10^{-4}	m
Eccentricity e	0.01	0.1	10^{-3}	-
Fin spacing angle (tail & wing)	30	70	0.1	°
Tail leading edge radius	5×10^{-3}	0.1	10^{-3}	m
Tail airfoil wedge angle	0	30	0.1	°
Tail root chord	Tail max semispan / 4	Tail max semispan	0.01	m
Tail tip chord	Tail max semispan / 8	Tail max semispan / 4	10^{-3}	m
Tail start position	Tail min start position	Tail max start position	0.01	m
Tail span	Tail max semispan / 4	Tail max semispan	10^{-3}	m
Wing leading edge radius	0.01	0.1	10^{-3}	m
Wing airfoil wedge angle	0	30	0.1	°
Wing root chord	Wing max semispan / 8	Wing max semispan / 4	0.01	m
Wing tip chord	Wing max semispan / 16	Wing max semispan / 8	0.01	m
Wing start position	Wing min start position	Wing max start position	0.01	m
Wing span	Wing max semispan / 8	Wing max semispan	10^{-3}	m

Table 6.2: List of constraints applied in the random individual creation of the body aerodynamics

- Propulsion: The length of the nose and the booster are the main parameters optimized in the aerodynamic phase having the most importance on propulsion design. Nose length is the restrictive parameter on intake design while booster length puts a limit on the amount of propellant the rocket motor can carry with it. The fitness function for propulsion is again splitted in two parts, the first concerning to the booster and the second to the scramjet.

– Rocket booster:

$$f = \frac{(\dot{\theta})^3 (q_{max})^2}{(v_{max})^4 (TWR)^4 (\theta_f)^4 (\sum h)^3 (\sum R)}$$

Parameter	Minimum Value	Maximum Value	Step Size	Units
Number of slots	3	12	1	-
Propellant outer radius	0.18	0.2	0.01	m
Slot length	0.1	0.16	0.01	m
Propellant inner radius	5×10^{-3}	10×10^{-3}	10^{-3}	m
Slot tip radius	5×10^{-4}	10×10^{-4}	10^{-4}	m
Pitch rate	1	5	0.1	° s ⁻¹
Final pitch	10	60	1	°

Table 6.3: List of constraints applied in the random individual creation of the propellant grain

– Scramjet engine:

$$f = \frac{(|h_{c_{desired}} - h_{c_{real}}|)(S(\dot{m}_f))}{S(\eta_c) S(\eta_{KE}) S(\eta_o) S\left(\frac{s_3 - s_0}{C_{pc}}\right) S\left(\frac{F}{\dot{m}_0}\right) S(I_{sp}) S(h_1) S(h_2) S(h_3) S(h_4) (M_4)^2}$$

Parameter	Minimum Value	Maximum Value	Step Size	Units
Ramp angle 1	1	7	0.1	°
Ramp angle 2	1	9	0.1	°
Ramp angle 3	1	14	0.1	°
Longitude ramp 1	0.01	1.5	0.01	m
Longitude ramp 2	0.01	1	0.01	m
Longitude lip	1	1.5	0.01	m
Altitude	20	30	0.1	km

Table 6.4: List of constraints applied in the random individual creation of the scramjet engine

- Trajectory: Although it is considered a different part of the optimization, it has strong relationship with propulsion, where they are evaluated together. The gravity turn is optimized together with the port of the propellant, whereas the scramjet is first optimized for cruise conditions and then its performance evaluated at lower altitudes and lower speeds for climbing to the desired cruise altitude. Here comes the meaning of iteration, where an aerodynamic solution must be good enough with low drag but it has a shorter booster length, carrying less propellant and thus, making difficult the start of the scramjet engine. Through this iteration, new limits and constraints are assigned inside the margin of pseudorandom numbers generators, and in this project it has been done manually, resulting in a practical but tedious method.

– Constant θ climb:

$$f = q_{max} t_c (m_f)^3 (\dot{q})^2$$

Parameter	Minimum Value	Maximum Value	Step Size	Units
TWR start	2	4	1	-
Climb angle	Final Pitch / 4	Final Pitch	10.25	°

Table 6.5: List of constraints applied in the random individual creation of the constant climb angle phase

CHAPTER 7. RESULTS

The results obtained in this project are only a measure of performance of the missile, and they can also be used to design the first conceptual CAD model. Those final results could also be improved by adding additional constraints and requirements to our missile design like minimum Radar Cross Section (RCS), structural analysis, complex heat transfer studies to evaluate the insulation materials of the airframe, Infrared emission due to radiation and coming out of the scramjet nozzle, etc. Those parameters are considered when evaluating the survivability of the missile in detail, however they require more advanced simulation tools and time.

7.1. Warhead

As we expected, the algorithm tried to find the lightest warhead while giving priority to a small charge to mass ratio, since the detonation velocity of the HE is small, and less energy is available to accelerate fragments. The velocity of those fragments adjust to the requirements of 1600 m/s while the blast wave is high enough to ensure lethality at a radius of 3 m (more or less the sphere radius of 100m³ explosion). To find the most optimal solution, 300000 random individuals were generated in Monte Carlo simulation, ensuring enough variability.

Parameter	Value	Units
Miss distance	3	m
Casing inner radius	0.1404	m
Casing outer radius	0.2186	m
Casing longitude	0.2469	m
Explosive	HNS	-
Explosive density	1700	kg m ⁻³
Detonation velocity	7	km s ⁻¹
Charge to fragment mass ratio	1.4	-
Warhead total weight	200	kg
Terminal speed	1391	m s ⁻¹
Length over diameter penetrator	26	-
Penetrator nose length percentage	34	%
Penetrator nose length	0.0526	m
Penetrator total length	0.1546	m
Penetrator weight	0.067	kg
Ballistic limit velocity	1106.57	m s ⁻¹
Peak pressure	3.298	MPa
Total energy	753.95	MJ
Velocity fragments	1578.75	m s ⁻¹
Duration time	0.9705	s
Time damaging	0.342	s

Table 7.1: Final Warhead dimensions and performance

7.2. Aerodynamics

In this part we must notice the size of the nose, which represents about the 40% of the missile length (with not accounting the booster). This excessive nose length is required to meet the compression requirements but it may suppose a challenge for seeker design where the signal get worse as longer is the nose. Another important fact to highlight is the dimensions of the tail which tend to be engulfed in the fuselage at high speeds, increasing the complexity of folding it to fit properly on the VLS launcher. In this case, the Monte Carlo simulation was initialized with 2000 individuals, less than the warhead case due to the complexity of calculations.

Parameter	Value	Units
Nose type	Power series 3/4	-
Nose length	1.61	m
Missile length	4.09	m
Total missile plus booster length	6.2	m
Missile radius	0.28	m
Semi-major axis at nose	0.051	m
Semi-minor axis at nose	0.0211833	m
Body eccentricity	0.038	-
Spacing between fins and axis	65.5	°
Wing leading edge radius	0.013	m
Wing delta wedge	12.6	°
Wing root chord	0.27	m
Wing tip chord	0.14	m
Wing start position	3.82	m
Wing semispan	0.0765	m
Wing surface	0.031365	m ²
Load factor per unit deflection in rad of the missile alone	-726.904184	g/rad
Tail deflection for 60 g	-4.73	°
Tail leading edge radius	0.02	m
Tail delta wedge	3.5	°
Tail root chord	1.11	m
Tail tip chord	0.44	m
Tail start position	4.91	m
Tail semi span	0.05	m
Tail surface	0.03875	m ²
Load factor per unit deflection in rad of the missile and booster	-742.77781	g/rad
Missile reference surface	0.24625251	m ²
Tail taper ratio	0.3963964	-
Tail aspect ratio	0.03225806	-
Tail outboard center of pressure	0.02139785	m
Mean tail aerodynamic chord	0.82326882	m
Wing taper ratio	0.51851852	-
Wing aspect ratio	0.37317073	-

Wing outboard center of pressure	0.06841463	m
Mean wing aerodynamic chord	0.21186992	m
Semi-major axis of the body	0.28007551	m
Semi-minior axis of the body	0.27986956	m
Max L/D body (booster and missile body)	2.68563223	-
Max L/D wing (booster and missile body)	1.30409745	-
Max L/D tail (booster and missile body)	1.32589872	-
Max L/D α body (booster and missile body)	13	°
Max L/D α wing (booster and missile body)	10.3	°
Max L/D α tail (booster and missile body)	11.4	°
Max L/D body (missile body)	2.87409695	-
Max L/D tail (missile body)	1.30409745	-
Max L/D α body (missile body)	12	°
Max L/D α tail (missile body)	10.3	°
dCN/d α (booster and missile body)	16.8241294	-
dCN/d δ (booster and missile body)	-8.35861253	-
dCm/d α (booster and missile body)	-3.60308592	-
dCm/d δ (booster and missile body)	-57.6467806	-
dCN/d α (missile body)	19.8473319	-
dCN/d δ (missile body)	8.77111343	-
dCm/d α (missile body)	22.463907	-
dCm/d δ (missile body)	36.0695111	-
$\bar{X}_{missile\ plus\ booster}$	-0.11993061	-
$\bar{X}_{missile}$	0.63382766	-
$C_{D_{0,body\ plus\ booster}}$	0.62269062	-
$C_{D_{0,body}}$	0.33008212	-
Missile body CM	1.636	m
Missile body plus booster CM	3.1	m
Missile weight body	702	kg
Missile maximum heat transfer	18.8	MW s^{-1}

Table 7.2: Final Missile aerodynamics and missile flight performance

Finally, the CFD results of the nose for different angles of attack for density, temperature, pressure and velocity. The most important angles of attack are 0° corresponding to level flight, 12° corresponding to the angle of maximum L/D and 20.5° , corresponding to the climb angle of the missile.

The images below (figures 7.1, 7.2, 7.3, 7.4) shows us how the inlet of the scramjet reacts at different angles of attack, increasing the inlet temperature and decreasing the performance of the total compression. From the aerodynamic point of view, high angles of attack induce high wave drag and a disruption of the streamlines going into the inlet. All the figures, despite their angle of attack, show high stagnation temperatures on the missile's nose, ranging between 2800 K at the lowest angle of attack and 3800 K at the highest since it is less aerodynamic.

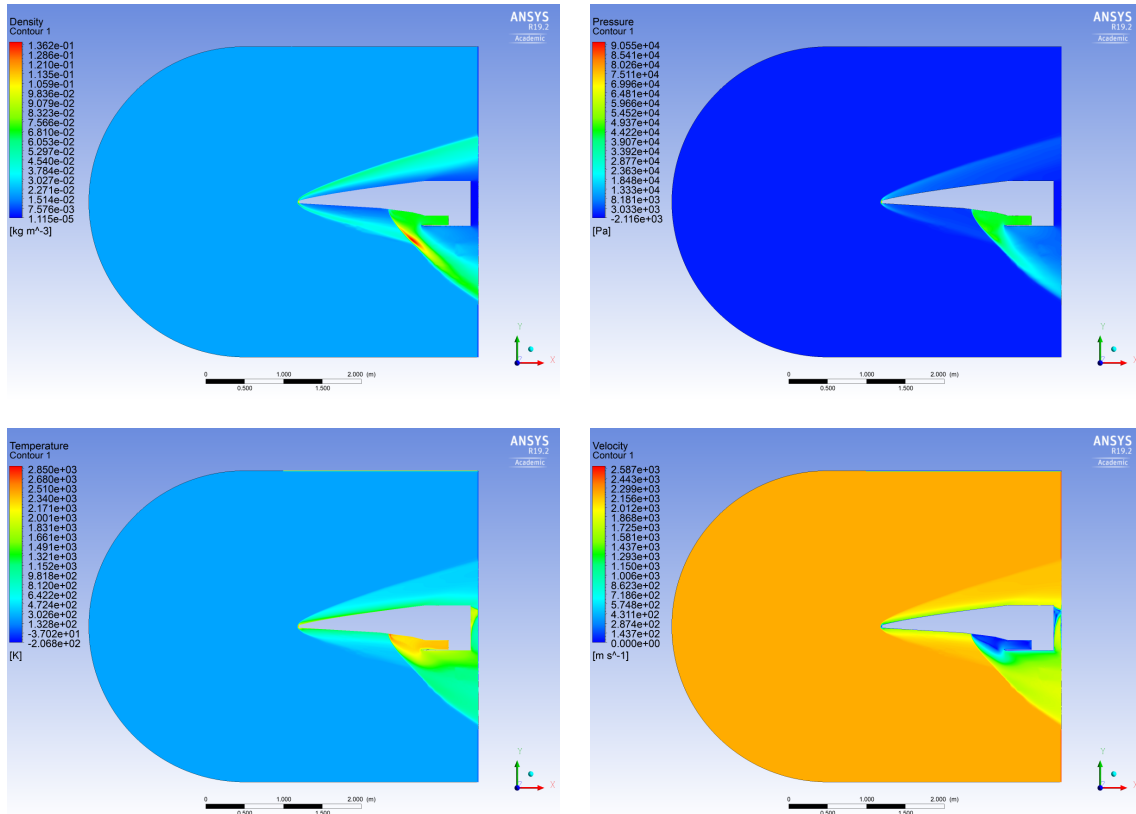


Figure 7.1: Nose and Scramjet inlet at $M = 7.35$ and $\alpha = 0^\circ$

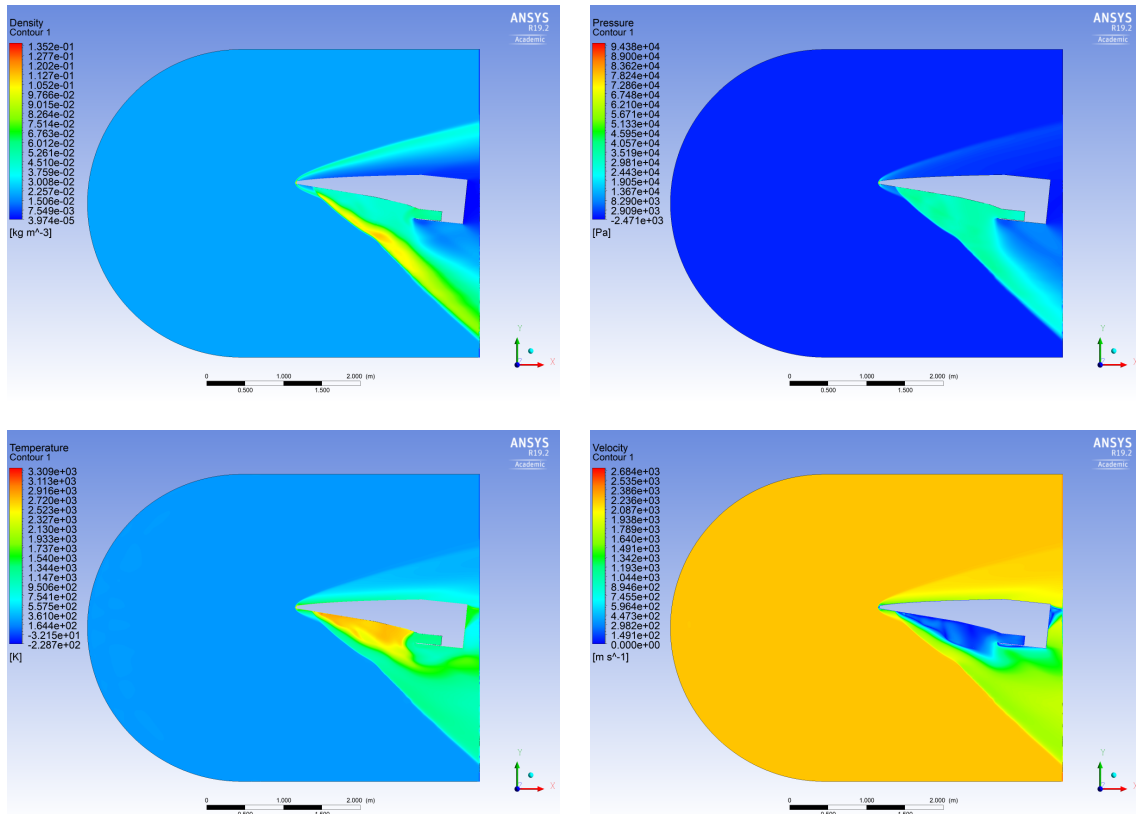


Figure 7.2: Nose and Scramjet inlet at $M = 7.35$ and $\alpha = 6^\circ$

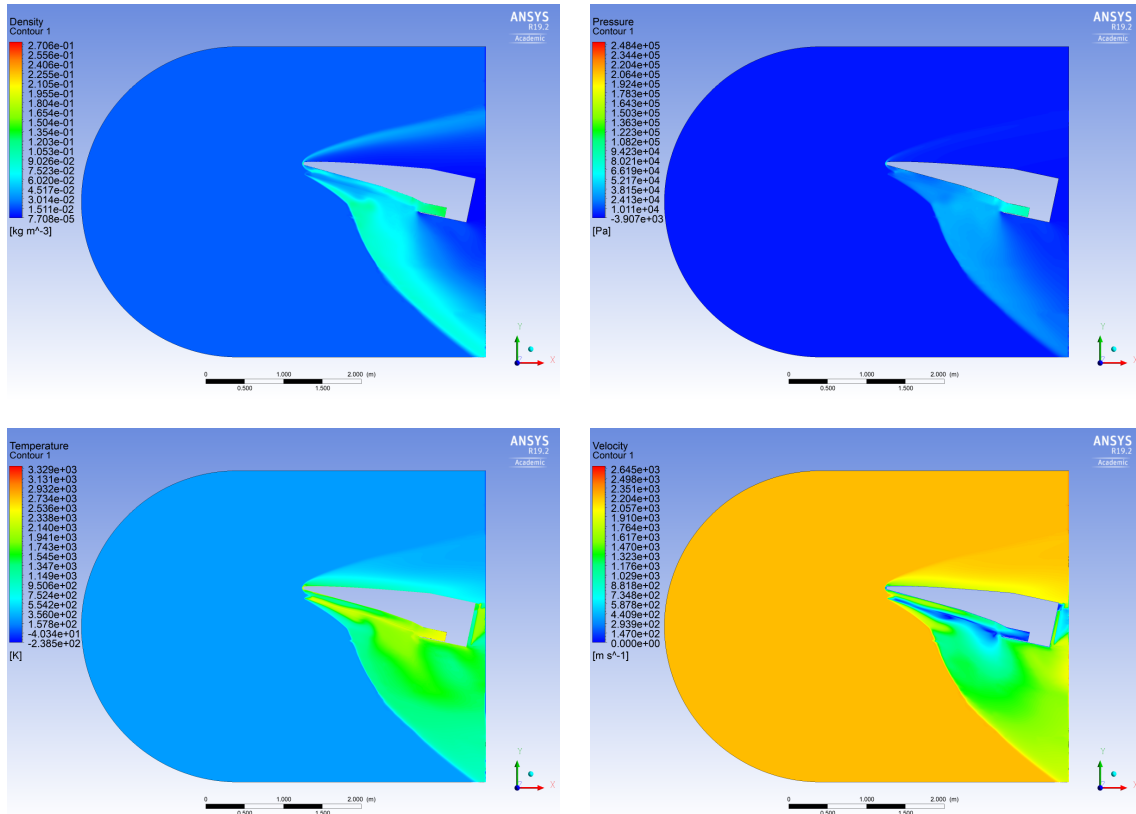


Figure 7.3: Nose and Scramjet inlet at $M = 7.35$ and $\alpha = 12^\circ$

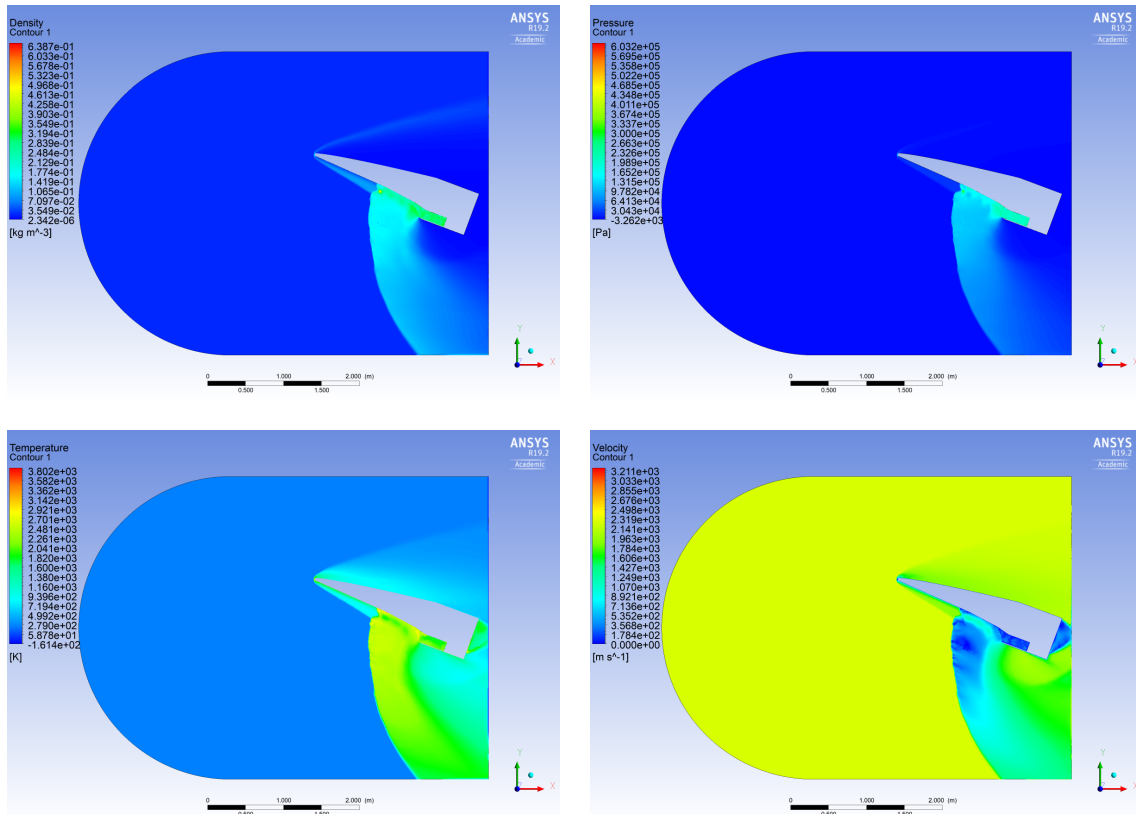


Figure 7.4: Nose and Scramjet inlet at $M = 7.35$ and $\alpha = 20.5^\circ$

7.3. Booster

The booster solution includes the 3D model of the propellant grain, and the evolution of thrust as a function of time. Notice that the nozzle takes an important part of the total booster size, decreasing the available propellant and thus the final ΔV . Taking into account that the required amount of propellant to accelerate the missile at almost Mach 5 speed (1715 m/s at SL) to start the scramjet was supposed to be 900 kg (assuming the worst I_{sp} of all the propellants eq. (D.9)), the total weight at the launch must be decreased by consider the volume filled by the nozzle an empty space. The propellant used in this case is PU/AP/Al or Polyurethane/Ammonium Perchlorate/Aluminium.

The genetic algorithm used in this case required 5 generations, 80 individuals and a mutation probability of 4 %. It was also calculated together with the take-off trajectory.

Parameter	Value	Units
Number of slots	9	-
Outer radius	0.2	m
Propellant slot length	0.16	m
Inner radius	0.008	m
Slot tip radius	0.0005	m
Propellant length	1.29	m
Diameter rocket booster	0.56	m
Pitch rate	0.2	$^{\circ} s^{-1}$
Final pitch	41	$^{\circ}$
Propellant type	PU/AP/Al	-
Nozzle exit area	0.246	m^2
Nozzle throat area	0.026	m^2
Nozzle length	0.82	m
Characteristic velocity	1615.96	$m s^{-1}$
Propellant mass	523.37	kg

Table 7.3: Final propellant grain dimensions and rocket performance

The cartridge of the propellant grain appears on figure 7.5.

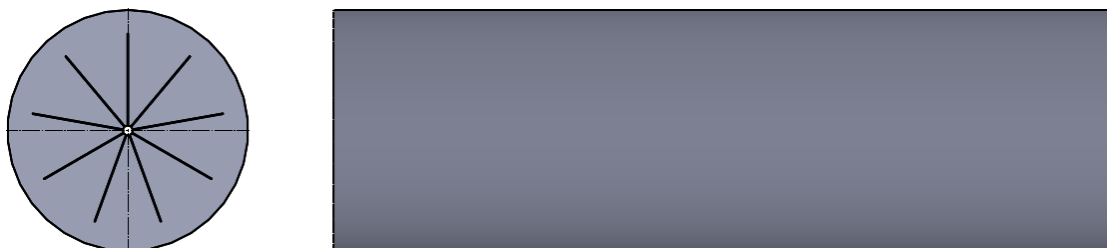


Figure 7.5: Propellant grain cartridge in different views

And in the following figures (7.6(a), 7.6(b), 7.6(c), 7.6(d)) there are represented different performance parameters of the solid rocket booster. Note that the vertical dashed line is the point where Scramjet must be turned on for a proper ascent to cruise altitude:

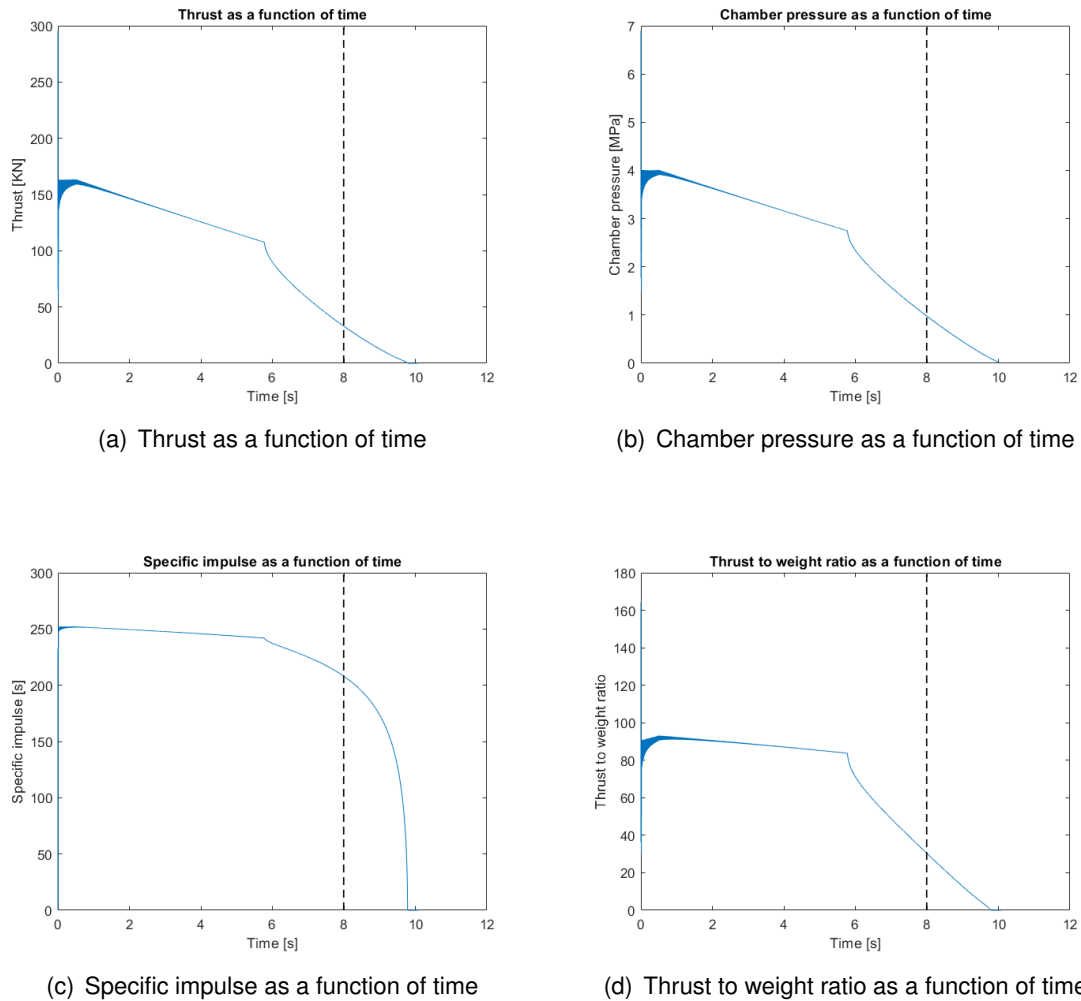


Figure 7.6: Missile booster technical data plots

7.4. Scramjet

Scramjet engine performance is analysed for 5 types of fuel and assuming 200 kg of it, and comparing which has the highest performance in cruising conditions. Methane has the highest specific impulse, and according to the Breguet range equation, it allows travelling further distances. The main problem of the analysed hydrocarbons in front of other military jet fuels like JP-10 and JP-7 studied by Wilson on reference [41], are their relatively low melting point temperatures and lower heating values. In other words, to storage methane a pressurized fuel vessel tank is required and thus increasing weight, the complexity of logistics and the danger for the crew operating the missile (more information about pressurized vessels in reference [47]). The genetic algorithm used in this case required 10 generations, 600 individuals and a mutation probability of 3 %.

Parameter	Methane	Ethane	Hexane	Octane	Ethylene	Units
δ_1	3.4	3.4	3.4	3.4	3.4	$^\circ$
δ_2	4	4	4	4	4	$^\circ$
δ_3	7.3	7.3	7.3	7.3	7.3	$^\circ$
δ_4	14.7	14.7	14.7	14.7	14.7	$^\circ$
h_1	0.0611	0.0611	0.0611	0.0611	0.0611	m
h_2	0.0545	0.0545	0.0545	0.0545	0.0545	m
h_3	0.0419	0.0419	0.0419	0.0419	0.0419	m
h_4	0.1218	0.1218	0.1218	0.1218	0.1218	m
$h_{c,desired}$	0.2795	0.2795	0.2795	0.2795	0.2795	m
L_1	1.03	1.03	1.03	1.03	1.03	m
L_2	0.42	0.42	0.42	0.42	0.42	m
L_3	0.16	0.16	0.16	0.16	0.16	m
L_{lip}	0.05	0.05	0.05	0.05	0.05	m
V_0	2234	2234	2234	2234	2234	ms^{-1}
Altitude	29400	29400	29400	29400	29400	m
Drag	1998.2716	1998.2716	1998.2716	1998.2716	1998.2716	N
$\frac{T_3}{T_0}$	3.3218	3.3218	3.3218	3.3218	3.3218	-
η_c	0.9402	0.9402	0.9402	0.9402	0.9402	-
η_{KE}	0.9855	0.9855	0.9855	0.9855	0.9855	-
M_3	3.567	3.567	3.567	3.567	3.567	Mach
P_3	53.271	53.271	53.271	53.271	53.271	kPa
$\frac{A_3}{A_0}$	76.124	76.124	76.124	76.124	76.124	-
T_4	2756.84	2771.53	2758.02	2755.34	2925.42	K
P_4	92.401	92.973	92.464	92.338	98.845	kPa
M_4	2.652	2.643	2.651	2.653	2.555	Mach
T_{10}	1367.72	1373.92	1368.17	1367.10	1439.03	K
V_{10}	3234.24	3236.45	3234.25	3234.06	3261.34	ms^{-1}
M_{10}	4.6839	4.6767	4.6832	4.6847	4.6062	Mach
$\frac{A_{10}^0}{A_0}$	4.3506	4.3845	4.3835	4.3824	4.581	-
π_c	0.7322	0.7317	0.7321	0.7322	0.7275	-
$\frac{F}{\dot{m}_0}$	1188.64	1204.45	1213.44	1214.83	1248.99	Ns kg^{-1}
C_{TS}	4.9×10^{-5}	5.18×10^{-5}	5.43×10^{-5}	5.46×10^{-5}	5.44×10^{-5}	$\text{kg N}^{-1} \text{s}^{-1}$
\dot{m}_f	0.0979	0.1035	0.1085	0.1092	0.1087	kg s^{-1}
η_{th}	0.9388	0.9252	0.9199	0.9193	0.88	-
η_p	0.8736	0.8768	0.8802	0.8807	0.8762	-
η_o	0.9594	0.9557	0.9598	0.9605	0.9156	-
I_{sp}	2080.74	1967.85	1877.16	1865.42	1874.03	s

Table 7.4: Final Scramjet dimensions and performance on cruise conditions

Finally, the results for the expansion nozzle with 120 characteristic lines are shown on figure 7.7. The maximum allowed height at the combustor exit is about 7 cm to allow the nozzle fitting properly on the missile. The total height of the nozzle at the end of the expansion is 54.68 cm and the total length of the nozzle is 2.335 m. The total available length of the scramjet combustor is 14.5 cm.

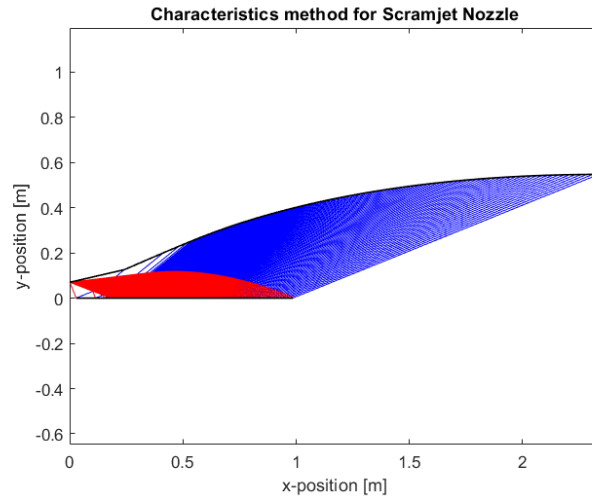
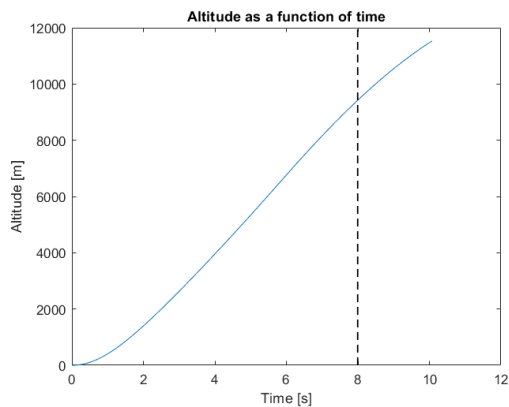


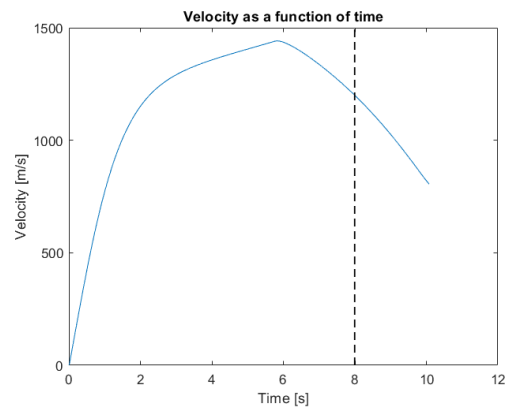
Figure 7.7: Characteristics method for Scramjet Nozzle

7.5. Trajectory

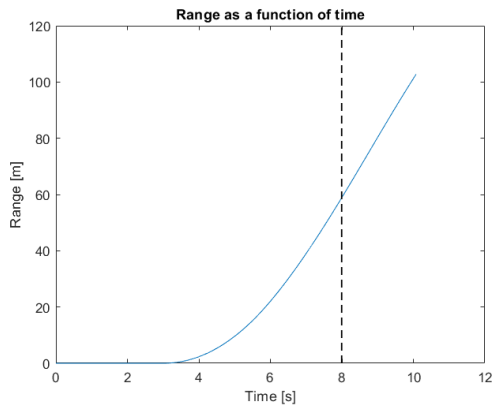
For the take-off phase. Note that the vertical dashed line is the point where Scramjet must be turned on for a proper ascent to cruise altitude, in this case at 9000 m and 1200 m s^{-1} :



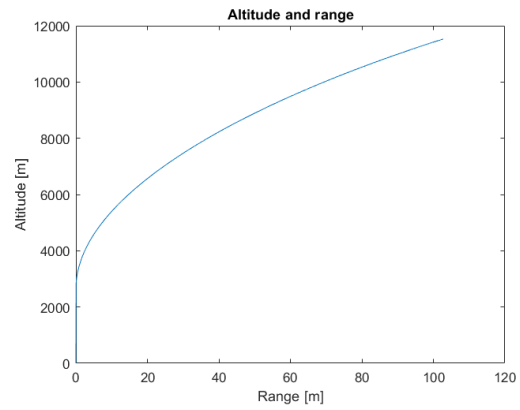
(a) Altitude as a function of time



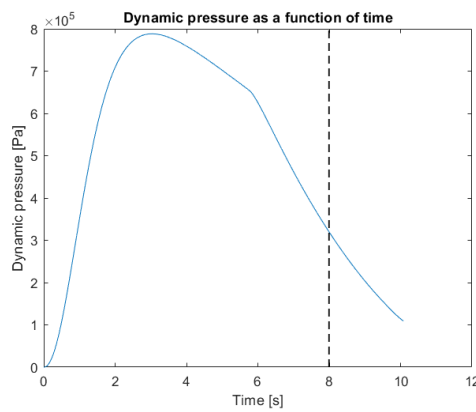
(b) Velocity as a function of time



(c) Range as a function of time



(d) Altitude and range



(e) Dynamic pressure as a function of time

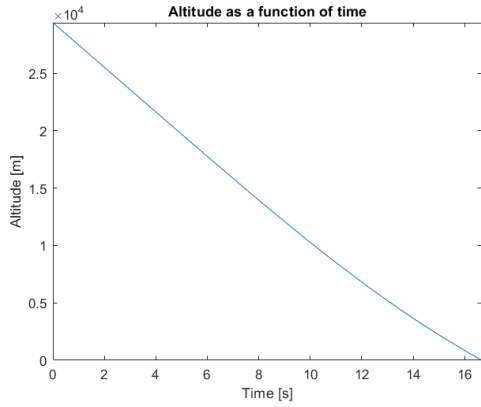
Figure 7.8: Take-off phase trajectory plots

For the constant climb angle phase:

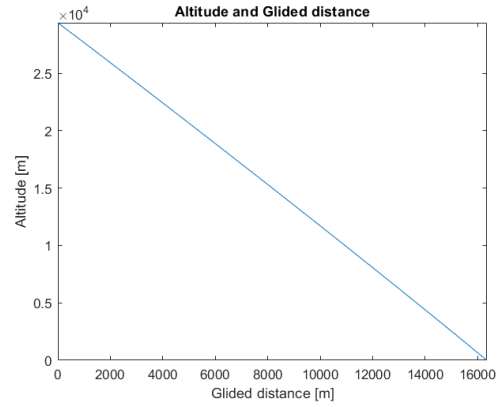
Parameter	Value	Units
TWR	2	-
Climb angle	20.5	$^{\circ}$
Fuel wasted	82.391	kg
Time to climb	40	s
Distance	53.75	km

Table 7.5: Parameters of the missile flying at a constant pitch angle

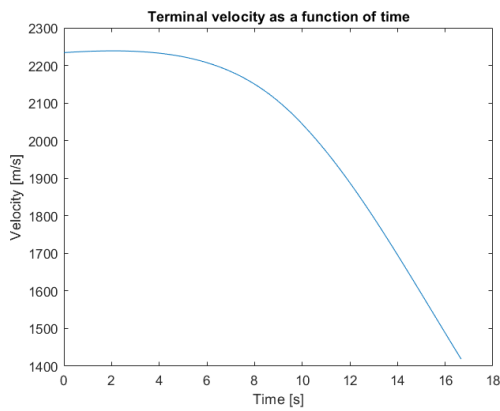
For the gliding phase:



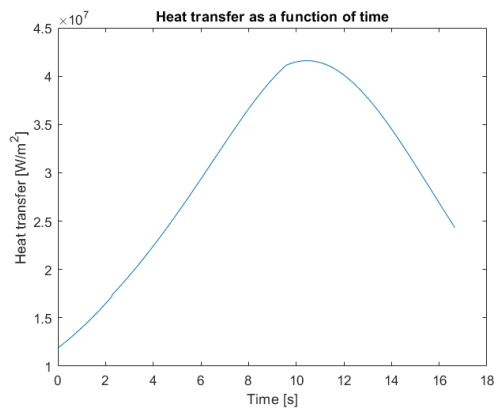
(a) Altitude as a function of time



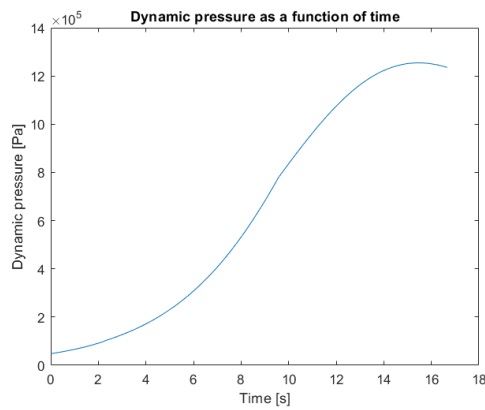
(b) Altitude and Glided distance



(c) Terminal velocity as a function of time



(d) Heat transfer as a function of time



(e) Dynamic pressure as a function of time

Figure 7.9: Gliding phase trajectory plots

7.6. General aspects

The following table contains the final data of the missile system, in round numbers and the images of the design.

Parameter	Value	Units
Launch Mass	1425	kg
Structural Mass (22%)	313.5	kg
Cruise Speed	7.35	Mach
Missile mass (no booster)	900	kg
Fuel mass (methane)	200	kg
Max range	2010	km
Ceiling	29400	m

Table 7.6: Technical data of the hypersonic missile

And finally, the CAD model of the hypersonic missile modelled with SolidWorks.

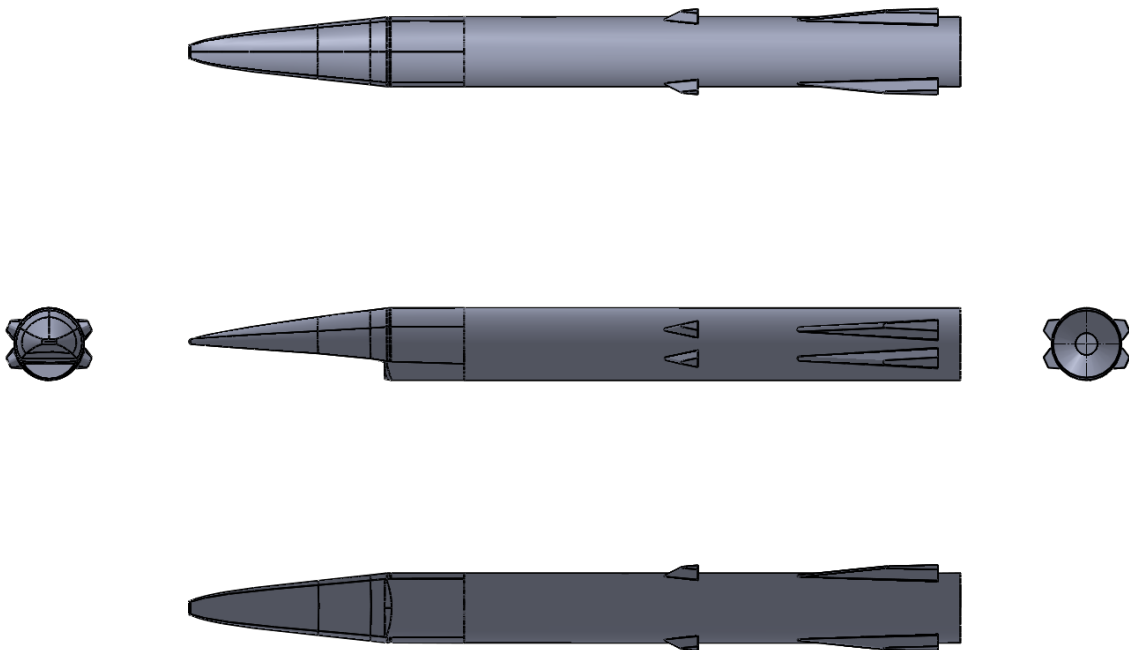


Figure 7.10: Final missile model with the booster in different views

CONCLUSIONS

Throughout this project, the main problems on designing a hypersonic cruise missile with very limiting constraints have emerged. Some of those problems are strongly related to a technological barrier, like the materials of the airframe and the scramjet combustor. Other problems such as the limited volume available for the solid propellant encourages scientists to investigate further on new higher density propellants with high specific impulses. Referring to scramjet engine, the most important technical challenge comes from the combustor, where low available lengths adds difficulties to a complete combustion of the fuel, meaning that new and high performance mixing methods must be developed. And at last but not least, the cruise Mach number is a reasonable value and an appropriate flight regime for hypersonic cruise missiles like 3M22 Zircon or BrahMos II missiles, but the total operational range is fairly optimistic.

In the aerodynamics field, the algorithm has been able to find an optimal solution for the nose, providing the minimum drag and the required amount of compression to start the scramjet at lower speeds. On the other hand, tail and wing fins have excessive sweepback angles, and tend to be engulfed by the main airframe, suiting to the predictions of reference [7], where the limits to consider a wing plus body configuration range between Mach 5 and 8. Above that limits, thicker wings to overcome heat transfer are required, but excessive leading edge radius cause a phenomena of viscous interactions with flow field and the body, caused by high pressure in front of the leading edge and a substantial reduction on L/D ratio as we have seen when designing the airfoil. Sharp leading edges improves L/D ratio but radiative cooling must be employed, and this technique is cost prohibitive for missiles.

One solution to avoid the usage of high sweepback control surfaces (especially in tail) is to use thrust vectoring control of the rocket motor. Two light weight candidates for a possible study are jet vanes and jet tabs, but the first needs to be coupled to an additional aerodynamic control. Jet tab is used in the Antiship Exocet MM40 and in the Tomahawk cruise missile whereas jet vanes are more likely to be used in SAM and AAM.

Regarding to genetic algorithms, they tend to find an optimal solution faster than the Monte Carlo simulation, but the best individual of a generation is susceptible to outperform in the crossover, if the best values of the fitness function are obtained on the first generation. Other disadvantages about genetic algorithm is its dependence on the initial generation of individuals, where if a bad set of individuals is created at the start, despite the crossover and mutation, there exists a high risk of having bad offspring at the end, or in other words, the probability of getting an acceptable fitness function value with bad parents is low. It seems obvious that to overcome this problem, high mutation rates are preferable, and then, an entire random population generated only once in Monte Carlo simulation resulted to be the possible answer to obtain better fitness function values.

Other improvements inside the algorithms are the use of other mathematical optimization techniques to better update the constraints of random parameters and avoid using the classical trial and error technique, which can be tedious and inefficient in some cases. One of the possible methods to improve our design consists on applying the local search method, which is useful when the number of possible variables is huge (large search space) and initially a good enough solution can be calculated. So far, the only requirements needed to start the optimization process are an initial solution, new operators to change the solution

and a fitness function to direct the search comparing different solutions and getting the best value among that neighbour solutions.

With this method, known as hill climbing (in this case we look for a minimum), only the first solution must be initialized with pure randomness while the following are only resetting the initial constraints and only focusing on the values which give at each iteration better fitness values. However, with this algorithm we must deal with the same problem as before, where a local minimum of the function is found but maybe it is not the global minimum. A method to solve this problem is by initializing different solutions at the start and try to find the global minimum from different positions.

Overall, it seems that the Mk-41 VLS is capable of handling an hypersonic missile but the constraints of the launcher are strong limiting factors, especially from the scramjet combustor point of view. Other VLS system is the Mk-57, but is only installed on the US Zumwalt Class Destroyer. Nowadays, the most effective platforms to launch hypersonic missiles are from aircrafts like the Kinzhal missile or from rockets when considering HGVs (Hypersonic Glide Vehicles) like the AHW or the Avangard. The benefits of launching from an aircraft are basically less amount of propellant in the booster.

BIBLIOGRAPHY

- [1] “Hypersonic Weapon Basics – Missile Defense Advocacy Alliance.” missiledefenseadvocacy.org/missile-threat-and-proliferation/missile-basics/hypersonic-missiles/. 3
- [2] J. White, et al. “Affordable Hypersonic Missiles for Long-Range Precision Strike.” *Johns Hopkins APL technical digest*, vol. 20(3), pp. 415-427, 1999.
- [3] Ghoshal, Debalina. “Hypersonic Weapons: The new age of weapon systems.” *Instituto Español de Estudios Estratégicos*, Sept. 2018.
- [4] Fleeman, Eugene L., and Joseph A. Schetz. *Missile Design and Systems Engineering*. American Institute of Aeronautics & Astronautics, 2012. ix, 19, 25, 26, 35
- [5] Christos, Ioannis. “Design Drivers for Anti-Ship and Land-Attack Missiles.” *Cranfield University*, Sept. 2013. 33, 39
- [6] N. Nielsen, Jack. “The Present Status and the Future of Missile Aerodynamics.” *National Aeronautics and Space Administration*, Jan. 1988.
- [7] J. Becker, John. “Studies of High Lift/ Drag Ratio Hypersonic Configurations.” *International Council of the Aeronautical Sciences*, 1964. ix, 13, 63
- [8] H. Carlson, Charles. “Preliminary Scramjet Design for Hypersonic Airbreathing Missile Application.” *National Aeronautics and Space Administration*, Nov. 1983.
- [9] Ender, Tom, and Erin McClure. “Development of an Integrated Parametric Environment for Conceptual High Speed Missile Sizing.” *AIAA’s Aircraft Technology, Integration, and Operations (ATIO) 2002 Technical Forum*, 2002. 5
- [10] Alkamdawi, Hani, et al. “Hypersonic Aircraft Design.” *The Ohio State University*, Nov. 1989.
- [11] Demiral, Ertan. “Conceptual Aerodynamic Design of Ramjet Missiles.” *Middle East Technical University*, Jan. 2017. 5
- [12] B. Anderson, Murray. “Conceptual Missile Design Using Genetic Algorithms.” *NATO/Von-Kármán Institute*, June 2003. 6, 43
- [13] R. Redmon, Danny. “Tactical Missile Conceptual Design.” *Naval Postgraduate School*, Sept. 1980. 6
- [14] “World Missiles.” *Missile Threat*, missilethreat.csis.org/missile/. 6
- [15] Arslan, Kivanç. “Aerodynamic Optimization of Missile External Configurations.” *Middle East Technical University*, Sept. 2014. 43
- [16] Broglia, Alessandro. “Preliminary Design of Waverider Aircraft.” *Politecnico di Milano*, Apr. 2016. 43
- [17] Advisory Group for Aerospace Research & Development. *Special Course on Missile Aerodynamics*. North Atlantic Treaty Organization, 1994. 9, 75

- [18] G. Moore, Frank, et al. "Second-Order Shock-Expansion Theory to include Real Gas Effects." *Naval Surface Warfare Center*, Feb. 1992. 10
- [19] Anderson, John D. *Hypersonic and High Temperature Gas Dynamics*. 2nd ed., AIAA, 2006. 11, 74
- [20] J. Hopkins, Edward. "Charts for predicting Turbulent Skin Friction from the Van Driest Method (II)." *National Aeronautics and Space Administration*, Oct. 1972. 12
- [21] A. Penland, Jim. "Aerodynamic Force Characteristics of a Series of Lifting Cone and Cone-Cylinder Configurations at a Mach Number of 6.83 and Angles of Attack up to 130°." *National Aeronautics and Space Administration*, June 1961. 12
- [22] S. Stivers, Louis. "Calculated Pressure Distributions and Components of Total-Drag Coefficients for 18 Constant-Volume Slender Bodies of Revolution at Zero Incidence for Mach Numbers from 2.0 to 12.0, with Experimental Aerodynamic Characteristics for Three of the Bodies." *National Aeronautics and Space Administration*, Oct. 1971. 12
- [23] L. Talbot, et al. "Hypersonic Viscous Flow Over Slender Cones." *University of California at Berkeley and University of Michigan* 12
- [24] Ming Lee, Hsiung, et al. "Hypersonic Flow Past a Slender Elliptic Cone." *University of Oklahoma*, Nov. 1978. 12
- [25] H. Jorgensen, Leland. "Prediction of Static Aerodynamic Characteristics for Space-Shuttle-Like and Other Bodies at Angles of Attack from 0° to 180°." *National Aeronautics and Space Administration*, Jan. 1973. 12, 76
- [26] H. Jorgensen, Leland. "A Method for estimating Static Aerodynamic Characteristics for Slender Bodies of Circular and Noncircular Cross Section Alone and with Lifting Surfaces at Angles of Attack from 0° to 90°." *National Aeronautics and Space Administration*, Apr. 1973. 12, 13, 77
- [27] W. Cleary, Joseph, et al. "Theoretical Aerodynamic Characteristics of Sharp and Circularly Blunt-Wedge Airfoils." *National Aeronautics and Space Administration*, July 1964. 14, 79
- [28] Tenney, D.R., et al. "MATERIALS AND STRUCTURES FOR HYPERSONIC VEHICLES." *National Aeronautics and Space Administration*, Oct. 1988. 15
- [29] Frazer, R. Kelly. "EVALUATION OF SILICON NITRIDE AS AN ADVANCED RADOME MATERIAL." *Johns Hopkins APL Technical Digest*, vol. 13(3), pp. 393-399, Nov. 1992. 16
- [30] Chen, Fei, et al. "ELECTROMAGNETIC OPTIMAL DESIGN AND PREPARATION OF BROADBAND CERAMIC RADOME MATERIAL WITH GRADED POROUS STRUCTURE." *Progress In Electromagnetics Research*, vol. 105, pp. 445-461, 2010. 16
- [31] Schwarz, Arman. "Experimental Study of Hypersonic Wing/Fin Root Heating at Mach 8." *The University of Queensland*, 2014. 14

- [32] Kasen, Scott. "Thermal Management at Hypersonic Leading Edges." *University of Virginia*, May 2013. ix, 10, 16, 83
- [33] Oriden, Daniel. "Parametric Analysis of a Hypersonic Inlet using Computational Fluid Dynamics." *Arizona State University*, Nov. 2013. 16
- [34] Mölder, Sannu, et al. "Hypersonic Air Intake Design for High Performance and Starting." *North Atlantic Treaty Organization* 26
- [35] El-Sayed, Ahmed F. "Pulsejet, Ramjet, and Scramjet Engines." *Fundamentals of Aircraft and Rocket Propulsion*, Springer, 2016, pp. 364-386.
- [36] Chin, S. S. *Missile configuration design*. 1961. 85, 101
- [37] Sutton, George P., and Oscar Biblarz. *Rocket Propulsion Elements*. 7th ed., John Wiley & Sons, 2001. 89
- [38] H. Sloan. "Preliminary Solid Rocket Motor Design Techniques." *Naval Weapons Center*, Jan. 1979.
- [39] Tola, Ceyhun, and Melike Nikbay. "Internal Ballistic Modeling of a Solid Rocket Motor by Analytical Burnback Analysis." *Journal of Spacecraft and Rockets*, vol. 56, (2), pp. 498-516, 2019. ix, 20, 21, 90
- [40] Heiser, William H., and David T. Pratt. "Hypersonic Airbreathing Propulsion". *AIAA*, 1994. ix, 20, 24, 27, 95
- [41] Roberts, Kristen, and Donald Wilson. "Analysis and Design of a Hypersonic Scramjet Engine with a Transition Mach Number of 4.00." *47th AIAA Aerospace Sciences Meeting including The New Horizons Forum and Aerospace Exposition*, 2009. 57
- [42] Weidner, J., et al. "Scramjet integration on hypersonic research airplane concepts." *12th Propulsion Conference*, 1976. 28
- [43] Hartfield, Roy, et al. "A Review of Analytical Methods for Solid Rocket Motor Grain Analysis." *39th AIAA/ASME/SAE/ASEE Joint Propulsion Conference and Exhibit*, 2003. 19, 20
- [44] Kubota, Naminosuke. *Propellants and Explosives: Thermochemical Aspects of Combustion*. John Wiley & Sons, 2002. xi, 22
- [45] Folly, Patrick, and Peter Maeder. "Propellant Chemistry." *Schweizerische Chemische Gesellschaft*, vol. 58, (6), pp. 374-382, 2004. 22
- [46] Ceviz, M.A., and İ. Kaymaz. "Temperature and air-fuel ratio dependent specific heat ratio functions for lean burned and unburned mixture." *Energy Conversion and Management*, vol. 46, (15-16), pp. 2387-2404, Feb. 2005. 28
- [47] Megyesy, Eugene F. "Pressure Vessel Handbook". 12th ed., 2008. 57
- [48] Ul Islam Rizvi, S. T., et al. "Optimal trajectory analysis of hypersonic boost-glide waverider with heat load constraint." *Aircraft Engineering and Aerospace Technology*, vol. 87, (1), pp. 67-78, 2015. 6, 34, 36, 103

- [49] Siouris, George M. *Missile Guidance and Control Systems*. Springer Science & Business Media, 2006. [ix](#), [2](#), [37](#)
- [50] J. Eggers, Alfred, et al. "A Comparative Analysis of the Performance of Long-Range Hypervelocity Vehicles." *National Advisory Committee for Aeronautics*, pp. 1141-1160, 1957.
- [51] Urzay, Javier. "Supersonic Combustion in Air-Breathing Propulsion Systems for Hypersonic Flight." *Annual Review of Fluid Mechanics*, vol. 50, (1), pp. 593-627, 2018. [ix](#), [34](#)
- [52] Zhou, Hao, et al. "Hypersonic vehicle trajectory design based on optimal control theory." *Sixth International Symposium on Instrumentation and Control Technology: Sensors, Automatic Measurement, Control, and Computer Simulation*, 2006. [34](#)
- [53] Chai, Dong, et al. "Boost-skipping trajectory optimization for air-breathing hypersonic missile." *Aerospace Science and Technology*, vol. 46, pp. 506-513, 2015. [34](#), [36](#)
- [54] Lloyd, Richard M. "Blast Warhead Concepts." *Conventional Warhead Systems Physics and Engineering Design*, American Institute of Aeronautics & Astronautics, 1998, pp. 253-314. [ix](#), [40](#), [105](#)
- [55] Cooper, Paul W. *Explosives Engineering*. John Wiley & Sons, 1996.
- [56] U.S. Army Materiel Command. "Engineering Design Handbook: Warheads-General." July 1964. [39](#)
- [57] Holkko, Niko. "Mechanisms of Armour Penetration." *Tampere University of Technology*, 2015. [41](#), [107](#)
- [58] "Earth Atmosphere Model - Metric Units." NASA Glenn Research Center, 5 May 2015, www.grc.nasa.gov/WWW/k-12/airplane/atmosmet.html. [71](#)
- [59] "Specific Heats - Calorically Imperfect Gas." NASA Glenn Research Center, 12 2014, www.grc.nasa.gov/WWW/BGH/realspec.html. [73](#)

APPENDICES

APPENDIX A. ATMOSPHERE MODEL

The following equations can be found on reference [58].

For $h \leq 11000$ (Troposphere):

$$T = 15.04 - 0.00649h \quad (\text{A.1})$$

$$P = 101290 \left[\frac{T + 273.1}{288.08} \right]^{5.256} \quad (\text{A.2})$$

For $11000 < h \leq 25000$ (Lower Stratosphere):

$$T = -56.46 \quad (\text{A.3})$$

$$P = 22650 e^{1.73 - 0.000157h} \quad (\text{A.4})$$

For $h > 25000$ (Upper Stratosphere):

$$T = -131.21 + 0.00299h \quad (\text{A.5})$$

$$P = 2488 \left(\frac{T + 273.1}{216.6} \right)^{-11.388} \quad (\text{A.6})$$

Atmospheric density:

$$\rho = \frac{P}{0.2869 (T + 273.1)} \quad (\text{A.7})$$

where h is in m, T in $^{\circ}\text{C}$, P in Pa and ρ in Kg m^{-3} .

APPENDIX B. AERODYNAMIC DESIGN EQUATIONS

Specific heat definitions:

Specific heat at constant volume:

$$c_v = \left(\frac{de}{dT} \right)_v \quad (\text{B.1})$$

Specific heat at constant pressure:

$$c_p = \left(\frac{dh}{dT} \right)_p \quad (\text{B.2})$$

Specific heat ratio:

$$\gamma = \frac{c_p}{c_v} \quad (\text{B.3})$$

Universal gas constant:

$$R = c_p - c_v \quad (\text{B.4})$$

The following equations can be found on reference [59].

Calorically imperfect gas (air case):

$$c_v = c_{v_{perf}} \left[1 + (\gamma_{perf} - 1) \left[\left(\frac{\theta}{T} \right)^2 \frac{e^{\frac{\theta}{T}}}{(e^{\frac{\theta}{T}} - 1)^2} \right] \right] \quad (\text{B.5})$$

$$c_p = c_{p_{perf}} \left[1 + \frac{(\gamma_{perf} - 1)}{\gamma_{perf}} \left[\left(\frac{\theta}{T} \right)^2 \frac{e^{\frac{\theta}{T}}}{(e^{\frac{\theta}{T}} - 1)^2} \right] \right] \quad (\text{B.6})$$

$$\gamma = 1 + \frac{\gamma_{perf} - 1}{1 + (\gamma_{perf} - 1) \left[\left(\frac{\theta}{T} \right)^2 \frac{e^{\frac{\theta}{T}}}{(e^{\frac{\theta}{T}} - 1)^2} \right]} \quad (\text{B.7})$$

Where c_v , c_p and R are expressed in $\text{kJ kg}^{-1} \text{K}^{-1}$, $\theta = 5500^\circ \text{R}$ and $\gamma_{perf} = 1.4$.

Local surface inclination methods:

The following equations can be found on reference [19].

Newtonian theory:

$$C_p = 2 \sin^2 \theta \quad (\text{B.8})$$

Modified Newtonian theory:

$$C_p = C_{p_{max}} \sin^2 \theta \quad (\text{B.9})$$

$$C_{p_{max}} = \frac{2}{\gamma M_\infty^2} \left(\frac{p}{p_\infty} - 1 \right) \quad (\text{B.10})$$

$$\frac{p}{p_\infty} = \left[\frac{(\gamma + 1)^2 M_\infty^2}{4\gamma M_\infty^2 - 2(\gamma - 1)} \right]^{\frac{\gamma}{\gamma - 1}} \left[\frac{1 - \gamma + 2\gamma M_\infty^2}{\gamma + 1} \right] \quad (\text{B.11})$$

Newton-Busemann method:

$$C_{p_i} = 2 \sin^2 \theta_i + 2 \left[\frac{d\theta}{dy} \right]_i \sin \theta_i \int_0^{y_i} \cos \theta dy \quad (\text{B.12})$$

where θ is the local surface inclination angle, C_p is the pressure coefficient and M_∞ the freestream Mach number.

Missile nose design:

Haack series type:

$$\theta = \cos^{-1} \left(1 - \frac{2x}{L} \right) \quad (\text{B.13})$$

$$y = \frac{R}{\sqrt{\pi}} \sqrt{\theta - \frac{\sin 2\theta}{2} + C \sin^3 \theta} \quad (\text{B.14})$$

where L is the total nose length, x the distance from the nose radome, y the height of the radome at a given point x , R the maximum radius, $C=0$ for a Von Kármán type (LD-Haack), $C = \frac{1}{3}$ for a LV-Haack and $C = \frac{2}{3}$ for a tangent type.

Power series type:

$$y = R \left(\frac{x}{L} \right)^n \quad (\text{B.15})$$

and for n ranging from 0 to 1.

Missile body aerodynamics:

The following equations can be found on reference [17].

Axial skin friction force coefficient:

Start by applying the Van Driest II Method for Skin Friction Drag

$$A = \sqrt{\left[\frac{(\gamma - 1) M_\infty^2}{2 \frac{T_W}{T_\infty}} \right]} \quad (\text{B.16})$$

$$B = \frac{1 + \frac{\gamma - 1}{2 M_\infty^2}}{\frac{T_W}{T_\infty}} - 1 \quad (\text{B.17})$$

$$C_1 = \frac{2A^2 - B}{\sqrt{B^2 + 4A^2}} \quad (\text{B.18})$$

$$C_2 = \frac{B}{\sqrt{B^2 + 4A^2}} \quad (\text{B.19})$$

$$\frac{T_W}{T_\infty} = 1 + 0.9 \frac{\gamma - 1}{2} M_\infty^2 \quad (\text{B.20})$$

$$\frac{\mu}{\mu_\infty} = \left(\frac{T_W}{T_\infty} \right)^n \quad (\text{B.21})$$

and from Sutherland viscosity law

$$\mu_{\infty} = \mu_0 \left(\frac{T}{T_0} \right)^{\frac{3}{2}} \left(\frac{T_0 + S}{T + S} \right) \quad (\text{B.22})$$

$$R_{e_{\infty}} = \frac{\rho_{\infty} V_{\infty} l}{\mu_{\infty}} \quad (\text{B.23})$$

$$\frac{0.242 (\sin^{-1} C_1 + \sin^{-1} C_2)}{A \sqrt{C_{f_{\infty}} \left(\frac{T_W}{T_{\infty}} \right)}} = \log_{10} (R_{e_{\infty}} C_{f_{\infty}}) - \left(\frac{1 + 2n}{2} \right) \log_{10} \left(\frac{T_W}{T_{\infty}} \right) \quad (\text{B.24})$$

where $C_{f_{\infty}}$ is calculated iteratively.

and finally we get the skin friction axial force coefficient

$$C_{AF} = C_{f_{\infty}} \frac{S_{wet}}{S_{ref}} \quad (\text{B.25})$$

where n the power law index of value equal to 1 for newtonian fluid (air in this case), $\mu_0 = 1.7894 \times 10^{-5}$ kg/ms, $T_0 = 273.11$ K, $S = 110.56$ K, S_{wet} the area in contact with the fluid and S_{ref} the frontal area of the missile.

The following equations can be found on reference [25].

Axial base force coefficient:

Initially, we calculate the base pressure coefficient

$$C_{PB} = \frac{2}{\gamma M_{\infty}^2} \left[\left(\frac{2}{\gamma + 1} \right)^{1.4} \left(\frac{1}{M_{\infty}} \right)^{2.8} \left[\frac{2\gamma M_{\infty}^2 - (\gamma - 1)}{\gamma + 1} \right] - 1 \right] \quad (\text{B.26})$$

and finally we get

$$C_{AB} = -C_{PB} \quad (\text{B.27})$$

Axial wave force coefficient:

$$\beta = \sqrt{M_\infty^2 - 1} \quad (\text{B.28})$$

$$\theta = \tan^{-1} \left(\frac{d}{2l_N} \right) \quad (\text{B.29})$$

$$C_{A_w} = \frac{(4 \sin^2 \theta) (2.5 + 8 \beta \sin \theta)}{1 + 16 \beta \sin \theta} \quad (\text{B.30})$$

θ is also known as the nose cone half-angle and $\gamma = 1.4$.

Finally the total axial force coefficient for an angle of attack of $\alpha = 0^\circ$

$$C_{A_{\alpha=0}} = C_{A_F} + C_{A_B} + C_{A_w} \quad (\text{B.31})$$

and for each angle of attack it yields to

$$C_A = C_{A_{\alpha=0}} \cos^2 \alpha \quad (\text{B.32})$$

The following equations can be found on reference [26].

Normal force coefficient:

$$\left(\frac{C_N}{C_{N_o}} \right)_{SB} = \left(\frac{C_m}{C_{m_o}} \right)_{SB} = \left(\frac{C_n}{C_{n_o}} \right)_{SB} \quad (\text{B.33})$$

$$\left(\frac{C_N}{C_{N_o}} \right)_{Newt} = \left(\frac{C_m}{C_{m_o}} \right)_{Newt} = \left(\frac{C_n}{C_{n_o}} \right)_{Newt} \quad (\text{B.34})$$

$$\left(\frac{C_n}{C_{n_o}} \right)_{SB} = \frac{a}{b} \cos^2 \phi + \frac{b}{a} \sin^2 \phi \quad (\text{B.35})$$

$$\left(\frac{C_n}{C_{n_o}} \right)_{Newt} = \frac{3}{2} \sqrt{\frac{a}{b}} \left[\frac{-\frac{b^2}{a^2}}{\left(1 - \frac{b^2}{a^2}\right)^{\frac{3}{2}}} \log \left[\frac{a}{b} \left(1 + \sqrt{1 - \frac{b^2}{a^2}}\right) \right] + \frac{1}{1 - \frac{b^2}{a^2}} \right] \quad (\text{B.36})$$

where the subscript o refers to a circular cross-section body, ϕ is the bank angle, a the semimajor axis and b the semiminor axis.

$$C_N = \left(\frac{A_b}{A_r} \sin 2\alpha \cos \frac{\alpha}{2} \right) \left[\frac{1}{l} \int_0^l \left(\frac{C_n}{C_{no}} \right)_{SB} dx \right] + \left(\eta C_{dn} \frac{A_p}{A_r} \sin^2 \alpha \right) \left[\frac{1}{l} \int_0^l \left(\frac{C_n}{C_{no}} \right)_{Newt} dx \right] \quad (\text{B.37})$$

$$C_m = \frac{\sin 2\alpha \cos \frac{\alpha}{2}}{A_r X} \int_0^l \left(\frac{C_n}{C_{no}} \right)_{SB} \frac{dA}{dx} (x_{cg} - x) dx + \frac{2\eta C_{dn} \sin^2 \alpha}{A_r X} \int_0^l \left(\frac{C_n}{C_{no}} \right)_{Newt} r (x_{cg} - x) dx \quad (\text{B.38})$$

$$C_{dn} = \frac{2}{3} C_{pmax} \quad (\text{B.39})$$

where C_{dn} is the crossflow drag coefficient and η the crossflow drag proportionality factor, which is 1 for hypersonic regime. Moreover, A_r is the reference area, X the reference length (taken as the diameter) and x_{cg} the body center of mass position.

Aerodynamic force center:

$$x_{ac} = \left(\frac{x_{cg}}{X} - \frac{C_m}{C_N} \right) X \quad (\text{B.40})$$

Center of pressure:

$$X_{cp} = l_n + \frac{1}{2}(l - l_n) \quad (\text{B.41})$$

where l_n is the nose length and l the missile length (with booster or the missile only).

Body Lift and Drag coefficients:

$$C_L = C_N \cos \alpha - C_A \sin \alpha \quad (\text{B.42})$$

$$C_D = C_N \sin \alpha + C_A \cos \alpha \quad (\text{B.43})$$

Missile tail airfoil aerodynamics:

Taper ratio:

$$\lambda = \frac{c_{tip}}{c_{root}} \quad (\text{B.44})$$

Aspect ratio:

$$AR = \frac{b^2}{S} = \frac{2b}{(1+\lambda)c_{root}} \quad (\text{B.45})$$

Outboard center of pressure:

$$y_{cp} = \frac{\left(\frac{b}{6}\right)(1+2\lambda)}{1+\lambda} \quad (\text{B.46})$$

Mean aerodynamic chord:

$$c_{mac} = \frac{\left(\frac{2}{3}\right)c_{root}(1+\lambda+\lambda^2)}{1+\lambda} \quad (\text{B.47})$$

Chord at any position on the span:

$$c(y) = \frac{2S}{(1+\lambda)b} \left[1 - \frac{1-\lambda}{b}y \right] \quad (\text{B.48})$$

Tail & Wing max semispan:

$$\left(\frac{b}{2}\right)_{max} = \frac{r(1-\cos\theta)}{\sin\theta} \quad (\text{B.49})$$

where b is the span of the missile, S the wing area, y the position of the airfoil along the span, r is the cannister radius (or maximum radius of the missile) and θ is the angle between each wing/tail fin and the axis of the missile body.

The following equations can be found on reference [27].

Pressure coefficient for a blunt-wedge airfoil:

$$C_p = \frac{2}{\gamma+1} \left[1 + \gamma \sin^2 (\alpha + \delta_w) - \cos (\alpha + \delta_w) \sqrt{1 - \frac{4}{M_\infty^2} - \gamma^2 \sin^2 (\alpha + \delta_w)} \right] \quad (\text{B.50})$$

Pressure coefficient at detachment point:

$$C_{pD} = \frac{2}{\gamma} \left[\frac{\gamma+1 - \left(\frac{4}{M_\infty^2}\right)}{\gamma+1} \right] \quad (\text{B.51})$$

Section lift coefficient:

$$(c_l - c_{l_e}) = C_p \cos (\alpha + \delta_w) \left[\frac{1 - \frac{R}{c} (1 - \sin \delta_w)}{\cos \delta_w} \right] \quad (\text{B.52})$$

$$c_{l_e} = -\frac{RC_{p_{max}}}{3c} \sin^3 (\alpha + \delta_w) \quad (\text{B.53})$$

$$C_L = \int_0^{\frac{b}{2}} c_l(y) dy \quad (\text{B.54})$$

note that since we are only considering one tail fin in the analysis, we only integrate over the half span b .

Section drag coefficient:

$$(c_d - c_{d_e}) = C_p \sin (\alpha + \delta_w) \left[\frac{1 - \frac{R}{c} (1 - \sin \delta_w)}{\cos \delta_w} \right] \quad (\text{B.55})$$

$$c_{d_e} = \frac{RC_{p_{max}}}{c} \left[\frac{2}{3} + \cos (\alpha + \delta_w) - \frac{1}{3} \cos^3 (\alpha + \delta_w) \right] \quad (\text{B.56})$$

$$C_D = \int_0^{\frac{b}{2}} c_d(y) dy \quad (\text{B.57})$$

Section pitching moment coefficient:

$$\left[c_m - \left(\frac{x'}{c} - \frac{R}{c} \right) (c_{l_{le}} \cos \alpha + c_{d_{le}} \sin \alpha) \right] = C_p \cos \delta_w \left(\frac{x'}{c} - \frac{\tilde{x}'}{c} \right) \left[\frac{1 - \frac{R}{c} (1 - \sin \delta_w)}{\cos \delta_w} \right] \quad (\text{B.58})$$

and finally, for the remaining constants

$$\frac{\tilde{x}'}{c} = \frac{R}{c} + \frac{1}{2 \cos \delta_w} \left[\frac{1 - \frac{R}{c} (1 - \sin \delta_w)}{\cos \delta_w} \right] \quad (\text{B.59})$$

$$\frac{x'}{c} = 0.4 \quad (\text{B.60})$$

where c is the chord length, R is the leading edge radius, δ_w the wedge inclination angle of the airfoil, α the angle of attack, x' the body axis coordinate and \tilde{x}' the center of pressure of windward wedge surface.

Tail-body interferences:

Interference factors of normal force coefficients for tail and body:

$$S = \frac{\frac{b}{2} + r}{r} \quad (\text{B.61})$$

$$k_b = \frac{2}{\pi(S-1)^2} \left[\frac{\pi(S^2-1)^2}{4S^2} - \frac{(S^2-1)}{S} + \frac{(S^2-1)^2}{2S^2} \sin^{-1} \left(\frac{S^2-1}{S^2+1} \right) \right] \quad (\text{B.62})$$

$$k_w = \frac{2}{\pi(S-1)^2} \left[\frac{\pi(S^2-1)^2}{4S^2} + \frac{(S^2-1)}{S} + \frac{(S^2-1)^2}{2S^2} \sin^{-1} \left(\frac{S^2-1}{S^2+1} \right) \right] \quad (\text{B.63})$$

where r is the missile radius and $\frac{b}{2}$ the span of one tail fin.

Correction for taper ratio:

$$r_m = \frac{r}{\frac{b}{2} + r} \quad (\text{B.64})$$

$$v_{b,\eta} = v_{w,\eta} = v_\eta = 1 + \frac{r_m(1-r_m)}{(1+r_m)^2} \left(1 - \frac{1}{\lambda}\right) \quad (\text{B.65})$$

Correction for boundary layer effect:

$$r' = r + \delta' \quad (\text{B.66})$$

$$\delta' = 0.125 \left(\frac{0.37}{R_{L_1}^{0.2}} \right) L_1 \quad (\text{B.67})$$

$$L_1 = X_w + \frac{c_{root}}{2} \quad (\text{B.68})$$

$$r_m = \frac{r'}{\frac{b}{2} + r} \quad (\text{B.69})$$

$$\bar{\delta}' = \frac{\delta'}{r} \quad (\text{B.70})$$

$$v_{b,bt} = v_{w,bv} = v_{bt} = 1 - \frac{r_m(1+r_m^2) \left[r_m + r_m(1+3r_m) - 1 \right] \bar{\delta}'}{\lambda} \quad (\text{B.71})$$

where X_w is the distance from missile nose to tail fin root, δ' is the thickness of the boundary layer, and R_{L_1} the reynolds number evaluated for a distance L_1 .

Wing-tail interferences:

Correction for not remote wing:

$$v_{b,f} = v_{w,f} = v_f = e^{0.05(1-M_\infty)} \quad (\text{B.72})$$

and is valid if and only if $M_\infty \leq 5$.

Correction for downwash:

$$\left(\frac{d\epsilon}{d\alpha} \right)_t = (1 - \eta_t) \Delta\epsilon \quad (\text{B.73})$$

$$\Delta\epsilon = \frac{S'_t}{S_t} \quad (\text{B.74})$$

$$\eta_t = 1 + \frac{i_c K_w C_{N_t} S_w}{8\pi(K_w + K_b)_t \left[\left(\frac{b}{2} + r \right)_t - r \right] (Z_v - r)} \quad (\text{B.75})$$

$$i_c = \frac{-4Z_v \left[(\bar{S}_m)_t - r \right] (K_w)_t}{(\bar{Y}_v^2 + \bar{Z}_v^2) (\bar{S}_m)_t} \quad (\text{B.76})$$

$$(\bar{S}_m)_t = \frac{\left(\frac{b}{2} + r \right)_t}{r} \quad (\text{B.77})$$

$$\bar{Z}_v = \frac{Z_v}{\left(\frac{b}{2} + r \right)_t} \quad (\text{B.78})$$

$$\bar{Y}_v = \frac{Y_v}{\left(\frac{b}{2} + r \right)_t} \quad (\text{B.79})$$

$$Z_v = r + \left(\left(\frac{b}{2} + r \right)_t - r \right) \left[0.885 + 0.2049 \left((r_m)_t + 0.5 \right) + 0.1072 \left((r_m)_t + 0.5 \right)^2 \right] \quad (\text{B.80})$$

$$Y_v = 2.75 (X_{cm})_t \quad (\text{B.81})$$

where t subscript refers to tail fin and X_{cm} is the center of mass of the tail fin.

Total interference factors computation:

$$(K_w + K_b)_w = (k_w v_{b,\eta} v_{w,bv} v_{w,f} + k_b v_{w,\eta} v_{b,bt} v_{b,f})_w \quad (\text{B.82})$$

$$(K_w + K_b)_t = (k_w v_{b,\eta} v_{w,bv} v_{w,f} + k_b v_{w,\eta} v_{b,bt} v_{b,f})_t \quad (\text{B.83})$$

The following equations can be found on reference [32]. The coefficients of the next 2 equations are well explained in the reference.

Missile aeroheating:

Heat flux over the leading edge:

$$q_{st} = 1.83 \times 10^{-4} \sqrt{\left(\frac{\rho_\infty}{R_{LE}} \right)} V_\infty^3 \quad (\text{B.84})$$

Heat flux on a flat surface:

$$q_f = 2.53 \times 10^{-5} \sin \varphi \sqrt{\left(\frac{\rho_\infty \cos \varphi}{\eta} \right)} V_\infty^{3.2} \quad (\text{B.85})$$

APPENDIX C. STABILITY, MANEUVERABILITY AND CONTROL

The following equations can be found on reference [36].

Static longitudinal stability:

Missile body and booster:

Total normal force coefficient as a function of α for the missile and the booster:

$$\begin{aligned}
 C_{N_\alpha} = & (C_{N_\alpha})_B + \left[((C_{N_\alpha})_{W1} + (C_{N_\alpha})_{W3}) \sin \theta + ((C_{N_\alpha})_{W2} + (C_{N_\alpha})_{W4}) \cos \theta \right] \\
 & (K_{W(B)} + K_{B(W)}) \frac{S_W}{S_{ref}} + \left[((C_{N_\alpha})_{T1} + (C_{N_\alpha})_{T3}) \sin \theta + ((C_{N_\alpha})_{T2} + (C_{N_\alpha})_{T4}) \cos \theta \right] \\
 & (K_{T(B)} + K_{B(T)}) \frac{S_T}{S_{ref}} (1 - \epsilon_\alpha)
 \end{aligned} \tag{C.1}$$

Total normal force coefficient as a function of δ for the missile and the booster:

$$\begin{aligned}
 C_{N_\delta} = & \left[((C_{N_\alpha})_{W1} + (C_{N_\alpha})_{W3}) \sin \theta + ((C_{N_\alpha})_{W2} + (C_{N_\alpha})_{W4}) \cos \theta \right] \\
 & (K_{W(B)} + K_{B(W)}) \frac{S_W}{S_{ref}} + \left[((C_{N_\alpha})_{T1} + (C_{N_\alpha})_{T3}) \sin \theta + ((C_{N_\alpha})_{T2} + (C_{N_\alpha})_{T4}) \cos \theta \right] \\
 & (K_{T(B)} + K_{B(T)}) \frac{S_T}{S_{ref}} (-\epsilon_\delta)
 \end{aligned} \tag{C.2}$$

Total pitching moment coefficient as a function of α for the missile and the booster:

$$\begin{aligned}
C_{m_\alpha} = & (C_{N_\alpha})_B \left(\frac{x}{d} \right)_B + \left[((C_{N_\alpha})_{W1} + (C_{N_\alpha})_{W3}) \sin \theta + ((C_{N_\alpha})_{W2} + (C_{N_\alpha})_{W4}) \cos \theta \right] \\
& (K_{W(B)} + K_{B(W)}) \frac{S_W}{S_{ref}} \left(\frac{x}{d} \right)_W + \left[((C_{N_\alpha})_{T1} + (C_{N_\alpha})_{T3}) \sin \theta + ((C_{N_\alpha})_{T2} + (C_{N_\alpha})_{T4}) \cos \theta \right] \\
& (K_{T(B)} + K_{B(T)}) \frac{S_T}{S_{ref}} \left(\frac{x}{d} \right)_T (1 - \epsilon_\alpha)
\end{aligned}
\tag{C.3}$$

Total pitching moment coefficient as a function of δ for the missile and the booster:

$$\begin{aligned}
C_{m_\delta} = & \left[((C_{N_\alpha})_{W1} + (C_{N_\alpha})_{W3}) \sin \theta + ((C_{N_\alpha})_{W2} + (C_{N_\alpha})_{W4}) \cos \theta \right] \\
& (K_{W(B)} + K_{B(W)}) \frac{S_W}{S_{ref}} \left(\frac{x}{d} \right)_W + \left[((C_{N_\alpha})_{T1} + (C_{N_\alpha})_{T3}) \sin \theta + ((C_{N_\alpha})_{T2} + (C_{N_\alpha})_{T4}) \cos \theta \right] \\
& (K_{T(B)} + K_{B(T)}) \frac{S_T}{S_{ref}} \left(\frac{x}{d} \right)_T (-\epsilon_\delta)
\end{aligned}
\tag{C.4}$$

where the subscript α and δ are the angles of attack and fin deflection referring to the derivatives of C_N , C_m , etc. while B , W , T subscripts refer to body, wing and tail, respectively. S_{ref} is the reference surface or the frontal area of the missile, S_W and S_T are the total surface for all the wing fins and tail fins in the missile, θ is the angle between each wing/tail fin and the axis of the missile body and $\frac{x}{d}$ is the difference of the pressure center position of any components (body, wing, tail measured from the missile nose), and the missile center of gravity, all divided by the missile diameter.

Missile body:

Total normal force coefficient as a function of α for the missile:

$$\begin{aligned}
C_{N_\alpha} = & (C_{N_\alpha})_B + \left[((C_{N_\alpha})_{W1} + (C_{N_\alpha})_{W3}) \sin \theta + ((C_{N_\alpha})_{W2} + (C_{N_\alpha})_{W4}) \cos \theta \right] \\
& (K_{W(B)} + K_{B(W)}) \frac{S_W}{S_{ref}}
\end{aligned}
\tag{C.5}$$

Total normal force coefficient as a function of δ for the missile:

$$C_{N\delta} = \left[((C_{N\alpha})_{W1} + (C_{N\alpha})_{W3}) \sin \theta + ((C_{N\alpha})_{W2} + (C_{N\alpha})_{W4}) \cos \theta \right] \frac{S_W}{(K_{W(B)} + K_{B(W)}) S_{ref}}$$

(C.6)

Total pitching moment coefficient as a function of α for the missile:

$$C_{m\alpha} = (C_{N\alpha})_B \left(\frac{x}{d} \right)_B + \left[((C_{N\alpha})_{W1} + (C_{N\alpha})_{W3}) \sin \theta + ((C_{N\alpha})_{W2} + (C_{N\alpha})_{W4}) \cos \theta \right] \frac{S_W}{S_{ref}} \left(\frac{x}{d} \right)_W$$

(C.7)

Total pitching moment coefficient as a function of δ for the missile:

$$C_{m\delta} = \left[((C_{N\alpha})_{W1} + (C_{N\alpha})_{W3}) \sin \theta + ((C_{N\alpha})_{W2} + (C_{N\alpha})_{W4}) \cos \theta \right] \frac{S_W}{S_{ref}} \left(\frac{x}{d} \right)_W$$

(C.8)

Manoeuvring and turning performance:

Static stability margin:

$$\frac{\bar{X}}{d} = \frac{C_{m\alpha}}{C_{N\alpha}}$$

(C.9)

Load factor capability:

$$\frac{n}{\delta} = \left(C_{N\delta} - C_{N\alpha} \frac{C_{m\delta}}{C_{m\alpha}} \right) \frac{q S_{ref}}{W}$$

(C.10)

Flat turns cruciform fins:

$$C_{N_{TR}} = C_{N_{\alpha}} \left(-\frac{C_{m_{\delta}} \delta}{C_{m_{\alpha}}} \right) + C_{N_{\delta}} \delta \quad (\text{C.11})$$

$$R = \frac{V^2}{ng} \quad (\text{C.12})$$

$$R = \frac{2W}{\rho g S_{ref} C_{N_{TR}}} \quad (\text{C.13})$$

$$\dot{\gamma} = \frac{ng}{V} \quad (\text{C.14})$$

$$\dot{\gamma} = \frac{\rho g S V}{2W} C_{N_{TR}} \quad (\text{C.15})$$

Pitch up maneuver:

$$R = \frac{V^2}{g(n-1)} \quad (\text{C.16})$$

$$\dot{\gamma} = g \left(\frac{\rho V}{2W} C_{N_{TR}} - \frac{1}{V} \right) \quad (\text{C.17})$$

Pitch down maneuver:

$$R = \frac{V^2}{g(n+1)} \quad (\text{C.18})$$

$$\dot{\gamma} = g \left(\frac{\rho V}{2W} C_{N_{TR}} + \frac{1}{V} \right) \quad (\text{C.19})$$

where d is the missile diameter, n the load factor, $\dot{\gamma}$ the pitch rate, g the gravity, V is the velocity, R is the turn radius and the subscript TR refers to the trim.

APPENDIX D. SOLID BOOSTER DESIGN EQUATIONS

The following equations can be found on reference [37].

Fundamentals of rocket propulsion:

Total impulse:

$$I_t = \int_0^t F dt \quad (D.1)$$

Specific impulse:

$$I_{sp} = \frac{\int_0^t F dt}{g_0 \int \dot{m} dt} \quad (D.2)$$

Rocket thrust:

$$F = \dot{m} v_e + (p_e - p_0) A_e \quad (D.3)$$

Characteristic velocity:

$$c^* = \frac{p_c A_t}{\dot{m}} \quad (D.4)$$

Exhaust velocity:

$$v_e = \sqrt{\frac{2\gamma}{\gamma-1} RT_c \left[1 - \left(\frac{p_e}{p_c} \right)^{\frac{\gamma-1}{\gamma}} \right]} \quad (D.5)$$

$$M_e = \frac{v_e}{\sqrt{\gamma RT_c}} \quad (D.6)$$

$$M = \frac{625 T_c}{(I_{sp})^2} \quad (D.7)$$

$$R = \frac{R'}{M} \quad (D.8)$$

Tsiolkovsky rocket equation:

$$\Delta V = v_e \ln \frac{m_0}{m_f} = I_{sp} g_0 \ln \frac{m_0}{m_f} \quad (D.9)$$

Nozzle area ratio:

$$\frac{A_t}{A_e} = \left(\frac{\gamma+1}{2} \right)^{\frac{1}{\gamma-1}} \left(\frac{p_e}{p_c} \right)^{\frac{1}{\gamma}} \sqrt{\frac{\gamma+1}{\gamma-1} \left[1 - \left(\frac{p_e}{p_c} \right)^{\frac{\gamma-1}{\gamma}} \right]} \quad (D.10)$$

Thrust coefficient:

$$C_F = \sqrt{\frac{2\gamma^2}{\gamma-1} \left(\frac{2}{\gamma+1} \right)^{\frac{\gamma-1}{\gamma+1}} \left[1 - \left(\frac{p_e}{p_c} \right)^{\frac{\gamma-1}{\gamma}} \right]} + \frac{p_e - p_0}{p_c} \left(\frac{A_e}{A_t} \right) \quad (D.11)$$

$$F = C_F p_c A_t \quad (D.12)$$

Conical nozzle length:

$$L = \frac{D_t}{2} \left(\sqrt{\frac{A_e}{A_t}} - 1 \right) \tan^{-1}(\alpha) \quad (D.13)$$

$$\alpha = \sin^{-1} \left(\frac{1}{M_e} \right) \quad (D.14)$$

where \dot{m} is the propellant mass flow, v_e is the propellant velocity of exhaust gases, m_0 the initial rocket mass, m_f the final rocket mass (no fuel), p_e is the pressure at nozzle exit (assume for this study atmospheric pressure), p_0 is the atmospheric pressure, A_e is the nozzle exit area, A_t is the nozzle throat area, p_c is the chamber pressure, γ is usually taken as 1.18 for solid propellants, D_t is the nozzle throat diameter, M_e the exit Mach number of the nozzle, T_c the flame temperature and R' the universal gas constant equal to 8314.3 J kg⁻¹ mol⁻¹ K⁻¹.

The following equations can be found on reference [39].

Additional properties of solid rocket motors:

$$\dot{m}_g = \frac{dM}{dt} + \dot{m} \quad (\text{D.15})$$

$$\dot{m}_g = \rho_p A_b r_b \quad (\text{D.16})$$

$$r_b = a p_c^n \quad (\text{D.17})$$

$$\frac{dM}{dt} = \frac{d(\rho_g V_p)}{dt} = \rho_g \frac{dV_p}{dt} + V_p \frac{d\rho_g}{dt} \quad (\text{D.18})$$

$$\rho_g = \frac{p_c}{RT_c} \quad (\text{D.19})$$

$$\frac{dp_c}{dt} = \frac{1}{V_i} \left[RT_c (\dot{m}_g - \dot{m}) - p_c \frac{dV_i}{dt} \right] \quad (\text{D.20})$$

where ρ_p is the propellant density, ρ_g is the density of the combustion gases, \dot{m}_g is the rate of mass addition to the combustion chamber, r_b is the burning rate, a is the burning rate coefficient, n is the burning rate exponent, V_i is the gas volume, T_c is the chamber temperature and R is the gas constant.

Internal ballistics to study grain burnback:

$$A_{bA_1} = 2NL \left[(y+f) \left(\frac{\pi}{2} \right) + R_p - \sqrt{(R_i+y)^2 - (f+y)^2} + (R_i+y) \left(\frac{\pi}{N} - \theta_s \right) \right] \quad (\text{D.21})$$

$$V_{pA_1} = V_{pA_2} = NL \left[\left[2R_p - \sqrt{(R_i+y_{s3=0})^2 - (f+y_{s3=0})^2} - (y-y_{s3=0}) \cot \left(\frac{\pi}{N} \right) \right] \right. \\ \left. (y+f) + \frac{1}{2} \pi (y+f)^2 \right] \quad (\text{D.22})$$

$$\theta_s = \sin^{-1} \left(\frac{f+y}{R_i+y} \right) \quad (\text{D.23})$$

$$A_{b_{A_2}} = 2NL \left[(y+f) \left(\frac{\pi}{2} \right) + R_p - \sqrt{(R_i + y_{s_3=0})^2 - (f + y_{s_3=0})^2} \right. \\ \left. - (y - y_{s_3=0}) \cot \left(\frac{\pi}{N} \right) \right] \quad (D.24)$$

$$A_{b_{A_3}} = 2NL \left[(y+f) \theta_c + R_p - \sqrt{(R_i + y_{s_3=0})^2 - (f + y_{s_3=0})^2} \right. \\ \left. - (y - y_{s_3=0}) \cot \left(\frac{\pi}{N} \right) \right] \quad (D.25)$$

$$V_{p_{A_3}} = NL \left[\left[2R_p - \sqrt{(R_i + y_{s_3=0})^2 - (f + y_{s_3=0})^2} - (y - y_{s_3=0}) \cot \left(\frac{\pi}{N} \right) \right] \right. \\ \left. (y+f) + \theta_c (y+f)^2 - R_o R_p \sin \theta_p + \theta_p R_o^2 \right] \quad (D.26)$$

$$\theta_c = \cos^{-1} \left[-\frac{R_o^2 - R_p^2 - (y+f)^2}{2R_p(y+f)} \right] - \frac{\pi}{2} \quad (D.27)$$

$$\theta_p = \sin^{-1} \left[\frac{(y+f) \sin \left(\theta_c + \frac{\pi}{2} \right)}{R_o} \right] \quad (D.28)$$

$$A_{b_{A_4}} = 2NL (y+f) (\theta_c - \alpha_1) \quad (D.29)$$

$$V_{p_{A_4}} = NL \left[R_p X_1 + (\theta_c - \alpha_1) (y+f)^2 - R_o R_p \sin \theta_p + \theta_p R_o^2 \right] \quad (D.30)$$

$$\alpha_1 = \tan^{-1} \left(\frac{Y_1 - R_p}{X_1} \right) \quad (D.31)$$

$$X_1 = \frac{2 \tan \left(\frac{\pi}{2} - \frac{\pi}{N} \right) R_p + \sqrt{4 \tan^2 \left(\frac{\pi}{2} - \frac{\pi}{N} \right) - 4 \left[1 + \tan^2 \left(\frac{\pi}{2} - \frac{\pi}{N} \right) \right] \left[R_p^2 - (f+y)^2 \right]}}{2 \left[1 + \tan \left(\frac{\pi}{2} - \frac{\pi}{N} \right) \right]} \quad (D.32)$$

$$Y_1 = X_1 \tan \left(\frac{\pi}{2} - \frac{\pi}{N} \right) \quad (\text{D.33})$$

$$\begin{aligned} A_b = & A_{b_{A_1}} [H(y-0) - H(y-y_{s_3=0})] + A_{b_{A_2}} [H(y-y_{s_3=0}) - H(y-R_o + R_p + f)] \\ & + A_{b_{A_3}} [H(y-R_o + R_p + f) - H(y-y_{s_2=0})] + A_{b_{A_4}} [H(y-y_{s_2=0}) - H(y-y_{max})] \end{aligned} \quad (\text{D.34})$$

$$\begin{aligned} V_p = & V_{p_{A_1}} [H(y-0) - H(y-y_{s_3=0})] + V_{p_{A_2}} [H(y-y_{s_3=0}) - H(y-R_o + R_p + f)] \\ & + V_{p_{A_3}} [H(y-R_o + R_p + f) - H(y-y_{s_2=0})] + V_{p_{A_4}} [H(y-y_{s_2=0}) - H(y-y_{max})] \end{aligned} \quad (\text{D.35})$$

$$A_p = \frac{V_p}{L} \quad (\text{D.36})$$

where N are the number of slots, L is the length of the propellant, y the amount of grain regression, f the slot tip radius, R_p the slot length, R_i the inner radius of the propellant, R_o the outer radius of the propellant, A_b the total burn area of the propellant, V_p the volume of the propellant, A_p the total port area of the propellant, H the heaviside function, and $y_{s_3=0}$ and $y_{s_2=0}$ the amount of grain regression when the perimeters S3 and S2 are equal to 0.

APPENDIX E. SCRAMJET DESIGN EQUATIONS

The following equations can be found on reference [40].

Intake phase (0-3):

Inlet geometry considerations (4 shocks and mixed compression):

$$h_c = h_1 + h_2 + h_3 + h_4 \quad (\text{E.1})$$

$$L_{lip} = L_1 + L_2 + L_3 - L_n \quad (\text{E.2})$$

$$h_c = \tan(\beta_1)L_{lip} \quad (\text{E.3})$$

$$h_1 = L_1 \tan(\delta_1) \quad (\text{E.4})$$

$$h_2 = L_2 \tan(\delta_1 + \delta_2) \quad (\text{E.5})$$

$$h_3 = L_3 \tan(\delta_1 + \delta_2 + \delta_3) \quad (\text{E.6})$$

where h_c is the inlet capture height, $h_{1,2,3,4}$ the remaining ramps heights and $L_{lip,1,2,3,n}$ the lengths of the cowl lip, ramps and nose.

Oblique shocks fundamentals:

$$M_2 = \sqrt{\frac{(\gamma - 1)M_1^2 \sin^2 \beta + 2}{\left[2\gamma M_1^2 \sin^2 \beta - (\gamma - 1)\right] \sin^2(\beta - \delta)}} \quad (\text{E.7})$$

$$\frac{P_2}{P_1} = \left[\frac{2\gamma M_1^2 \sin^2 \beta - (\gamma - 1)}{\gamma + 1} \right] \quad (\text{E.8})$$

$$\frac{T_2}{T_1} = \frac{\left[2\gamma M_1^2 \sin^2 \beta - (\gamma - 1)\right] \left[(\gamma - 1)M_1^2 \sin^2 \beta + 2\right]}{(\gamma + 1)^2 M_1^2 \sin^2 \beta} \quad (\text{E.9})$$

$$\frac{\rho_2}{\rho_1} = \frac{(\gamma + 1)M_1^2 \sin^2 \beta}{2 + (\gamma - 1)M_1^2 \sin^2 \beta} \quad (\text{E.10})$$

$$\frac{P_{02}}{P_{01}} = \left[\frac{(\gamma+1)M_1^2 \sin^2 \beta}{(\gamma-1)M_1^2 \sin^2 \beta + 2} \right]^{\frac{\gamma}{\gamma-1}} \left[\frac{\gamma+1}{2\gamma M_1^2 \sin^2 \beta - (\gamma-1)} \right]^{\frac{1}{\gamma-1}} \quad (\text{E.11})$$

where subscript 1 refers to the conditions upstream the shock, subscript 2 to downstream conditions, δ is the wedge angle, β the shock wave angle, $P_{1,2}$ to the static pressure, $P_{01,02}$ to the total pressure, T to the static temperature and ρ to the density.

Inlet performance parameters:

$$\pi_c = \frac{P_{03}}{P_{00}} = \frac{P_3}{P_0} \left(\frac{T_0}{T_3} \right)^{\frac{\gamma}{\gamma-1}} \quad (\text{E.12})$$

$$\eta_c = \frac{\frac{T_3}{T_o} - \left(\frac{1}{\pi_c} \right)^{\frac{\gamma-1}{\gamma}}}{\frac{T_3}{T_o} - 1} \quad (\text{E.13})$$

$$\eta_{KE} = 1 - \frac{2}{(\gamma-1)M_0^2} \left(\frac{T_3}{T_0} - 1 \right) (1 - \eta_c) \quad (\text{E.14})$$

$$\frac{A_3}{A_0} = \frac{T_3}{T_0} \frac{p_0}{p_3} \frac{V_0}{V_3} \quad (\text{E.15})$$

$$M_3 = \sqrt{\frac{2}{\gamma-1} \left[\frac{T_0}{T_3} \left(1 + \frac{\gamma-1}{2} M_0^2 \right) - 1 \right]} \quad (\text{E.16})$$

$$T_{03} = T_3 \left[1 + 0.5(\gamma-1)M_3^2 \right] \quad (\text{E.17})$$

and according to Military standars for minimum inlet pressure recovery specified in MIL Spec E-5007D

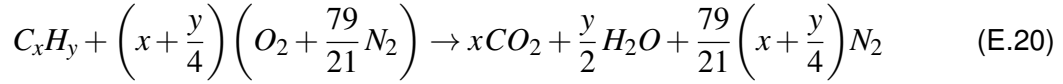
$$\frac{P_{03}}{P_{00}} = 1 - 0.0776(M_0 - 1)^{1.35} \quad \text{for } (1 < M_0 < 5) \quad (\text{E.18})$$

$$\frac{P_{03}}{P_{00}} = \frac{800}{M_0^4 + 935} \quad \text{for } (5 < M_0) \quad (\text{E.19})$$

where subscript 0 refers to the intake start position, subscript 3 to the combustion chamber entrance, A to the reference area, P_{00} to the total pressure at the intake start, P_{03} to the total pressure at the combustion chamber entrance, A to the reference area.

Combustion phase (3-4):

Stoichiometric fuel to air ratio for hydrocarbons:



$$f_{st} = \frac{36x + 3y}{103(4x + y)} \quad (E.21)$$

$$\gamma_h = \gamma_0 - k_1 e^{-\frac{k_2}{T}} \quad (E.22)$$

where C_{pc} is equal to 1090 kJ/kg, C_{ph} is equal to 1510 kJ/kg, γ_0 is equal to 1.38 and k_1 and k_2 have a value of 0.2 and 900, respectively.

$$T_{04} = \frac{f \eta_b h_{pr} + C_{pc} T_{03}}{C_{ph} (1 + f)} \quad (E.23)$$

$$\frac{T_{04}}{T_{03}} = \frac{M_4^2}{M_3^2} \left[\frac{1 + \gamma M_3^2}{1 + \gamma_h M_4^2} \right]^2 \left[\frac{1 + 0.5(\gamma_h - 1)M_4^2}{1 + 0.5(\gamma - 1)M_3^2} \right] \quad (E.24)$$

and here we need to isolate numerically M_4 .

$$P_4 = P_3 \frac{1 + \gamma M_3^2}{1 + \gamma_h M_4^2} \quad (E.25)$$

$$T_4 = \frac{T_{04}}{1 + 0.5(\gamma_h - 1)M_3^2} \quad (E.26)$$

Nozzle phase (4-10):

$$T_{10} = T_4 (1 - \eta_e) \left[1 - \left(\frac{P_0}{P_4} \right)^{\frac{\gamma_h - 1}{\gamma_h}} \right] \quad (E.27)$$

$$V_{10} = \sqrt{2C_{ph}(T_{04} - T_{10})} \quad (E.28)$$

$$\frac{A_{10}}{A_0} = (1 + f) \frac{p_0}{p_{10}} \frac{T_{10}}{T_0} \frac{V_0}{V_{10}} \quad (\text{E.29})$$

Method of characteristics:

Prandtl-Meyer function:

$$\nu = \sqrt{\frac{\gamma+1}{\gamma-1}} \left[\tan^{-1} \sqrt{\left(\frac{\gamma-1}{\gamma+1}\right)(M_e^2 - 1)} - \tan^{-1} \sqrt{\left(\frac{\gamma-1}{\gamma+1}\right)(M_4^2 - 1)} \right] - \left[\tan^{-1} \sqrt{M_e^2 - 1} - \tan^{-1} \sqrt{M_4^2 - 1} \right] \quad (\text{E.30})$$

Mach angle:

$$\mu = \sin^{-1} \frac{1}{M} \quad (\text{E.31})$$

Maximum nozzle angle:

$$\theta_{w,max} = \frac{\nu(M_{10})}{2} \quad (\text{E.32})$$

Centerline characteristics:

$$(s_-)_j = 2\theta_j \quad (\text{E.33})$$

$$(s_+)_j = \theta_j - \nu(M_j) = 0 \quad (\text{E.34})$$

Centerline slope of characteristics:

$$\lambda_{-j} = \tan(\theta_j - \mu_j) \quad (\text{E.35})$$

where M_e is the mach number behind the shock wave.

Engine performance relationships:

$$F = (\dot{m}_f + \dot{m}_0) V_{10} - \dot{m}_0 V_0 + (p_{10} - p_0) A_{10} \quad (\text{E.36})$$

$$\frac{F}{\dot{m}_0} = (1 + f) V_{10} - V_0 \quad (\text{E.37})$$

$$C_{TS} = \frac{\dot{m}_0 f}{F} \quad (\text{E.38})$$

$$f = \frac{\dot{m}_f}{\dot{m}_0} \quad (\text{E.39})$$

$$\eta_{th} = \frac{\frac{V_{10}^2}{2} - \frac{V_0^2}{2}}{f h_{PR}} \quad (\text{E.40})$$

$$\eta_p = \frac{2}{\frac{V_{10}}{V_0} + 1} = \frac{2}{\sqrt{\eta_{th} \frac{2f h_{PR}}{V_0^2} + 1} + 1} \quad (\text{E.41})$$

$$\eta_o = \eta_{th} \eta_p \quad (\text{E.42})$$

$$I_{sp} = \frac{h_{PR}}{g_0 V_0} \eta_o \quad (\text{E.43})$$

where F is the thrust force, \dot{m}_f the fuel mass flow, \dot{m}_0 the air mass flow, V_0 the missile velocity, V_{10} the exhaust velocity, C_{TS} the thrust specific fuel consumption, η_{th} the thermal efficiency, η_p the propulsive efficiency, η_o the overall efficiency and I_{sp} the specific impulse.

APPENDIX F. TRAJECTORY DESIGN EQUATIONS

The following equations can be found on reference [36].

Take-off trajectory with gravity turn:

$$q = \frac{1}{2} \rho V^2 \quad (\text{F.1})$$

$$D = C_{D_0} q S \quad (\text{F.2})$$

$$a_1 = \frac{(T - D)g}{W} \quad (\text{F.3})$$

$$a_2 = -g \sin \theta \quad (\text{F.4})$$

$$\sum a = a_1 + a_2 \quad (\text{F.5})$$

$$\Delta V = (3a_{n-1} - a_{n-2}) \frac{\Delta t}{2} \quad (\text{F.6})$$

$$V = V_{n-1} + \Delta V \quad (\text{F.7})$$

$$\theta = \theta_{n-1} + \dot{\theta} \Delta t \quad (\text{F.8})$$

$$\bar{\theta} = (\theta_{n-1} + \theta) \frac{\Delta t}{2} \quad (\text{F.9})$$

$$\bar{V} \sin \bar{\theta} = \frac{(V_{n-1} + V)}{2} \sin \bar{\theta} \quad (\text{F.10})$$

$$\bar{V} \cos \bar{\theta} = \frac{(V_{n-1} + V)}{2} \cos \bar{\theta} \quad (\text{F.11})$$

$$\Delta h = (\bar{V} \sin \bar{\theta}) \Delta t \quad (\text{F.12})$$

$$\sum h = h_{n-1} + \Delta h \quad (\text{F.13})$$

$$\bar{h} = \frac{h_{n-1} + h}{2} \quad (\text{F.14})$$

$$\Delta R = (\bar{V} \cos \bar{\theta}) \Delta t \quad (\text{F.15})$$

$$\sum R = R_{n-1} + \Delta R \quad (\text{F.16})$$

where q is the dynamic pressure, D is the drag force, a is the acceleration, n is the iteration step, ΔV is the velocity increment, Δt is the time step, V the velocity, θ the pitch angle, $\dot{\theta}$ the pitch rate, h the altitude, R the range and the $-$ symbol the mean value between two steps of the iteration.

Constant rate of climb ascent:

$$\sin \gamma_c = \frac{T - D}{W} = \frac{R}{C} \quad (\text{F.17})$$

$$\frac{R}{C} = \frac{(T - D) V}{W} \quad (\text{F.18})$$

Time to climb expression:

$$\int_{t_1}^{t_2} dt = \int_{h_1}^{h_2} \frac{1}{\frac{R}{C}} dh \quad (\text{F.19})$$

Rate of climb correction for accelerating aircraft (excess thrust):

$$\sin \gamma_c = \frac{T - D}{W} - \frac{a}{g} \quad (\text{F.20})$$

$$a = \frac{dV}{dt} = \frac{dV}{dh} \frac{dh}{dt} = \frac{dV}{dh} V \sin \gamma_c \quad (\text{F.21})$$

Cruise:

Equilibrium flight condition:

$$L = W \quad (\text{F.22})$$

$$T = D \quad (\text{F.23})$$

Breguet range equation:

$$R_{max} = V I_{sp} \left(\frac{L}{D} \right) \ln \left[\frac{m_{bc}}{(m_{bc} - m_f)} \right] \quad (\text{F.24})$$

The following equations can be found on reference [48].

Gliding towards target:

$$\frac{dr}{dt} = V \sin \gamma \quad (\text{F.25})$$

$$\frac{dR}{dt} = V \cos \gamma \quad (\text{F.26})$$

$$\frac{dV}{dt} = -\frac{D}{m} - g \sin \gamma \quad (\text{F.27})$$

$$\frac{d\gamma}{dt} = \frac{1}{V} \left[\frac{L}{m} \cos \sigma - \left(g - \frac{V^2}{r} \right) \cos \gamma \right] \quad (\text{F.28})$$

where r is the height, V is the velocity, R the distance, D the Drag force, L the Lift force, θ the bank angle and γ the pitch angle.

APPENDIX G. WARHEAD AND PENETRATOR DESIGN EQUATIONS

The following equations can be found on reference [54].

Gurney velocity coefficient:

$$\sqrt{2E_c} = \frac{D}{2.97} \quad (\text{G.1})$$

where D is the detonation velocity in mms^{-1} .

Relative Effectiveness factor:

$$RE = \frac{E_c}{E_{cTNT}} \quad (\text{G.2})$$

Total warhead mass:

$$M_T = C + M \quad (\text{G.3})$$

where C is the charge mass and M the total mass of fragments.

(G.4)

Equivalent charge weight using Fano approach:

$$C' = C \left[0.2 + \frac{0.8}{2\left(\frac{M}{C}\right) + 1} \right] \quad (\text{G.5})$$

Total explosive charge energy:

$$E = E_c C' \quad (\text{G.6})$$

Total missile energy vs total explosive charge energy:

$$\frac{E_T}{E} = \frac{0.5 M_{missile} V^2 + E}{E} \quad (G.7)$$

Scaled distance (not confuse R (miss distance) with RE):

$$Z = \frac{R}{\sqrt[3]{C'}} \quad (G.8)$$

Pulse duration time:

$$t_d = \sqrt[3]{C'} \left[\frac{980 \left[1 + \left(\frac{Z}{0.54} \right)^{10} \right]}{\left[1 + \left(\frac{Z}{0.02} \right)^3 \right] \left[1 + \left(\frac{Z}{0.74} \right)^6 \right] \left[\sqrt{1 + \left(\frac{Z}{6.9} \right)^2} \right]} \right] \quad (G.9)$$

Peak pressure:

$$\frac{p}{p_0} = \frac{808 \left[1 + \left(\frac{Z}{4.5} \right)^2 \right]}{\sqrt{1 + \left(\frac{Z}{0.048} \right)^2} \sqrt{1 + \left(\frac{Z}{0.32} \right)^2} \sqrt{1 + \left(\frac{Z}{1.35} \right)^2}} \quad (G.10)$$

where p_0 is the atmospheric pressure.

Fragment velocity:

$$V_f = \sqrt{\frac{1.6 E_c \left(\frac{C}{M} \right)}{1 + \left(\frac{C}{2M} \right)}} \quad (G.11)$$

Arrival time to target:

$$t_a = \frac{1}{a_x} \left(\frac{7 p_0 + 6 p}{7 p_0} \right)^{-\frac{1}{2}} (R - r_i) \quad (G.12)$$

Speed of sound:

$$a_x = \sqrt{\gamma R T} \quad (G.13)$$

Mach wave front:

$$M_x = \sqrt{1 + \left(\frac{6p}{7p_0}\right)} \quad (\text{G.14})$$

Blast pressure as a function of time:

$$p(t) = p e^{-\frac{t}{t_d}} \left(1 - \frac{t}{t_d}\right) \quad (\text{G.15})$$

Penetration distance:

$$\frac{P_{distance}}{d_p} = \left[\left(\frac{l_p}{d_p}\right) - 1 \right] \sqrt{\frac{\rho_p}{\rho_t}} + 3.67 \sqrt[3]{\left(\frac{\rho_p}{\rho_t}\right)^2 \left(\frac{\rho_t V^2}{\sigma_t}\right)} \quad (\text{G.16})$$

where σ_t is the yield stress of the target in psi, d_p is the penetrator diameter, l_p is the penetrator length in feet, ρ_p and ρ_t the density of the penetrator and the target in lb/in³ and V the velocity in ft/s

The following equations can be found on reference [57].

Ballistic limit velocity:

$$v_{bl} = \sqrt{\frac{2t \sigma_r}{\rho_p L}} \quad (\text{G.17})$$

$$\sigma_r = (2 + 0.8 \ln K) \sigma_p \quad (\text{G.18})$$

$$K = \frac{P_{distance}}{d_p} \quad (\text{G.19})$$

where σ_r is the ability of the armour to resist penetration (penetration strength).